CENTRIFUGE MODELLING OF ICE SCOUR IN SAND

FRANK HYNES

CENTRIFUGE MODELLING OF ICE SCOUR IN SAND

by

© FRANK HYNES, B.Eng.

A thesis submitted to the School of Graduate Studies
in partial fulfilment of the requirements for
the degree of Master of Engineering

Faculty of Engineering and Applied Science
Memorial University of Newfoundland

January 1996

St. John's Newfoundland Canada

Abstract

The interaction of icebergs (of glacial origin) and pressure ridge ice keels (formed from frozen sea water) with the seabed is recognized as an important consideration in the development of hydrocarbon resources in both the arctic and eastern offshore regions of Canada. To understand the detrimental effect of a scouring ice mass upon the integrity of seafloor facilities such as wellheads, pipelines and submarine cables, a large amount of analytical, experimental and phenomenological research into ice keel scour has been undertaken.

Concerns related to the ice keel scour phenomenon are currently being addressed within a joint industry and government sponsored research program entitled the Pressure Ridge Ice Scour Experiment (PRISE). The objective of this program is to develop the expertise and understanding required for the safe and economical engineering of offshore pipelines in regions prone to ice keel scour. Under the auspices of the PRISE program, a series of centrifuge modelling tests involving ice keel scour were undertaken. The centrifuge modelling program involved towing an instrumented model ice keel of set geometry across a model testbed at a set scour depth while under the influence of a centrifugal force. The objective of the tests was to measure scour-induced stresses and pore pressures, horizontal and vertical loads and model keel/ soil interface pressures.

The results obtained during the experimental program involving ice keel scour in sand highlighted the importance of the static soil "dead wedge" beneath the model ice keel with respect to variation in scour loads and subscour soil displacements. Analysis of the results served to support Been's (1990) shear dragging hypothesis. The results also suggest that a linear relationship can be used to describe the variation of scour loads with depth.

Acknowledgements

The completion of this thesis was due in part to the helpful contributions and assistance provided by others. Special thanks are due to:

(i) My supervisors Dr. J.I. Clark and Dr. R. Phillips under whose guidance and supervision the project was completed.

(ii) Dr. Woodworth-Lynas for his insight into the phenomena of ice scour.

(iii) The members of the geotechnical group at C-CORE for their help and cooperation.

(iv) The sponsors of PRISE including the National Energy Board, the Natural Sciences and Engineering Research Council, the U.S. Department of the Interior Minerals Management Service, Petro-Canada Resources, ARCO Alaska Inc., Mobil Oil Canada Properties and Exxon Production Research Company.

(v) And finally, Cynthia for her patience, understanding and support.

Contents

List of Figures

List of Tables

List of Symbols

Acceleration	a
Acceleration or Scaling Factor	N
Angular Velocity	ω
Angle of internal friction	ϕ
Area	A
Attack Angle of The Keel	α
Cone Tip Resistance	q_c
Cone Penetration Test	CPT
Centrifuge Radius	r
Density	ρ
Effective Grain Size	d_{10}
Force	F
Gravity ($9.81 m/s^2$)	g
Horizontal Scour Force	F_H
Linear Distance	h
Horizontal Load Cell	TC
Vertical Load Cell	LC
Mean Grain Size	d_{50}
Model	Subscript-m
Mass	M,m
Prototype	Subscript-p
Pore Pressure Transducer	PPT
Pressure Transducer	PT
Scour Depth	D_S
Scour Width	B
Strain	ϵ
String Pot	SP
Total Stress Cell	TLC
Unit Weight	γ
Vertical Scour Force	F_V
Vertical Stress, Effective	σ_v'
Volume	V

Chapter One

Introduction

1.1 Opening remarks

An ice keel scour is formed when the base of an iceberg or pressure ridge ice keel is propelled laterally while in contact with the seabed. Scours are typically characterized by an elongated curvilinear or linear seafloor incision. The ability of an ice keel to scour is dependent upon a variety of factors including soil resistance, ice strength, keel geometry and driving force. The latter is a result of a combination of wind, wave, ice and tide action. Scouring of the seabed can occur when there are sufficient environmental forces to overcome soil resistance. The interaction of icebergs (of glacial origin) and pressure ridge ice keels (formed from frozen sea water) with the seabed is recognized as an important consideration in the development of hydrocarbon resources in both the arctic and eastern offshore regions of Canada.

1.2 Problem Definition

To help understand the detrimental effect of a scouring ice mass upon the integrity of seafloor facilities such as wellheads, pipelines and submarine cables, a large amount of

analytical, experimental and phenomenological research into ice keel scour has been undertaken. From a design perspective, the research has been successful in expanding the level of understanding of the process of ice keel scour. However, it has also been instrumental in identifying additional concerns, the potential for large subscour soil deformations to occur beneath a scouring ice keel being prominent.

Concerns related to the ice keel scour phenomenon are currently being addressed within a joint industry and government sponsored research program entitled the Pressure Ridge Ice Scour Experiment (PRISE). The objective of this program is to develop the expertise and understanding required for the safe and economical engineering of offshore pipelines in regions prone to ice keel scour. The PRISE program consists of five phases. Specific components include; phenomenological field studies, physical and numerical modelling, the establishment of pipeline design criteria and full scale physical modelling exercises.

Phase One of PRISE involved initial project planning, as well as a feasibility study of the Extreme Gouge Dating Project. Phase One was completed in the spring of 1992. Phase Two involved the implementation of the Extreme Gouge Dating Project. This project consisted of a field program which was undertaken in the Alaskan Beaufort Sea during the summer of 1992. The objective of this program was to verify a radiometric dating technique that could be used to determine the absolute age of seabed sediments filling deep scours. This information would aid in the determination of a return period for extreme scour events.

Phase Three involved both centrifuge and numerical modelling of ice scour, as well as the development of pipeline design guidelines. Initial centrifuge model tests of ice scour were undertaken in 1992 on the Cambridge University geotechnical centrifuge. Coincident with centrifuge modelling, a finite element model of ice/soil interaction was also developed. A second suite of centrifuge modelling exercises examining ice keel scour was undertaken at the Centre for Cold Ocean Resources Engineering (C-CORE) centrifuge facility. Designated Phase 3(a), it consisted of a series of model scour events in which the effect of attack angle, scour depth, keel width and seabed material upon ice keel scour as well as possible subscour soil deformation were examined. The development of an engineering model, calibrated using the centrifuge modelling and other data, was also undertaken during this time period. The development of the engineering model was designated Phase 3(b). Phases Four and Five will consist of monitoring a full-scale ice scour event and the burial and monitoring of an experimental pipeline respectively. As part of Phase 3(a), this thesis presents both the results of the centrifuge modelling of ice keel scour in sand, as well as an analysis of the measured scour forces.

1.3 Thesis Outline

For clarity of presentation this thesis comprises nine chapters, augmented by additional information presented within an appendix. The remaining chapters are as follows:

Chapter Two examines the various phenomenological, analytical and experimental studies

involving ice scour that have been undertaken by previous researchers. In keeping with the experimental nature of this thesis, emphasis is placed upon the experimental efforts involving small-scale physical modelling of ice scour. Chapter Three presents the rationale behind the centrifuge model sand tests as well as the experimental objectives. Chapter Four establishes the principles of centrifuge modelling, including a discussion of scaling relationships, effect of lateral acceleration and the use of the method of "modelling of models" in the verification of results. Chapters Five and Six provide a descriptive review of the experimental equipment and facilities and establish the experimental procedure used during the course of the experiments. Chapters Seven and Eight present experimental results and analysis. The analysis involves a comparison of the various data sets, specifically in terms of measured loads. A discussion of the results and the conclusions reached are presented in the final chapter.

Chapter Two

Literature Review

The phenomenon of ice keel scour has been examined through extensive offshore field studies (Woodworth-Lynas and Barrie, 1985; Woodworth-Lynas *et al.*, 1991; Hodgson *et al.*, 1988; Gilbert 1990); excavation of relic scours on land (Woodworth Lynas *et al.*, 1986; Woodworth-Lynas and Guigne, 1991; Woodworth-Lynas, 1992; Longva and Bakkejord, 1990); physical modelling (Chari, 1975; Green, 1984; Prasad, 1985; Poorooshasb *et al.* 1989; Poorooshasb and Clark, 1990; Paulin, 1992; Lach and Clark, 1994); and analytical approaches (Chari, 1975; FENCO, 1975; Palmer *et al.*, 1989; Been *et al.*, 1990a).

2.1 Phenomenological (Field) Studies

Offshore phenomenological scour data originating from high resolution sub-bottom profiling, sidescan sonagraphs and visual inspections using remote operated vehicles (ROV's) and manned submersibles have provided a wealth of data in terms of scour characteristics, including depth, width, orientation, length, frequency and spatial density. Analysed statistically this information is useful in the selection of pipeline routes which minimize the probability of scour damage.

A region prone to ice keel scour, the Canadian Beaufort Sea has been the focus of many offshore field studies (Pelletier and Shearer, 1972; Lewis, 1977; Hnatiuk and Wright, 1983; Gilbert, 1990; Lewis and Blasco, 1990). Associated with pressure ridge ice keels, scours in this region occur predominantly in water depths ranging from 10 to 40 m, have mean dimensions of 0.5 m deep (7.1 m maximum), 26 m wide (1375 m maximum) and are on the order of 5 to 10 km in length (Lewis and Blasco, 1990). Other offshore phenomenological studies have focused upon the eastern offshore region of Canada. Reported in Woodworth-Lynas and Barrie (1985); Hodgson *et al.* (1988); Woodworth-Lynas *et al.* (1991) and Lewis and Blasco (1990), scours present in this region are associated with icebergs. Typically, such scours are found in water depths less than 110 m, have mean dimensions of 1.3 m deep (5 m maximum) and 25 m wide (100 m maximum) (Lewis and Blasco, 1990).

In addition to offshore studies, field studies have also focused upon the excavation of relic scours present on land. Scour studies at King William Island, as described by Woodworth-Lynas *et al.* (1986), examined scours in poorly sorted sediments, whereas scour studies in the Lake Agassiz basin (Woodworth-Lynas and Guigne, 1991; Woodworth-Lynas 1992) examined relic ice keel scours preserved in a clayey and silty stratum. Excavation of the latter identified the existence of visible faults and slip planes beneath the scour mark. The deformation was attributed to bearing capacity failure beneath the scouring ice mass (Poorooshasb and Clark, 1990). The presence of deformation structures identified beneath the Lake Agassiz features have also been identified in other regions (Longva and Bakkejord,

1990). In addition to relic scour studies, small-scale field observations have also been used in the investigation of ice keel scour (Poorooshasb and Clark, 1990; Woodworth-Lynas, 1992). These investigations appear to confirm the potential for subscour soil deformations.

2.2 Experimental Studies of Ice Keel Scour

2.2.1 Small-scale Physical Modelling

Traditionally, small-scale physical models have played an integral role in the investigation of ice keel scour. The investigations range from ice soil interaction as addressed by Chari (1975), Green (1984) and Prasad (1985), to specific experimental programs aimed at defining subscour soil movements as reported by Poorooshasb *et al.* (1989) , Poorooshasb and Clark (1990) and Paulin (1992). In addition, industry sponsored programs as reported in Abdelnour *et al.* (1981), Abdelnour and Graham (1984), Dunwoody *et al.* (1984) and Been *et al.* (1990a), have also focused on questions associated with ice/soil interaction and possible failure mechanisms associated with the soil beneath the ice keel.

As one of the early pioneers in the investigation of ice keel scour, Chari (1975) used a small-scale physical model to investigate iceberg model/soil interaction. The model iceberg, made from aluminum, was idealised as a rectangular prismatic shape with dimensions 0.23 m (length) x 0.45 m (width) x 0.40 m (height). The experiment consisted of a series of scour events into a submerged sloping test-bed constructed of potters clay. Visual observations,

facilitated by a glass-sided flume tank, revealed the existence of failure surfaces propagating from the toe of the model, oriented 25-30° to the horizontal, as well as failure planes extending to the soil surface 0.5 m ahead of the model. Based upon the results, Chari (1975) attributed soil resistance to a combination of both passive soil deformation in front of the model and soil movement in front of and below the iceberg model.

Questions surrounding soil model interaction were also addressed by Green (1984). As part of the investigation into ice scour in sand, Green (1984) conducted a series of physical model tests in a sloping test-bed constructed of dry coarse masonry sand. Parameters examined included possible scale effects, the effect of attack angle and the zone of scour influence. The experiment was conducted in a large rectangular tank, with dimensions of 6 m (width) x 14 m (length) x 1 m (depth). The iceberg models consisted of rectangular prismatic shapes of varying size and shape. Green (1984) concluded that: (i) the primary resistance to scour for the horizontal ploughing action of an iceberg is the passive soil pressure developed on the front face on an iceberg, with the failure mechanism characterized by a series of successive failure planes; (ii) the frictional component of soil resistance on the sides and base for the scouring model iceberg in a frictional soil is insignificant compared to the total soil resistance; and (iii) the shape of the iceberg keel was determined to be an important factor affecting soil resistance during the scour process, with an inclination of the keel by 30° from vertical resulting in as much as a 35% increase in soil resistance.

In keeping with the recommendations of Green (1984), Prasad (1985) experimented with various ice keel model shapes in a cohesionless medium, measuring both the soil resistance and the pressures generated upon the face of the iceberg model as it encountered a sloping model seabed composed of dry sand. Prasad (1985) concluded that the soil resistance encountered was dependent on both the inclination of the model from vertical as well as the shape of the model in plan view.

In an effort to acquire insight into the phenomenon of ice scour, the Arctic Petroleum Operators Association (APOA) sponsored several small-scale physical modelling experiments. The first, reported by Abdelnour *et al.* (1981) and Abdelnour and Graham(1984), involved a series of dry scour events in sand, silt and clay. The objectives of these experiments included; (i) to gain insight into the effect of shape, soil medium, cut depth and forward velocity upon the horizontal force required for an ice mass to scour, (ii) measurement of the variation in pressure distribution measured on the front face of the model as well as in the surrounding soil in both horizontal and vertical directions relative to the model, and (iii) analysing the behaviour of the soil during the scouring process and the scour profile characteristics behind the ice mass relative to its shape and cut depth. The ice keel was idealised as either an inverted pyramid, or a rectangular prismatic shape. The results were presented as dimensional and non-dimensional semi-empirical relationships.

A second experimental program reported in Dunwoody (1984) into ice / berm interaction was also undertaken under the auspices of APOA. The objective of this experiment involved an analysis of the forces and possible uplift associated with the penetration of a soil berm by the leading edge of an ice sheet. Parameters examined included: the attack angle, the geometry of the soil berm, the buoyant specific weight of the soil, the internal angle of friction and the angle of friction between the soil and ice. The ice sheet was simulated using an aluminum model with a width of 0.50 m and an attack angle which ranged between 30° to 105 ° degrees to the horizontal. Springs attached to the model enabled stiffness to be examined. The soil berm was constructed of clean dry quartz sand, with a slope of 5:1. Dunwoody (1984) makes particular reference to the ability of the model to rise-up as it penetrates the soil berm, as well as the formation of failure planes in front of the model.

A series of ice keel scour experiments using the ice scour facility of the Faculty of Engineering, at Memorial University of Newfoundland, were undertaken in order to investigate ice/soil interaction as well as possible subscour soil deformations (Poorooshasb *et al.* 1989; Poorooshasb and Clark, 1990; Paulin, 1992). The potential for such displacements had been previously identified beneath relic scours such as those excavated in Lake Agassiz soils (Woodworth-Lynas and Guigne, 1990). The initial experiments involved small-scale modelling of ice scour in a submerged test-bed filled with a gravity-consolidated silt, using a model iceberg with a complex prismatic shape. The experimental program consisted of two scour events, with a scour incision depth of 0.04 m and 0.07 m

respectively. Distortion of soil laminations present beneath the scour mark confirmed the potential for subscour soil deformation.

Further insight into potential subscour soil deformation was acquired through an additional four ice scour experiments in a dry model test-bed constructed of dense and loose sand (Poorooshasb, 1989). In addition to potential subscour soil displacements, the effect of attack angle, model width and sand density on scour forces were also investigated. Solder strands were incorporated in the model test-bed in order to document sub-scour displacements. The attack angle was varied between 15° and 30° from the horizontal, with the model width being either 0.430 m or 0.860 m. A scour depth of 0.075 m was used. Based upon the results, Poorooshasb (1989) concluded that sand density appeared to have a considerable effect on soil deformations beneath a scouring indentor. It was observed that both the magnitude and extent of deformations decreased with increasing sand density.

Using the same ice scour facility as Green (1984), Prasad (1985) and Poorooshasb (1989), Paulin (1992) conducted four scour experiments in loose sand under dry and saturated conditions. As in previous efforts the experimental objectives involved measurement and analysis of subscour soil displacements, magnitude of scour forces as well as the stress response of the soil beneath the ice keel model. In addition the pore pressure response of the submerged soil beneath the scour was also examined. The ice keel was idealised as a rectangular prismatic shape with dimensions of 0.43 m (width) x 1.2 m (length) with an

attack angle of 15° to the horizontal. The model seabed was prepared loose using type O silica sand characterized by an internal angle of friction equal to 35°. The incision depth for all of the tests was approximately 0.04 m while the scour width was held constant at 0.430 m. Based upon the results, Paulin (1992) concluded that: (i) the vertical forces were of sufficient magnitude in some cases to cause general shear bearing capacity failure, and (ii) the successive failure surfaces observed during scour are believed to have been caused by passive earth pressure failure of the soil in front of the model.

Been *et al.* (1990a) reviewed the results of a series of small indentor tests conducted in both sand and clay soils. The objective of these experiments was to gain insight into soil deformations surrounding a scouring indentor. In terms of the indentor tests in sand, Been (1990) makes reference to (i) the absence of bearing capacity failure and passive failure planes below the indentor, and (ii) the presence of a static soil wedge. Been (1990) examined the observed subscour deformations in terms of (i) rupture surfaces due to passive or bearing capacity failure, or (ii) shear dragging beneath the ice keel. In response to a lack of experimental evidence to support the former, Been (1990) suggested that shear dragging was responsible. The scour mechanisms as envisioned by Been (1990) are presented in Figure 2.1.

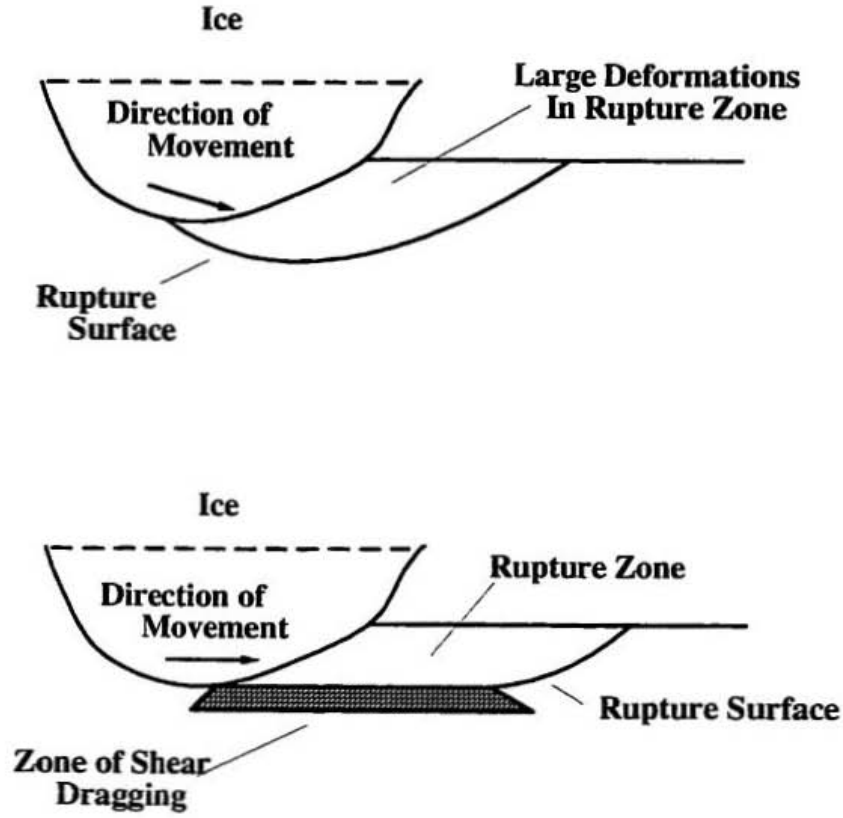

Figure 2.1 Diagram Showing Potential Soil Failure Mechanisms During Scour (Been, 1990)

2.2.2 Centrifuge Modelling of Ice Keel Scour

Centrifuge modelling has been used in the investigation of ice keel scour (e.g. Lach, 1996). The tests, conducted at a nominal acceleration of 100g using a 1/100 scale model, were designed to examine the effect of soil stress history, attack angle, keel width and model buoyant weight upon ice keel scour, including subscour soil deformations and pore pressure changes in the soil. The model ice keel was idealised as a rigid body with a defined attack angle and width. The experimental test-bed was formed from a consolidated kaolin clay slurry. Subscour soil deformations were documented using a combination of embedded lead trails, spaghetti markers and surface markers. Lach and Clark (1994) concluded that the centrifuge models were capable of replicating physical features observed in both modern and relic scours and provided a better understanding of the mechanics of ice scouring.

Centrifuge models also form a significant component of the PRISE program. The tests were conducted at a nominal acceleration of 150g using a 1/150 scale model. The tests were designed to examine the effect of soil type, attack angle, keel width and scour depth upon ice keel scour forces, as well as the magnitude and extent of subscour soil deformations and pore pressure changes in the soil. The seven centrifuge modelling tests involving ice keel scour in sand are the subject of this thesis.

2.3 Theoretical and Analytical Studies of Ice Keel Scour

Analytical studies have been carried out by various researchers in an endeavour to predict various aspects of ice scour. Initial efforts in this area involved either a force balance or work energy approach (FENCO, 1975; Chari, 1975). Later efforts were associated with the use of plasticity theory (e.g. Been *et al.*, 1990b).

The dynamic force-balance model of FENCO (1975) solved the differential equations of motion describing the interaction of a block-shaped body encountering a sloping seabed. The vertical soil reaction can be analysed using either plastic or elastic theory, the former assuming that the soil reaction is the product of the bearing capacity and effective area beneath the base of the iceberg while the later involves an estimate of the soil's spring constant. The horizontal soil resistance is determined based on the assumption that the soil passive pressure is fully mobilized, and is calculated using a trial wedge solution with a plane failure surface. The surcharge is assumed to contribute to the overall passive resistance, but is considered to have no shear resistance. FENCO (1975) also proposed a simple energy balance model to describe the interaction of an iceberg undergoing horizontal translation into a sloping seabed. The passive soil resistance is assumed to be fully mobilized and is given by Coulomb's earth pressure theory. The surcharge is assumed to contribute to the passive resistance, but is considered to have no strength as it is remoulded. The FENCO model considers a shear force equal to the active lateral earth pressure multiplied by the soil / ice

friction coefficient to act on the sides of the iceberg.

The work energy model of Chari (1975) equates a driving force, idealised as the momentum possessed by the iceberg as it encounters the seafloor sediment, against the work done as the soil is displaced. Using this model, theoretical iceberg scour lengths and depths can be calculated for an assortment of physical criteria. It is noted that while Chari's model initially ignored the effect of both current and wind, it was subsequently modified to take into consideration the positive effect of current drag (Chari and Muthukrisknaiah,1978), the effects of side friction, (Chari and Green, 1981), as well as the effect of nonlinear velocity experienced by the iceberg during a scouring event (Prasad, 1985).

Been *et al.* (1990b) presented an incremental force and work balance model which was based on plasticity theory to predict an ice scour event associated with a pressure ridge ice keel. Considerations included uplift of the ice keel, flexural stiffness of the pressure ridge in relation to the ice sheet, environmental forces acting upon the ice keel, ice / soil friction and surcharge. Soil resistance was calculated based on passive resistance, determined by the method of stress characteristics of Sokolovski, (Been *et al.*, 1990b). The characteristics method of Sokolovski was modified to take into consideration the formation of soil dead wedges in the failure zone. The results of this model were in agreement with an observed Beaufort Sea scour, including uplift over an extended distance.

As outlined by Palmer *et al.* (1990), the question of ice / soil / pipeline interaction can be examined in terms of deformation features, specifically in terms of possible zones of deformation. As illustrated in Figure 2.2, Palmer (1990) hypothesized three distinct zones of deformation. These zones are characterized as: Zone 1 - a zone of large deformation in which the soil is ploughed, entrained into the frontal spoil mound and eventually deposited laterally forming the side berms; Zone 2 - a zone of large deformation in which the soil deforms plastically and is located beneath the ice keel, and Zone 3 - a zone characterized by small elastic deformation but which is subject to scour-induced stresses.

A pipeline located in Zone 1 will be subjected to scour loads of sufficient magnitude as to cause failure whereas a pipeline located in Zone 3 will be safe from scouring action, (Palmer *et al.*, 1990). However, a pipeline located in Zone 3 may be uneconomic due to its depth of burial. The alternative is to located the pipeline in Zone 2. Although conceptual, it is believed that a pipeline located in Zone 2 would be subject to scour loads as well as the effect of soil displacement. The combination of scour loads and soil displacement may be of sufficient magnitude to damage a pipeline in this zone. In order to design a pipeline for such loading conditions it is important to determine the magnitude and extent of large soil deformations in the region designated as Zone 2.

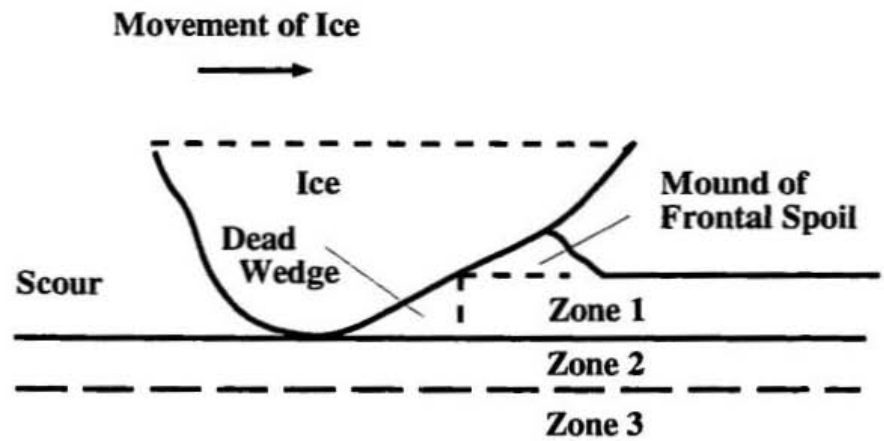

Figure 2.2 **Diagram Showing Zones of Ice Scour Deformation (Palmer, 1990)**

2.4 Closing Remarks

The varied nature of the analytical, experimental and phenomenological research into ice keel scour is testimony to the significance given to ice keel scour in terms of offshore development. Understanding of possible scour mechanisms is impeded by difficulties in observing and documenting actual ice scour events. However, physical and mathematical modelling have been successful in expanding the level of understanding in regard to the process of ice keel scour and have been instrumental in identifying additional concerns, the potential for subscour soil deformation being prominent. The results obtained from research into ice scour, or ice / soil interaction would suggest that soil failure in front of the advancing ice keel can be attributed mainly to passive earth pressure failure. However, there is little consensus as to the nature of potential subscour soil deformations. Current understanding has attributed this to either shear dragging beneath the ice keel, or bearing capacity failure, or a combination of both. In the absence of understanding of the deformation process, the ability to predict loading conditions is also the subject of uncertainty.

Chapter Three

Experimental Scope and Objectives

In reference to the preceding chapter, it is evident that the uncertainty associated with an absence of understanding as to the nature of the deformation process as well as the nature of the imposed loading are impediments to the safe and economical engineering of offshore pipelines in regions prone to ice keel scour. Small-scale physical modelling of scour conducted in normal (1g) gravity conditions as discussed in Chari (1979); Green (1984); Prasad (1985); Poorooshasb (1989); and Paulin (1992), has offered some insight into the mechanics governing ice scour. However, the results of these modelling exercises vary, in part due to the idealization of field conditions in terms of the model ice keel geometry, the degrees of freedom allowed in the model, the soil type and state. The rationale behind the current research stems in part from these uncertainties.

3.1 Experimental Scope and Rationale

Although the incentive behind the current research stems from uncertainties associated with the nature of subscour deformation and loading conditions, the rationale behind the current research takes into consideration aspects of ice scour such as; the extrapolation of

results obtained from small-scale physical modelling to full-scale ice scour events, the nature of the driving forces behind a scour event, as well as possible questions associated with the geometry and structural integrity of the ice keel.

Uncertainties associated with the extrapolation of results obtained from small-scale physical modelling to full-scale ice scour events highlights the important role that effective stress and stress history of the soil has in regard to soil behaviour. Such uncertainties can be avoided using centrifuge modelling because it is possible to replicate both the effective stress as well as the stress history of a soil. It has also been established that the centrifuge is capable of replicating various physical features observed in both modern and relic scours (Woodworth-Lynas *et al.* 1995).

In reference to the present centrifuge tests involving ice scour in sand, the parameters under consideration include: soil state, attack angle, scour depth and scour width. The soil state includes both loose and medium dense sand, thus enabling the effects of density upon subscour deformation to be investigated. In order to examine the effect of model keel geometry upon the measured forces and subscour soil deformation, the attack angle of the model ice keels was set at 15° and 30° and the scour width was either 15 or 30 m. Finally, the scour depth was varied from 1 to 2 m in order to examine the effect of scour depth on the scour loads. The ice keel was idealised as a rigid body possessing sufficient strength to withstand the forces developed during scouring. The modelling apparatus used in the current

test series restricted the keel to a single degree of freedom representation in which the model ice keel was constrained to translate horizontally at a constant velocity through a horizontal testbed at a fixed scour depth. This approach assumed that the forces driving a scouring ice mass are sufficient to ensure a continuous forward motion. The approach models steady state ice scour, during which there are no other translational or rotational keel movements. This is a reasonable assumption because offshore field data show scour marks characteristically maintain constant dimensions over long distances.

3.2 Experimental Objectives

In terms of the centrifuge modelling component of PRISE the established experimental objectives included;

(i) modelling up to 20 scour events using clay, sand and layered sand / clay media,

(ii) describing and quantifying the general cases for each soil type and to highlight the similarities and differences in the responses of the different soils to the same ice keel loads,

(iii) and the verification of the physical model results against field data from modern and relic scour marks.

In this thesis emphasis is placed on describing and quantifying the nature of ice keel scour in sand.

Chapter Four

Centrifuge Modelling

In modelling geotechnical phenomena, it is known that soil behaviour is governed both by the applied effective stress as well as the effective stress history of the soil. It is for this reason that the results of small-scale physical modelling exercises under normal gravitational conditions cannot be easily applied to large scale prototype conditions. The degree of uncertainty present with small-scale physical modelling can be avoided using a centrifuge since it permits stress similarity between the model and the prototype. Moreover, if the external loads are scaled such that the resulting stresses in the prototype and model are similar, the reaction of the model to the external loading will be similar to the prototype behaviour (Poorooshasb, 1990). Centrifuge technology is considered a proven and effective tool when modelling gravity-dependent phenomena (Schofield, 1980).

4.1 Theory of Centrifuge Modelling

Centrifuge modelling utilizes the radial acceleration experienced by an object rotated around a central axis. The increased radial acceleration is equal to $r\omega^2$, where ω is the angular velocity of rotation expressed in radians per second and r is the distance between the

object and its axis of rotation. The increase in radial acceleration (Ng) experienced by an object at the end of a rotating arm is determined using;

$$Ng = r\,\omega^2 \qquad \textbf{[4-1]}$$

where 'g' is equivalent to earth's gravitational acceleration.

As shown in Figure 4.1, the rationale behind centrifuge modelling can be illustrated clearly in terms of the effective vertical confining stress (σ_v'), expressed as;

$$\sigma_v' = \rho\, g\, h \qquad \textbf{[4-2]}$$

where ρ represents mass density, g represents earth's gravitational acceleration and h is the prototype height. A model which is geometrically inversely proportional to the prototype by a scale factor (n) will have a height of (h/n). The effective vertical confining stress in the model with the same mass density as the prototype is 1/n than that experienced by the prototype. In order to maintain similarity of stresses, it is apparent that either the material density or the gravitational acceleration must be increased in order to compensate for the reduction in stress level in the model. Since large variations in density are unrealistic, the gravitational component 'g' must therefore be increased N times, where N = n. This relationship is shown in equation 4-3.

$$\sigma_v' = \rho\, N\, g\, h\, (1/n) \qquad \textbf{[4-3]}$$

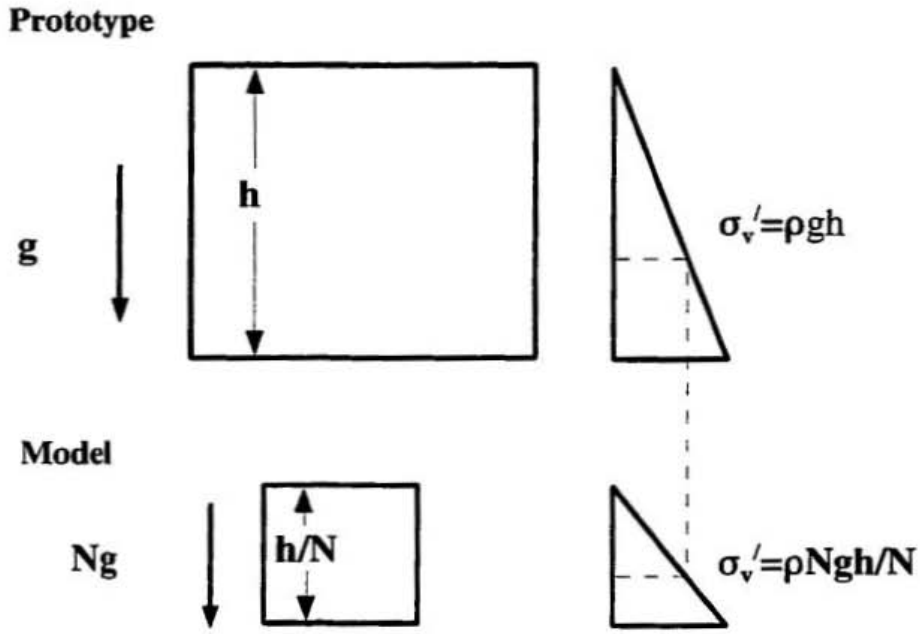

Figure 4.1 **Diagram Showing Theory of Centrifuge Modelling In Terms of the Effective Confining Stress (σ'_v)**

The relationship shown in Equation [4-3] implies that the acceleration field experienced by the model must be N times the acceleration field present in the prototype. An alternative expression to Equation [4-3] is given in equation [4-4],

$$a_m = N\, a_p \qquad \textbf{[4-4]}$$

where "a" is defined as the gravitation acceleration and the subscripts "m" and "p" are used in reference to the model and prototype respectively.

4.2 Centrifuge Scaling Relationships

The manner in which centrifuge scaling laws are derived is illustrated with respect to force (F). Using the inverse relationship between model and prototype length as a starting point, the volume (V) occupied by the model (V_m) in relation to the volume of the prototype (V_p) is given as;

$$V_m = \frac{1}{N^3}\, V_p. \qquad \textbf{[4-5]}$$

Since mass is a function of an object's volume and mass density and the mass density is assumed to remain constant, the model mass is therefore inversely related to the prototype mass, expressed in equation [4-6] as;

$$m_m = \frac{1}{N^3} m_p. \qquad \textbf{[4-6]}$$

Combining equations [4-4] and [4-6], the scaling relationship for F_p (prototype) and F_m (model) is given as;

$$F_m = m_m a_m = \left(\frac{1}{N^3} \right) m_p \; N \; a_p. \qquad \textbf{[4-7]}$$

The simplified version of Equation [4-7] is;

$$F_m = \left(\frac{1}{N^2} \right) F_p \qquad \textbf{[4-8]}$$

The prototype force is therefore equivalent to the increased acceleration (N) experienced by the model squared, multiplied by the measured model force.

Other common centrifuge scaling relationships include;

area,

$$A_m = 1/N^2 \; A_p, \qquad \textbf{[4-9]}$$

strain,

$$\epsilon_m = \epsilon_p, \qquad \textbf{[4-10]}$$

and unit weight,

$$\gamma_m = N \gamma_p \qquad [4\text{-}11]$$

The implications of the preceding discussion in reference to the modelling of ice scour is relatively simple. In terms of geometrical considerations the corresponding dimension of the model is essentially the increase in acceleration, N, multiplied by the given dimension. A model ice keel with a width of 0.1 m at an acceleration of 150g would be equivalent to 15 m at equivalent prototype scale. A model with a width of 0.2 m at an acceleration of 75g would also be equal to 15 m at equivalent prototype scale.

4.3 Lateral Acceleration

A feature of centrifuge modelling which must be taken into consideration is the presence of a lateral force, commonly referred to as 'lateral g'. It is a geometrical consideration arising from a change in radial distance from the model to the centre of axis of rotation. In reference to the model package used in modelling ice scour, the effect of lateral g is illustrated in Figure 4.2.

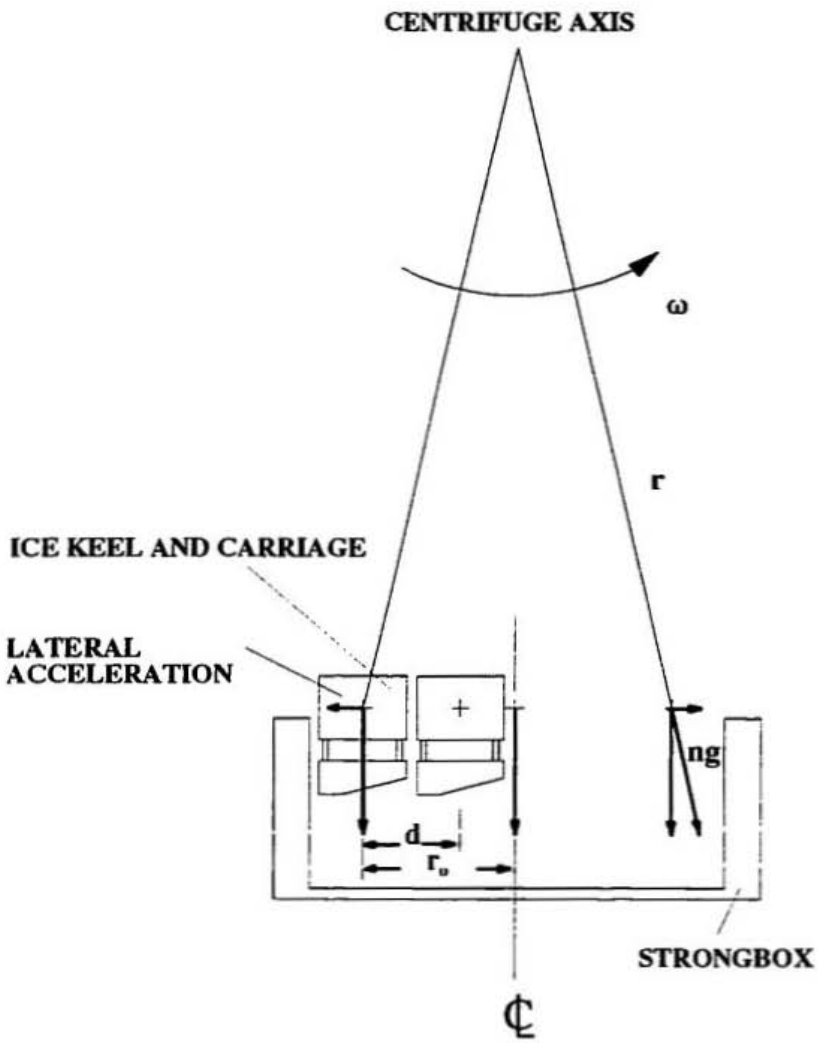

Figure 4.2 **Schematic Diagram Showing Theory of Lateral Acceleration**

The geometry of the model test package in reference to the axis of rotation imposes a radial component of acceleration upon the model ice keel as it is pulled across the model testbed. The measured horizontal force is therefore a measure of the soil resistance plus the lateral component of acceleration. The magnitude of radial acceleration varies with the distance between the centerline of the strongbox and the centre of mass of the model carriage assembly. The magnitude of the radial force is given by the following expression:

$$F_r = M_c |r_0 - d| \omega^2 \qquad \textbf{[4-12]}$$

where r_0 is the initial distance from the carriage centroid to the centerline of the strongbox. d is the displacement of the keel, M_c is the total mass of the model carriage assembly and ω is the angular velocity of the centrifuge in radians per second (C-CORE, 1995a).

4.4 Modelling of Models

A technique known as "modelling of models" can be used to verify results obtained from a centrifuge modelling program. Prototype behaviour is predicted from the results of two or more tests conducted at different scales. If the observed results are repeatable using different scale models, the results are considered representative of the behaviour present in the prototype. As an example of modelling of models, the current centrifuge tests involving ice scour utilized two scales: 1/75 and 1/150.

4.5 Closing Remarks

Due to the efforts of many researchers, centrifuge modelling has become a proven and accepted tool in the investigation of gravity dependent phenomenon. It is used both in confirmation of theoretical solutions and in the calibration of numerical and constitutive models. The versatility of centrifuge modelling is emphasized by the variety of applications that have been undertaken. These include soil dynamics (Craig *et al.*, 1988), earthquake modelling (Pilgrim and Zeng, 1994), cold regions studies (Smith, 1991), contaminant transport and flow problems (Mitchell and Stratton, 1994), ice mechanics (Lovell and Schofield, 1986), hydrodynamics (Zelikson, 1995; Poorooshasb, 1990), shallow and deep foundations (Kutter *et al.*, 1984) and structural geology (Dixon, 1988; Peltzer and Garnier, 1988). Centrifuge modelling has also been used in the investigation of ice keel scour (Lach and Clark, 1994; Lach,1996).

Chapter Five

Experimental Facilities and Equipment

5.1 C-CORE Centrifuge Facility

5.1.1 Acutronic 680-2 Geotechnical Centrifuge

Described in detail by Phillips *et al.* (1994), C-CORE's centrifuge facility is located on the St. John's campus of Memorial University of Newfoundland. The facility comprises a circular containment chamber housing an Acutronic 680-2 geotechnical centrifuge and an adjacent two-story building containing offices, laboratories, mechanical and electrical workshops.

The Acutronic 680-2 geotechnical centrifuge, illustrated in Figures 5.1 and 5.2, is a beam centrifuge with a radius of 5.5 m from its axis of rotation to the working base of a pivoting platform. Features of the Acutronic 680-2 geotechnical centrifuge include two parallel steel tubes, a swinging platform, an adjustable 20.2 tonne counterweight and a central drive box. Power is provided by an AC variable speed motor, with power consumption mainly due to aerodynamic drag within the centrifuge chamber.

The Acutronic 680-2 Geotechnical Centrifuge has a maximum rotational speed of 189 rpm, corresponding to a centripetal acceleration approximately equivalent to 200 gravities at a radius of 5 m. The payload, which is contained within an aerodynamic shroud to reduce drag, is limited dimensionally to 1.1 m by 1.4 m in plan and 1.1 m in height. The payload capacity of the Acutronic 680-2 Centrifuge varies from 2.2 tonnes at an acceleration of 100 gravities to 0.65 tonnes at an acceleration of 200 gravities, the reduction in payload capacity due to the increased self-weight of the platform.

5.1.2 Ancillary Equipment

Centrifuge models are contained within a rectangular or circular vessel referred to as a 'strongbox' or 'tub'. The purpose of this vessel is to contain the model testbed and to provide a base for securing ancillary experimental equipment. The rectangular strongbox used in modelling ice keel scour has internal dimensions of 1.18 m (length) x 0.94 m (width) x 0.4 m (height). At an acceleration of 150 gravities, the prototype model testbed has an equivalent plan area of 141 m x 177 m. The rectangular strongbox weighs approximately 3.15 kN empty. Channels are machined into the base of the strongbox. These channels form part of a system used to maintain a constant water level during the course of a centrifuge test and to permit drainage once the test has been completed.

As illustrated in Figure 5.3, the strongbox also serves as a pad for securing actuator units,

cone penetrometer apparatus, as well as data acquisition apparatus including signal conditioning boxes and signal leads, cameras and power cables. The cone penetration test is used to obtain a measure of soil strength during the centrifuge test. The cone consists of a hollow steel shaft 11 mm in diameter, the point of which has an angle of 60° and a cross-sectional area of 100 mm^2.

5.2 Experimental (Model) Testbed

5.2.1 Experimental Testbed Soil

Each experimental model testbed was fabricated using approximately 0.2 m^3 of clean dry silica sand (Type F110) supplied by U.S. Silica. The model testbed was prepared by pluviating the sand from an overhead hopper. The relative density of the model testbed was controlled by varying the elevation of the hopper as well as the mass rate at which the sand was placed. The properties of the sand used in constructing the model testbed are presented in Table 5.1. The grain size analysis is presented in Figure 5.4. The internal angle of friction of the sand was determined, from both triaxial extension and compression tests on loose and medium dense samples, to be on the order of 36.5° (C-CORE ,1995e).

Figure 5.1 **The 680-2 Acutronic Geotechnical Centrifuge At Rest**

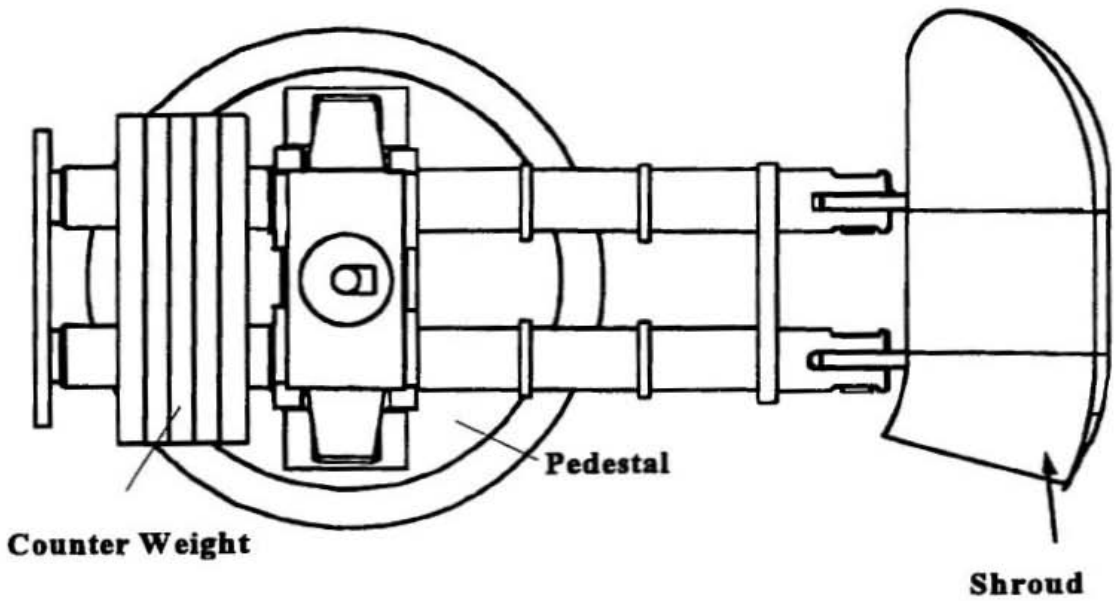

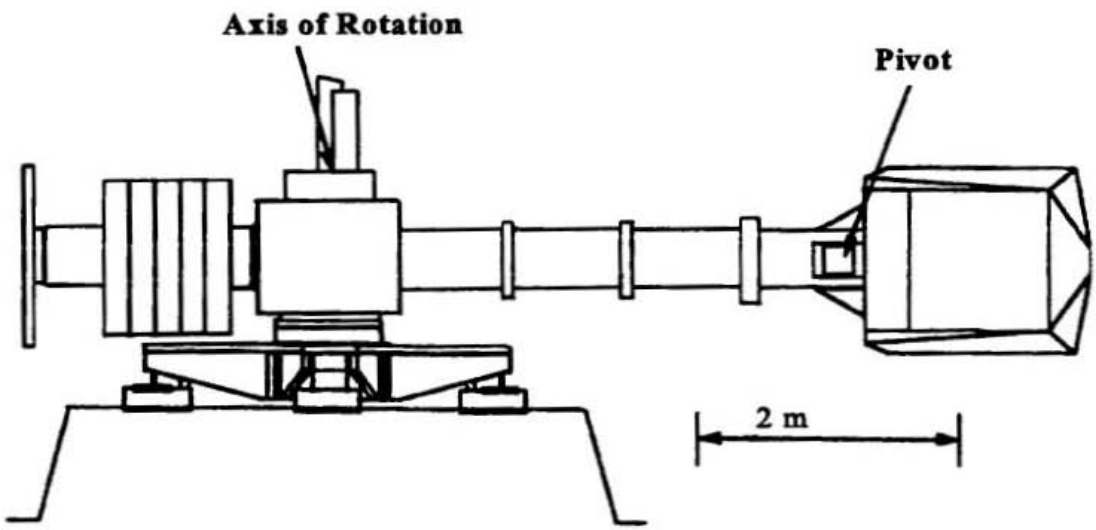

Figure 5.2 **Schematic of the 680-2 Acutronic Geotechnical Centrifuge**

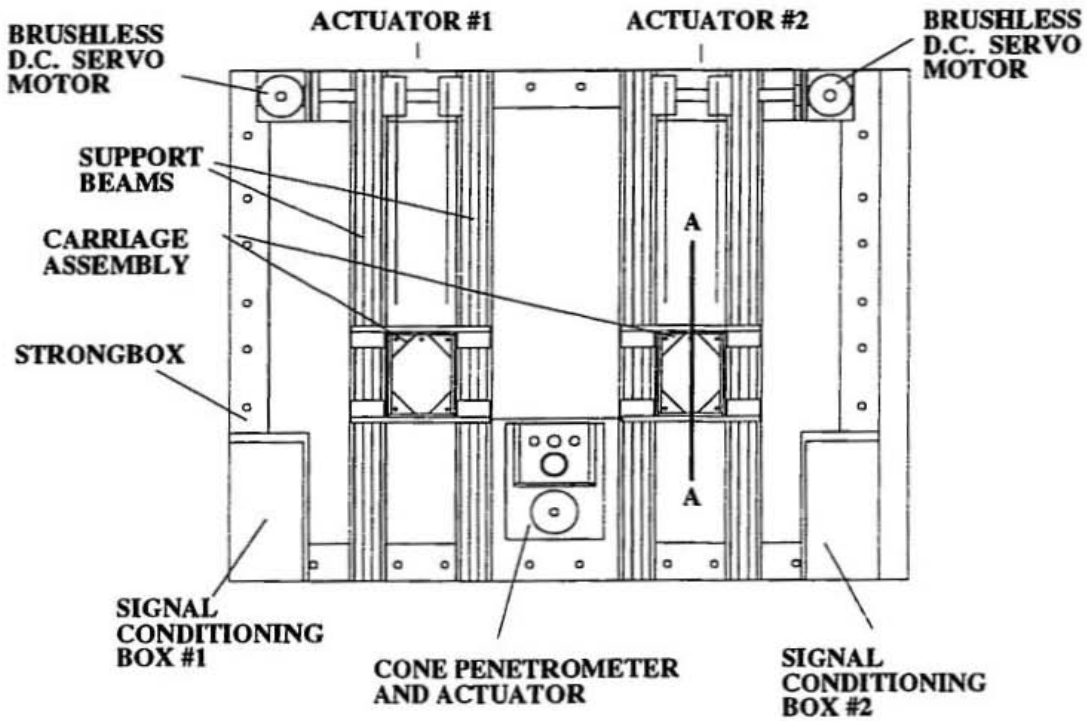

Figure 5.3 **Schematic of the Model Test Package Used in Centrifuge Modelling of Ice Keel Scour - Plan View**

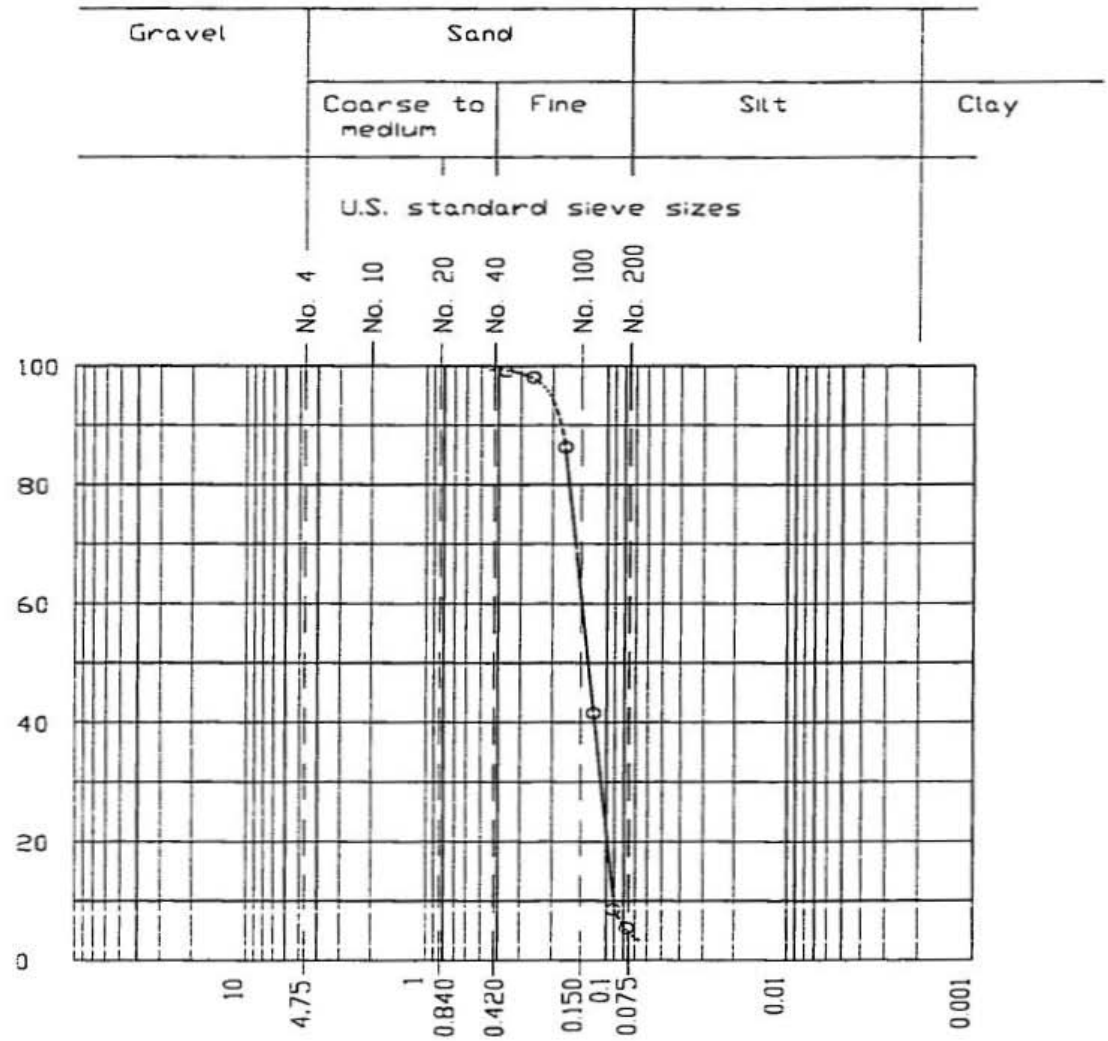

Figure 5.4 **Grain Size Analysis of the Sand Used in the Experimental Program**

Table 5.1 **Sand Properties**

Maximum Dry Density (γ_{dmax})	1.684 g/cm^3
Minimum Dry Density (γ_{dmin})	1.409 g/cm^3
Specific gravity (G_s)	2.66
Effective Grain Size (d_{10})	0.095 mm
Mean Grain Size (d_{50})	0.13 mm
Uniformity Coefficient (C_u)	1.47
Internal Angle of Friction (ϕ')	36.5°

5.2.2 Experimental Testbed Instrumentation

In order to investigate the pore pressure response beneath the model ice keel, miniature pore water pressure transducers (PPT's) and Lebow 4531-150 subminiature pressure transducers (TLC's) were embedded in the model test bed. The Druck model PDCR 81 pore pressure transducers (PPT's) have a working range of 0 to approximately 0.7 MPa. They measure the differential pressure between the atmospheric pressure and a fluid pressure. (Köenig *et al.*, 1994). Each transducer was fitted with a sintered bronze stone which permitted the fluid pressure to act upon the diaphragm, yet resisted the effective stress of the sand. At least two pore water pressure transducers (PPT's) were buried beneath each scour event. The Lebow 4531-150 subminiature pressure transducers have a working range of 0 to 3.5 MPa. These transducers were used in order to provide a measure of total vertical stress beneath the scouring keel. Due to a difference in stiffness between the instrument and the soil medium, the interpretation of data associated with these transducers was subject to

possible errors. For example, the difference in stiffness will cause the transducer to overestimate (stress concentration) or underestimate (arching effect) the actual stresses present in the soil medium. Passive markers in the form of dyed sand layers and coloured spaghetti strands were also placed in the model testbed. The coloured sand was obtained by mixing the model test sand material with a commercially available machinist layout dye, in liquid form. The mixture was then air dried and sieved. The spaghetti strands were also dyed using an aerosol form of machinist layout dye.

5.3 Model Test Package

The model test package was designed to investigate various parameters including; the effect of scour width, scour depth and attack angle upon the scour process. A means of adjusting the elevation of the model keels was used to vary the incision depth of the scour. The single degree of freedom criterion imposed upon the model ice keel was an important feature of the modelling exercise. The model ice keel was constrained to translate horizontally at a fixed scour depth.

5.3.1 Model Ice Keels

The model ice keels were constructed from aluminum plate welded together and precision machined to the required dimensions. Both the attack face and the base of the model ice keels were knurled in order to ensure that the friction developed at the interface between the

model keel and the sand was comparable with the angle of internal friction for the sand.

5.3.2 Actuator Units

The assembled test package had provision for two scour events to be conducted per centrifuge flight. The actuator units, designated DRIVE #1 and DRIVE #2 were designed such that they provided the required horizontal force necessary to create the scour, as well as the vertical reaction force to uplift. Design criteria considered these forces to be on the order of 5 kN and 4 kN respectively (Cunnard, 1993). Each drive unit utilized a brushless D.C. servo motor connected to a drive shaft and spool assembly, which was in turn connected to the model keel through steel cables. Rotation of the drive shaft served to advance the model keel across the testbed at a predetermined velocity of 0.1 m/s. The carriage holding the model keel, as illustrated in Figure 5.5 was constrained to move along the guide rails. The speed of the servo motor controller was controlled by a preset analog control voltage. A scour event was initiated through a switch in the control room which triggered a series of relays on the centrifuge which in turn energized the servo system. The displacement of the model keel was measured using a Celesco PT101-0050-111-1110 position transducer (SP).

5.3.3 Model Keel Instrumentation

Shown in Figure 5.5, the model keels were instrumented to measure total vertical load, total horizontal load and contact pressure between the soil and the model ice keel. The notation LC, TC and PT represent load cell, tension cell and pressure transducer, respectively. Each model keel was attached to the carriage assembly and actuator via three 2.2 kN Sensotec Model 31/1432-08 tension/compression load cells (LC), one at each corner of the rear of the keel and one centred in front of the model ice keel. These load cells have a working range of 0-2.2 kN. Summation of the three load cell outputs provided a measurement of the net vertical force. Horizontal loads were measured using a tension load cell (TC) attached to the leading face of the model ice keel. Tow cables attached to the load cell provided the required force to move the model keel across the testbed. The tension load cell (TC) recorded the tension force present within each cable. Summation of the forces present within each cable provided a measurement of the net horizontal force. In order to compensate for the radial component of acceleration, ie. 'lateral g', the measured horizontal force was manipulated as outlined in Section 4.3. The pressures present on both the base and leading face of each model ice keel were measured using a flush-mount pressure transducer (PT) or face pressure cell. These pressure transducers (Sensotec Model S/1542-07) have a working range of 0 to 3.45 MPa gauge.

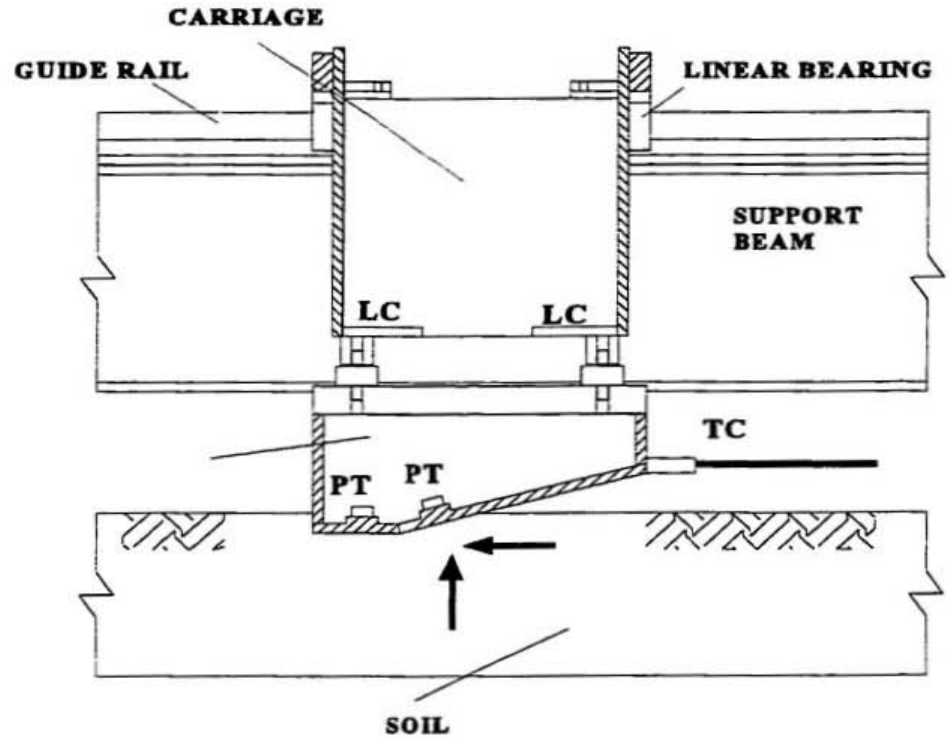

SECTION A-A

Figure 5.5 A Schematic Diagram of The Model Package Used In Centrifuge Modelling of Ice Keel Scour - Profile View.

5.4 Data Acquisition System

The data acquisition system consisted of; (i) a signal conditioning (S/C) sub-system mounted on the test package, (ii) a slipring arrangement, (iii) a filter chassis, (iv) a 64-channel multiplexer, (v) an analogic HSDAS-16 (16 bit A/D converter), (vi) a ± 15 Volt lambda power supply and (vii) a 486 DX-40 PC compatible computer running SnapMaster for Windows. Each signal conditioning box contained dual channel printed circuit cards, mounted in a 12 card chassis. Each channel had a selectable gain and excitation voltage for the attached instrumentation. The filter chassis was a 48-channel unit, with a selectable cut-off frequency between 1 to 500 Hz. The cut-off frequency used during centrifuge tests involving ice keel scour was 19.72 Hz. Amplified analogue signals from the various transducers after passing through the signal sliprings were filtered. The signals then entered the 64-channel multiplexer / ANALOGIC HSDAS-16 (16 bit A/D converter) where they were digitized and stored. A thinwire Ethernet enabled the instrument response to be displayed in the Centrifuge Control Room during the test.

5.5 Laser Profile System

The laser profiling system used to profile the post-scour features of the experimental testbed consisted of a Keyence Model LB-70 Controller, a Keyence LB-11 Sensor head and a Celesco PT101-0050-111-1110 string potentiometer. The LB series Keyence laser

displacement sensor is classified as a Class IIIb laser product. It has a measurement range of ±40 mm. The horizontal position is defined by a string potentiometer. Using a mobile PC computer system operating SNAP-MASTER data acquisition package, time, displacement and vertical displacement data were acquired.

5.6 Miscellaneous Equipment

In addition to the above equipment, other pieces of equipment were used during this experimental research program. These included a sand hopper, a vacuum system, density cups and a portable water reservoir. Placement of the sand through pluviation was accomplished using an overhead cylindrical hopper. The hopper was hoisted using a chain hoist attached to a mobile gantry. As part of the density control, density cups with a volume of 100 cm^3 were used. These containers were placed at various locations in the model testbed during preparation. Once filled, they were levelled, removed and weighed. A density determination based upon the weight and the volume was then made. Levelling of the individual sand layers was accomplished using a vacuum system, consisting of a wide nozzle, a clamping device, a guide rail assembly and a commercially available wet/dry vacuum system. The vacuum nozzle was set at the desired elevation. Since control on the order of ±1 millimetres was necessary, several passes were made across the model testbed, each pass lower until the required testbed elevation was obtained.

Chapter Six

Experimental Procedure

Model preparation comprises a major component of the experimental procedure. It involved the careful preparation of the model testbed. Model preparation was labour intensive, with test preparation requiring as much as several weeks. The centrifuge test involved acceleration of the model testbed to a predetermined level, a brief period during which the instruments were allowed to stabilize, followed by the scour event. A typical centrifuge test of ice keel scour in sand required approximately two hours from start to completion. Post-test excavation and data reduction was also labour intensive, and was undertaken over a period of several weeks.

6.1 Preparation of Model Testbed

Each model testbed was constructed in a rectangular strongbox described and illustrated in Section 5.1.1 and Figure 5.3 respectively. In order to prevent the ingress of sand into drainage channels, the base of the strongbox was covered with a layer of geotextile fabric. A dense, 130 mm-thick layer of coarse quartz sand (d_{10}=0.325 mm) served as a foundation for the model testbed. It was used to reduce the quantity of fine silica sand used in

constructing the model testbed. The model test package was designed such that the actuators were secured to the top of the strongbox.

As illustrated in Figure 6.1, the model testbed was constructed in a series of layers, (thick at the base and thin at the top). Each layer was placed by pluviating dry quartz sand from an overhead hopper. The relative density of the model testbed was controlled by varying the mass flow rate of the sand. Model tests described as loose or with a low relative density were formed using a low mass flow rate with an elevation drop of about 0.02 m. Medium dense model testbeds were constructed using an elevation drop of 0.3 to 0.5 m with a higher flow rate. Verification of the relative density of the model testbed was achieved using density cups. The individual sand layers were levelled using a vacuum system, and a thin layer of dyed sand spread evenly over the surface. The procedure was repeated until the model testbed reached an elevation of +300 mm above the base of the strongbox, or -100 mm from the top of strongbox. The model testbed had a nominal thickness of 170 mm.

Miniature pore pressure transducers (PPT's) and total stress cells (TLC's) embedded in the model testbed were incorporated into the model during the assembly process. Electrical leads from the transducers were secured to the side of the strongbox in order to prevent possible displacement of the transducer during model preparation. Horizontal spaghetti strands oriented perpendicular to the scour mark were also placed during the assembly process. With the completion of the final sand layer, vertical spaghetti strands along the

centerline of the scour, as well as perpendicular to the scour, were placed with the aid of a plexi-glass template.

Saturation of the model testbed with water while under vacuum enabled a high degree of saturation to be achieved. The saturation process involved placing the model testbed in a reduced atmosphere, using a 20 mm thick steel plate (vacuum plate) bolted to the top of the strongbox. A seal between the strongbox and the plate was formed using silicon sealant. A closed system between the strongbox and the water reservoir was then established as illustrated in Figure 6.2. This combined system was then connected to a vacuum line and a vacuum of approximately 70 kPa applied. Ordinary tap water was siphoned into the reservoir container where it was allowed to equalize over a period of several hours. The reduced atmosphere served to de-aerate the water. An arrangement of valves, designated A through E in Figure 6.2 enabled the strongbox containing the model testbed to be isolated, while the water reservoir was being filled. Saturation of the model testbed commenced when a valve connecting the reservoir to the strongbox (ie. valve D in Figure 6.2), and valves B and E, were opened, allowing water to flow under the influence of gravity from the reservoir to the base of the model testbed. Model saturation occurred at a rate of approximately 5 litres per hour. The flow rate was governed by the need to prevent fluidization of the model testbed during saturation. It was controlled by varying the height of the water reservoir relative to the height of the strongbox. Once the surface of the model testbed was submerged, the reduced atmosphere in the strongbox was slowly relieved to atmospheric

pressure. The vacuum plate was removed and the strongbox cleaned in preparation for the installation of the actuator units and other apparatus.

6.2 Ice Keel Model Preparation

Preparation of the ice keel model commenced with the installation of face pressure transducers in the base and attack face of the model ice keel. Each transducer was sealed with an 'O' ring. The model ice keel was attached to the carriage of the drive assembly via three 2.2 kN tension/compression load cells. The horizontal load cell was attached to the leading face of the model ice keel. The carriage height was adjusted vertically as required by the desired scour depth (to within ± 1 mm).

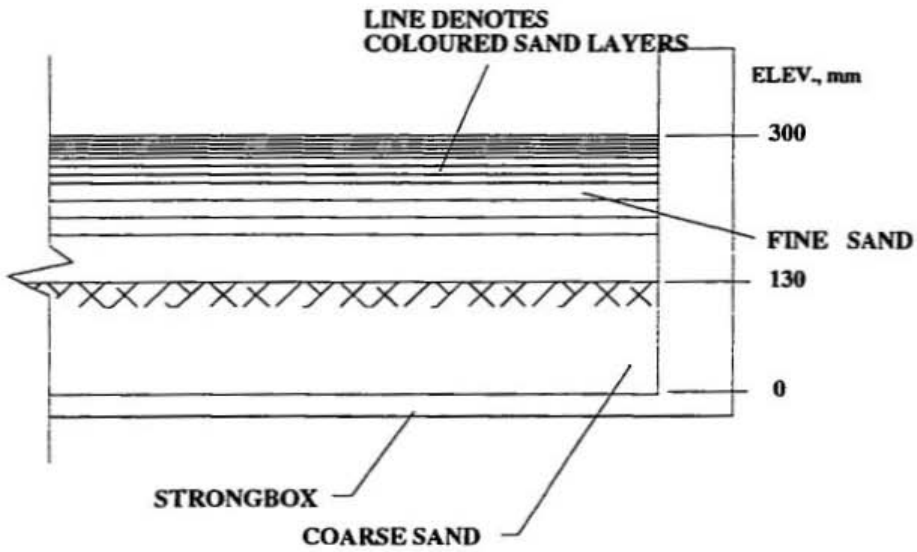

Figure 6.1 **A Cross Section of a Model Testbed Showing The Elevation Of The Coloured Sand Layers**

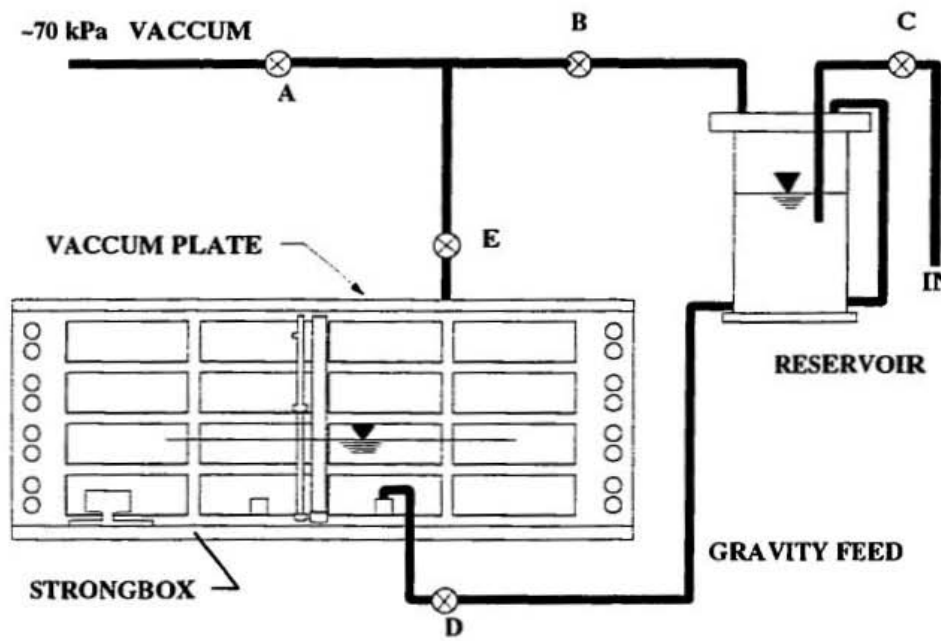

Figure 6.2 **A Schematic Diagram Showing Apparatus Used In The Saturation Of The Model Testbed With Water**

6.3 Model Assembly

Assembly of the model test package involved securing the actuator units to the strongbox, along with the cone penetrometer assembly as well as other apparatus, including camera mounts, signal conditioning (S/C) plates and boxes. The leads from the transducers were connected to the appropriate signal conditioning (S/C) box.

6.4 Centrifuge Testing of Ice Scour Models

Prior to the centrifuge test, components of the experimental package were checked in order to verify operation. Upon the successful completion of these checks, the steel cables to the individual keels were secured to the horizontal load cell located on the leading face of the ice keel model. Initially at rest, the centrifuge was accelerated in stages to either 114.3 rpm (75g test) or 161.3 rpm (150g test). The acceleration is defined at the base of the model keel, with the radius equivalent to the distance between the base of the model keel and the axis of rotation. For a 150g test, this distance was approximately 5.137 m. Knowing the required acceleration (**Ng**) and the distance from the axis of rotation to the base of the model keel (r), the rotational speed of the centrifuge was determined in terms of radians per second (ω) according to the following equation.

$$\omega = \left(\frac{Ng}{r} \right)^{\frac{1}{2}} \qquad \textbf{[6-1]}$$

Upon completion of the experiment, the centrifuge was decelerated in stages. During this time, the excess surface water was allowed to drain into the centrifuge chamber through the solenoid valve located at the base of the strongbox. The centrifuge was then stopped and data acquisition system halted. Steps outlined in Section 6.3 were undertaken in reverse order. Following inspection and photographs of the model testbed, the model test package was removed from the centrifuge chamber to a secure area for post-test excavation and analysis.

6.5 Data Acquisition

As indicated previously, the Windows-based PC SNAP-MASTER program was used to control data acquisition. The program was run from the centrifuge control room. Data acquisition was subdivided into the following specific tasks; pretest monitoring, swing-up, scour event #1, cone penetration test, scour test #2 and finally swing down. Individual components were monitored as specific data acquisition files, the purpose being clarity and simplicity during data processing.

As part of the data acquisition process, the excitation voltage and gain for each transducer, as well as the sampling rate were determined prior to each centrifuge test. The gain was set for each transducer in anticipation of both static and dynamic loading. A sample rate of 50 Hz was used during the scour events, whereas a sample frequency rate of 0.1 Hz was used

for pretest monitoring, swing-up and swing-down.

Video documentation of each test was accomplished using two CCD cameras mounted between the drive units opposite the cone penetrometer assembly. Images from these cameras were recorded during the centrifuge test using a VHS video tape recorder. Each scour event was on the order of six (6) seconds duration.

6.6 Post-test Analysis

Post-test analysis consisted of photographic documentation of the surface morphology of the scour marks, general observations, laser profiling of the scoured surface and finally excavation of the passive markers and in-situ instrumentation. Using the laser profiling system described in Section 5.5, cross-section profiles of the model testbed were conducted at approximately 25-50 mm intervals along the scour mark. In addition, a profile along the centerline of each scour mark was also taken.

A typical post-test excavation of the model test bed was governed by the features that were of interest. The excavation faces are shown schematically in Figure 6.3. Initial excavations had a vertical face (Line #1) oriented perpendicular to the scour direction. This provided a cross-section of both scour events. At approximately Y + 350 mm, the model was excavated in parallel to the scour mark (Line #2), with the information of interest being both

the spaghetti markers along the centerline of the scour and the features delineated by the dyed layers of sand in the frontal spoil berm. In addition, the location of the transducers were recorded when exposed during the excavation process.

As a means of documenting the observed subscour deformations, soil peels were taken from the excavated surfaces. The technique involved pressing a transparency that had been previously coated with a contact cement against the excavated surface. A layer of sand several grains in thickness adhered to the transparency once it was removed. The transparency, when dried, was digitized, preserving the observed subscour deformations in electronic form for subsequent analysis. The peels were saved for future reference.

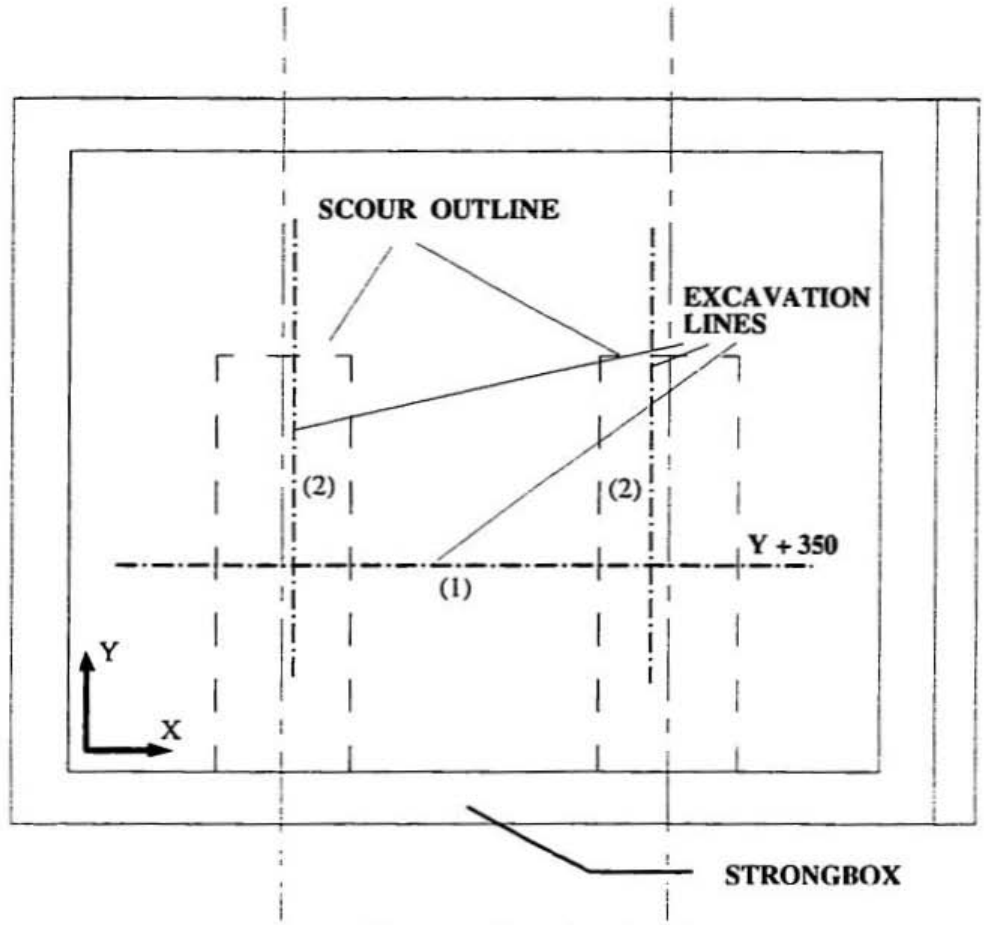

Figure 6.3 **A Schematic Diagram Showing the Excavation Sequence of a Typical Model Testbed**

Chapter Seven

Experimental Results

Centrifuge modelling of ice keel scour proved successful. The acquired data, consisting of seven distinct sets of numerical and semi-qualitative data, represent a range of scour conditions and parameters. A detailed summary of the acquired data set is presented in a series of individual data reports (C-CORE, 1995a, C-CORE, 1995b; C-CORE, 1995c; C-CORE, 1995d). The notation used in the identification of scour events in the data reports has been modified for use in this document such that the individual scour events are now represented by the letters A to H. In order to reduce confusion arising from this change, the notation used within this thesis along with the corresponding identification used in the data reports is presented in the following table.

Table 7-1 Test Identification.

Scour Event	Test Identification	Test Date
A	PRISE 01B Drive 1	01 Dec., 1994
B	PRISE 01B Drive 2	01 Dec., 1994
C	PRISE 01C Drive 1	15 Jan., 1995
D	PRISE 01C Drive 2	15 Jan., 1995
E	PRISE 09 Drive 1	01 Feb., 1995
F	PRISE 09 Drive 2	01 Feb., 1995
G	PRISE 10 Drive 1	23 Feb., 1995
H	PRISE 10 Drive 2	23 Feb., 1995

A test matrix describing the seven test configurations as defined by the various scour conditions and parameters is shown in Table 7.2. An eighth scour event designated Scour A was unsuccessful and is therefore omitted from Table 7.2 and subsequent discussions.

Table 7.2 Test Matrix

Scour	B	C	D	E	F	G	H
Sand Description	Loose	Loose	Loose	Dense	Dense	Dense	Dense
Scour Depth (m)	1.70	0.98	1.10	1.20	2.14	1.16	1.19
Scour Width (m)	15	15	15	15	15	30	30
Attack Angle (°)	15°	30°	15°	15°	15°	30°	15°
Acceleration Level (g)	150g	75g	75g	150g	150g	150g	150g

7.1 Post-Test Scour Profiles

As depicted in Figures 7.1 and 7.2, each scour event was characterized topographically by the formation of a surcharge mound located in front of the model ice keel and berms on each side. The topography of the scoured testbed was profiled in order to determine the scour depth and corresponding surcharge height. Profiles taken perpendicular to the length of the scour were used to determine scour depth. Profiles taken along the scour mark were used to determine the height of the frontal surcharge mound. The depth of each scour expressed in equivalent prototype units and the height of the corresponding surcharge mound is given in Table 7.3. It was noted that the height of the surcharge mound expressed in equivalent prototype scale was approximately 3.4 m for the 15 m wide scours and 5 m for the 30 m wide scours. It was concluded that the height of the surcharge mound was therefore

dependent upon the width of the scour event.

Table 7.3 Profile Data

Scour	B	C	D	E	F	G	H
Scour Width (m)	15	15	15	15	15	30	30
Scour Depth (m)	1.70	0.98	1.10	1.20	2.14	1.19	1.16
Surcharge Height (m)	3.5	3.1	3.1	3.6	3.6	5.0	5.0

7.2 Load Displacement Data

7.2.1 Horizontal Loads

As shown in Figure 7.3, the measured horizontal load was characterized by an increase from zero to an approximate steady state value. The magnitude of the horizontal load data expressed in equivalent prototype scale varies from 10 MN to approximately 50 MN. The peak horizontal load in equivalent prototype units for each scour event is presented in Table 7.4. Due to the configuration of the model testbed relative to the axis of rotation of the centrifuge, a radial component or lateral acceleration was superimposed upon the measured horizontal force. In order to compensate for the lateral acceleration, the calculated radial force component has been subtracted from the measured horizontal force. The horizontal load data presented in Figure 7.3 has been manipulated such that the radial component of acceleration has been removed. Plots from each scour event illustrating the response of the horizontal load cell versus both model displacement and time are presented in Appendix A.

Figure 7.1 **Plan View of Model Testbed Showing Scours C (Left) and D (Right)**

Figure 7.2 **Oblique View of Scour C Showing Surcharge In Front of Scour (Top) and Side Berms**

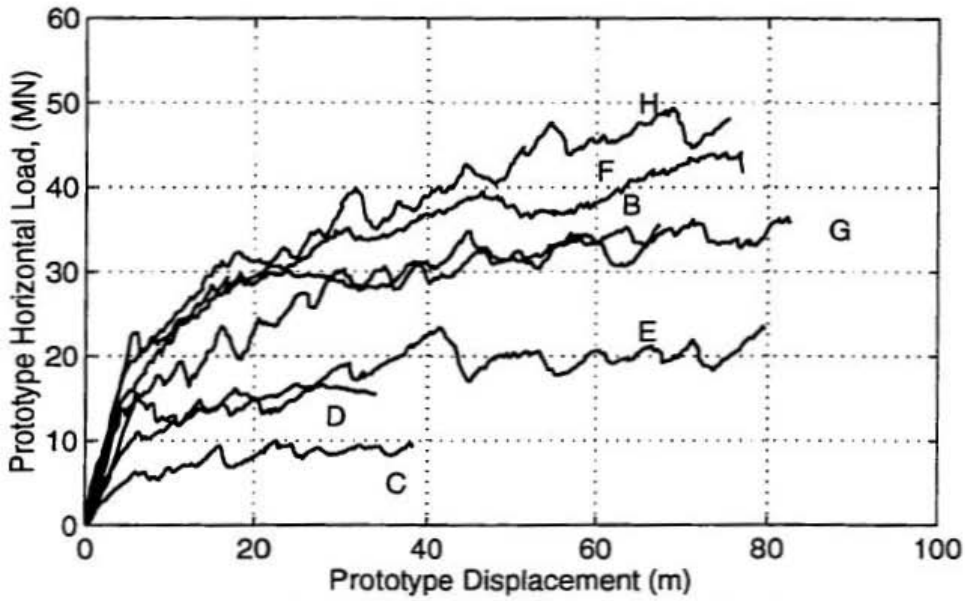

Figure 7.3 **Horizontal Load Expressed in Equivalent Prototype Scale Versus Model Ice Keel Displacement Expressed in Equivalent Prototype Scale**

7.2.2 Measured Vertical Loads

As shown in Figure 7.4, the total vertical load encountered by the model ice keel as it scours the model seabed is characterized by an increase from zero to an approximate steady state value. The magnitude of the vertical load displacement data expressed in equivalent prototype scale varies from 12 MN to approximately 56 MN. The peak equivalent prototype vertical load obtained for each scour event is tabulated in Table 7.4.

7.2.3 Ratio of Vertical to Horizontal Loads

The ratio between the measured vertical and horizontal load displacement data for each of the documented scour events presented in Table 7.4 and Figure 7.5, ranged from 1.03 to 1.18. In comparing the vertical and horizontal load displacement data, it was noted that both data sets were similar in form. For example, the cyclic variation present in the vertical load displacement data was also evident in the horizontal load displacement data. In addition, it was also noted that the cyclic response of the measured vertical and horizontal load displacement plots for each of the scour events were in phase. The close similarity between the vertical and horizontal load displacement plots is illustrated in Figure 7.6.

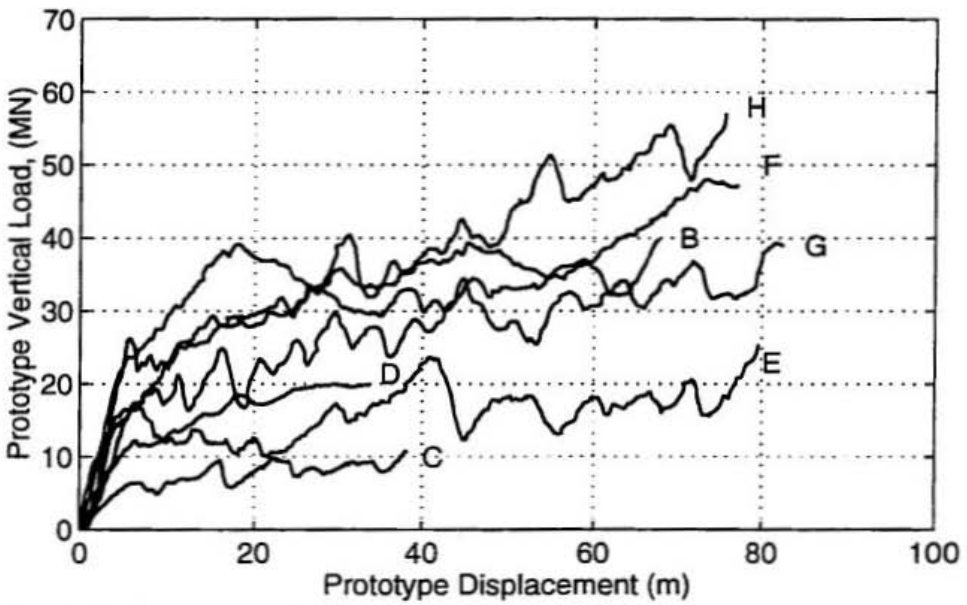

Figure 7.4 **Vertical Load Expressed in Equivalent Prototype Scale Versus Model Ice Keel Displacement Expressed in Equivalent Prototype Scale**

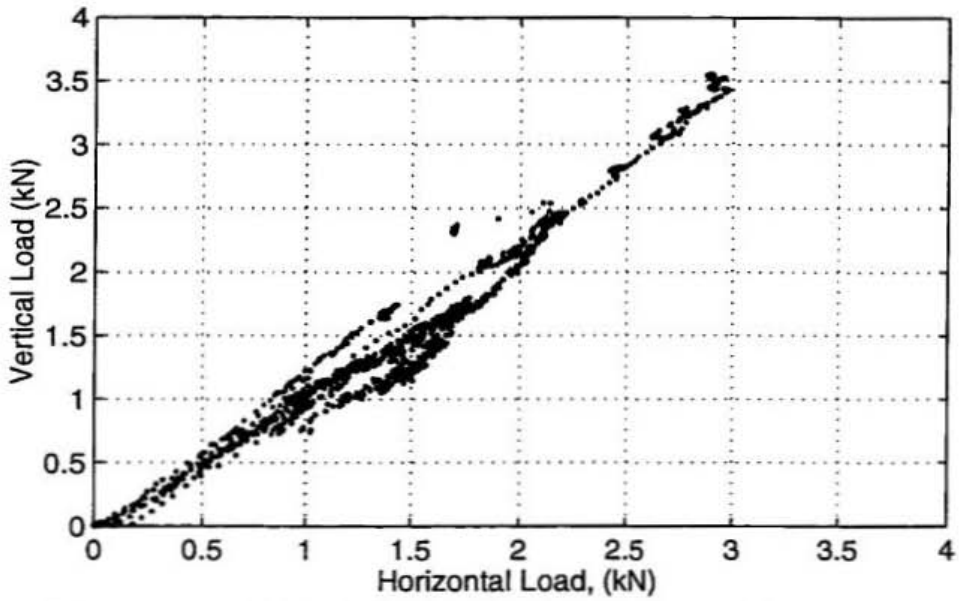

Figure 7.5 **Ratio of Vertical Load to Horizontal Load (Scours B through H)**

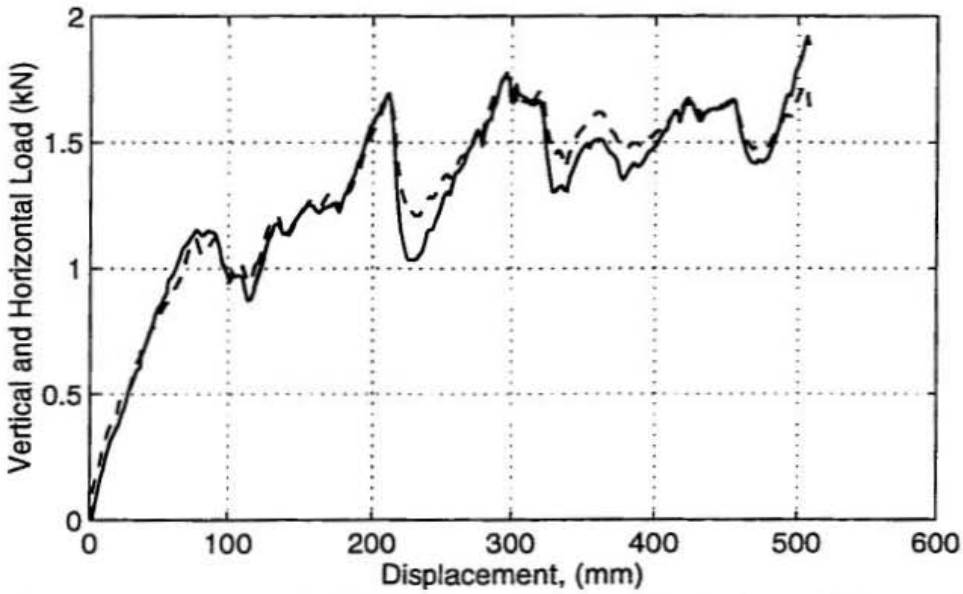

Figure 7.6 **Scour C, Phase Relationship Between Measured Vertical Load (Solid Line) and Horizontal Load (Dashed Line) Expressed in Equivalent Prototype Scale**

Table 7.4 **Vertical and Horizontal Load Displacement Data**

Scour	B	C	D	E	F	G	H
Sand Description	Dense	Loose	Loose	Dense	Dense	Dense	Dense
Scour Depth (m)	1.70	0.98	1.10	1.20	2.14	1.19	1.16
Scour Width (m)	15	15	15	15	15	30	30
Attack Angle (°)	15°	30°	15°	15°	15°	30°	15°
Acceleration Level (g)	150g	75g	75g	150g	150g	150g	150g
F_V (MN)	38.3	10.9	19.9	25.9	49.5	39.4	56.3
F_H (MN)	33.8	9.8	16.9	23.6	43.9	38.3	49.5
F_V/F_H	1.10	1.11	1.18	1.10	1.13	1.03	1.14

7.3 Pressure Transducer Data

A typical pressure transducer response versus model displacement for a pressure transducer (PT) embedded in the leading face of the model ice keel is shown in Figure 7.7. Plots from each scour event illustrating the pressure transducer response versus both model displacement and time are presented in Appendix A. The plots have been zeroed in order to reflect the magnitude of the interface pressures exerted by the model testbed on the model ice keel.

The pressure transducers embedded in the leading face of the model ice keel showed a sharp increase in pressure followed by an approximate steady state value. The pressure transducers embedded in the base of the model ice keel were characterized by a slight negative response during scouring. From the data presented in Table 7.5, it is noted that the

peak and mean response of the pressure transducers embedded in the leading face of the model ice keel were on the order of 200 to 300 kPa and 100 to 200 kPa respectively. The negative response of the pressure transducers located in the base of the model keel model was on the order of -15 to -25 kPa.

Table 7.5 Pressure Transducer Response

Scour	Equivalent Scour Depth (m)	Attack Angle (°)	Sand	Face Pressure Transducer Response (kPa)		
				Model Ice Keel, Face (Mean)	Model Ice Keel, Face (Peak)	Model Ice Keel, Base (Peak)
B	1.70	15	Loose	196.1	282.2	-15
C	0.98	30	Loose	170.1	259.6	-20
D	1.10	15	Loose	152.7	227.5	-15
E	1.20	15	Dense	160.5	312.0	-15
F	2.14	15	Dense	199.5	294.6	-25
G	1.19	30	Dense	185.3	275.3	-20
H	1.16	15	Dense	116.8	201.2	-15

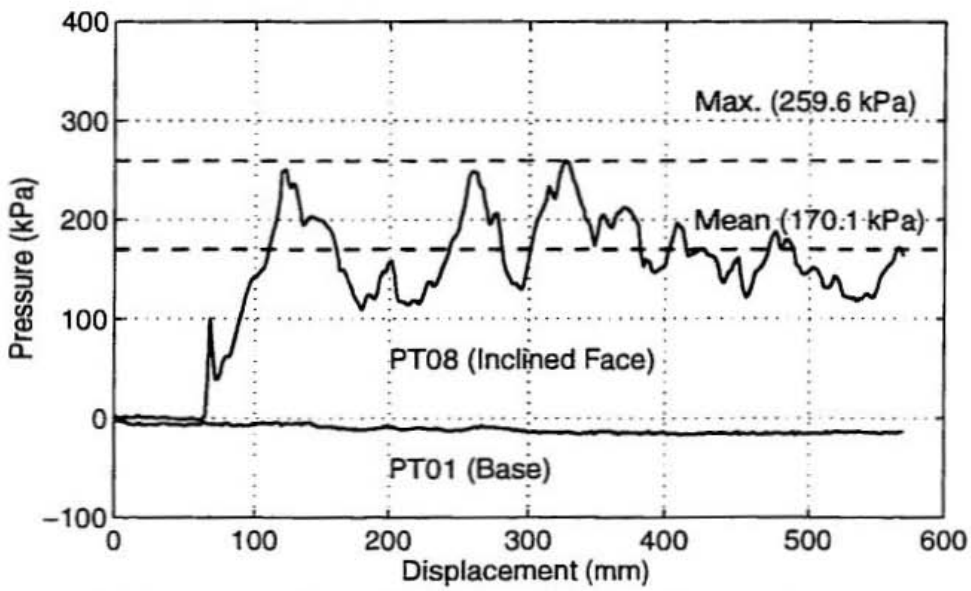

Figure 7.7 **Scour C - Excess Soil Keel Contact Pressure Response Versus Model Displacement**

7.4 Pore Pressure Transducer Response

As shown in Figure 7.8, the typical pore pressure transducer response was limited in magnitude. The plot depicted in Figure 7.8 has been zeroed in order to reflect pore pressure response above hydrostatic. The dashed vertical line present in Figure 7.8 represents the location of the pore pressure transducer (PPT) relative to the back of the model ice keel. Plots from each scour event illustrating the response of the pore pressure transducer versus both model displacement and time are presented in Appendix A.

In general, the pore pressure response was characterized by a slight positive increase as the model ice keel approached the pore pressure transducer followed by a negative dip. With the passage of the model ice keel over the buried pore pressure transducer, a zero shift in the positive direction was observed. The zero shift was on the order of 0.5 to 2 kPa. It is noted that an increase of this magnitude is representative of a vertical decrease in the elevation of the pore pressure transducer on the order of several millimetres at model scale. Table 7.6 summarizes the peak positive, peak negative and zero shift values for each of the pore pressure transducers. The pore pressure data in Table 7.6 are presented along with the scour identification, scour depth and the depth of the pore pressure transducer relative to the base of the scour.

Table 7.6 **Pore Pressure Transducer Data**

Scour Identification					Pore Pressure Transducer Response (kPa)		
Scour	Equivalent Scour Depth (m)	PPT #	Equivalent Depth Below Scour (m)	Sand	Peak (+ve)	Peak (-ve)	Offset
B	1.70	PPT # 7	4.5	Loose	0	0	1.5
C	0.98	PPT # 9	1.1	Loose	1.5	-7.5	0.5
C	0.98	PPT # 10	3.9	Loose	1	-0.7	0.4
D	1.10	PPT # 11	3.7	Loose	2.3	-2.3	-7.5
D	1.10	PPT # 12	2.8	Loose	8.2	0	1.7
E	1.20	PPT # 12	5.1	Dense	2.0	-1.6	0.5
E	1.20	PPT # 11	1.8	Dense	0	-3.7	1.1
F	2.14	PPT # 10	4.3	Dense	4.9	0	1.1
F	2.14	PPT # 9	2.7	Dense	1.5	0	1.6
G	1.19	PPT # 7	1.8	Dense	0	0	0.6
G	1.19	PPT # 11	4.8	Dense	0	0	0.4
H	1.16	PPT # 5	1.8	Dense	0	0	0.6
H	1.16	PPT # 12	4.8	Dense	0	0	0.3

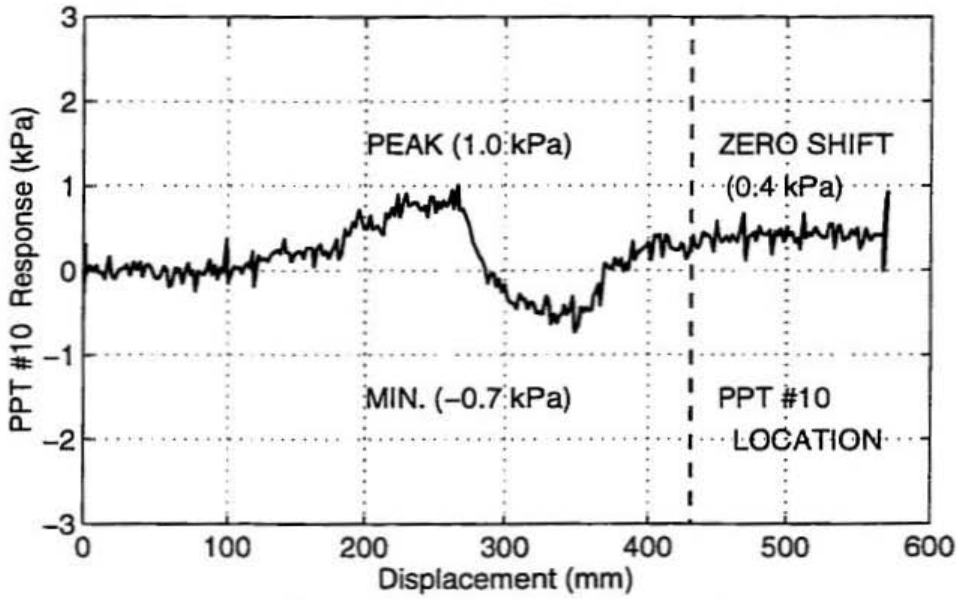

Figure 7.8 **Scour C, Excess Pore Pressure Response Versus Displacement**

7.5 Total Stress Cell Response

A typical response from a total stress cell (TLC) is shown in Figure 7.9. The dashed vertical line in Figure 7.9 is used to indicate the position of the transducer relative to the displacement of the model ice keel. Peak total stress values from each scour event are tabulated in Table 7.7. Plots from each scour event illustrating the response of the total stress cell transducers versus both model displacement and time are presented in Appendix A.

In general, the response of each total stress cells was similar in shape. It was noted that as the model ice keel approached the total stress cell, there was a rapid increase in the measured total stress up to a peak value followed by a return to a steady state condition. A zero shift in the negative direction was observed for most of the total stress cell (TLC) data. In reference to Scour D, the zero shift was on the order of 50% of the total response of the transducer. The observed zero shift was attributed to either a reduction in the effective stress associated with the removal of overlying material due to the scouring action, or a difference in stiffness between the model testbed and the total stress cell transducer. The uncertainty over the total stress data confirms an earlier statement that the response of the total stress cells beneath the model ice keel was dependent upon the stiffness of the transducer relative to the medium in which it was embedded.

Table 7.7 Total Stress Cell Data

Scour Identification					Total Stress Cell Response (kPa)	
Scour	Scour Depth	TLC #	Equivalent Depth Below Scour (m)	Sand	Peak (kPa)	Offset (kPa)
B	1.70	TLC # 2	2.5	Loose	176.7	-34.8
B	0.98	TLC # 6	4.8	Loose	175.4	-15.5
C	0.98	TLC # 2	3.9	Loose	69.3	-20.8
C	1.10	TLC # 6	0.2	Loose	102.6	5.1
D	1.10	TLC # 3	3.8	Loose	111.9	-51.0
E	1.20	TLC # 6	3.3	Dense	299.0	-7.5
F	2.14	TLC # 3	4.2	Dense	224.5	-26.0
F	2.14	TLC # 2	2.4	Dense	156.3	-27.2
G	1.19	TLC # 3	1.8	Dense	144.7	-4.2
H	1.19	TLC # 6	4.8	Dense	121.3	0.0
H	1.19	TLC # 3	1.8	Dense	105.9	30.1

7.6 Cone Penetrometer Test (CPT) Data

The cone penetrometer apparatus was used to obtain an indication of soil strength with depth. As illustrated in Figure 7.10, the cone penetration test provided an indication of the relative density of the test bed for each scour event. For example, the loose sand used for Scours C and D was characterized by a lower cone penetration resistance than the medium dense sand used for Scours E, F, G and H. Mechanical failure of the cone penetrometer prevented acquiring cone penetration data for Scour B.

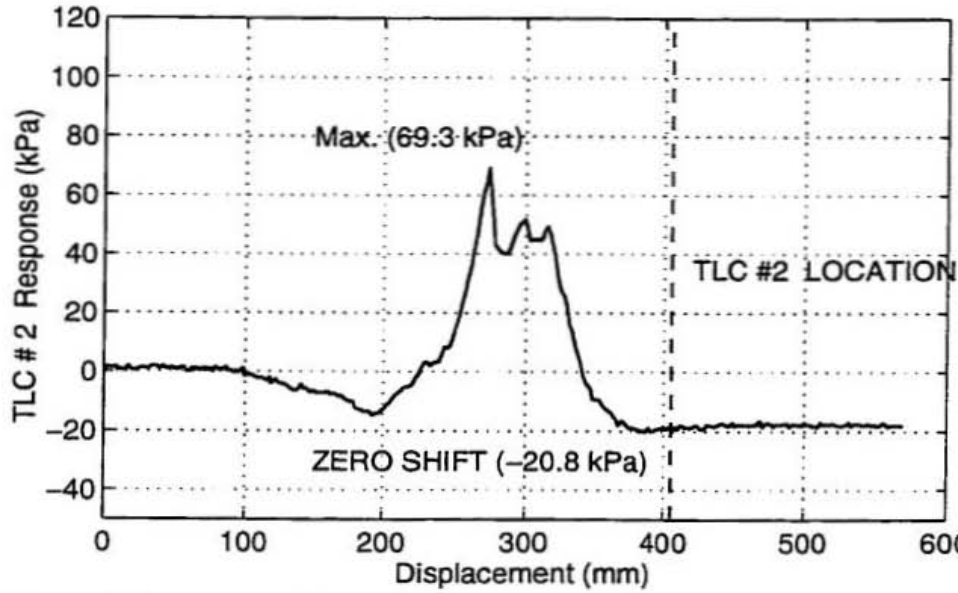

Figure 7.9 **Scour C, TLC #2 Response Versus Model Displacement**

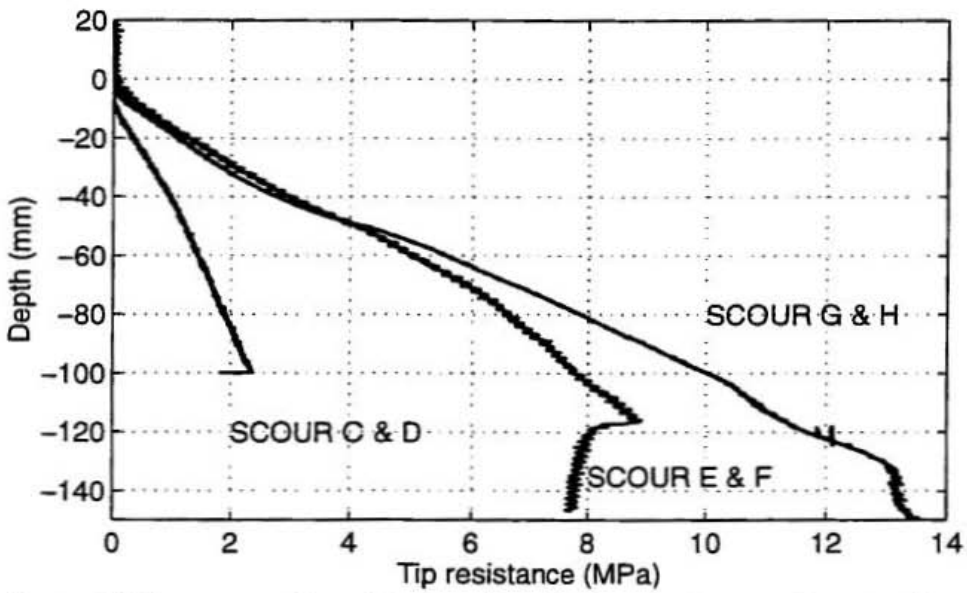

Figure 7.10 **Cone Penetration Resistance Versus Penetration Depth**

7.7 Passive Markers

Post-test analysis involved the documentation of both the observed surface features and subscour deformations. The identification of features beneath the ice keel scour was possible due to the presence of deformable spaghetti strands and coloured sand layers. Although semi-qualitative, the passive markers incorporated in the model testbed provided insight into the failure mechanism associated with the passage of a scouring ice mass. For example, as shown in Figure 7.11 (a) and (b), the coloured sand layers served to identify the presence of a static soil "dead wedge", located beneath the inclined portion of the model ice keel. The coloured sand layers were also instrumental in defining the presence of distinct rupture planes in the frontal spoil mound in each of the scour events. Depicted in Figures 7.11 (a) and (b), 7.12 (a) and (b) and 7.13 (a) and (b), the rupture planes are identified by short segments of coloured sand projecting upward through the surcharge mound. The low angle rupture planes are believed to be associated with the cyclic nature of the vertical and horizontal load displacement plots and will be addressed in the following chapter.

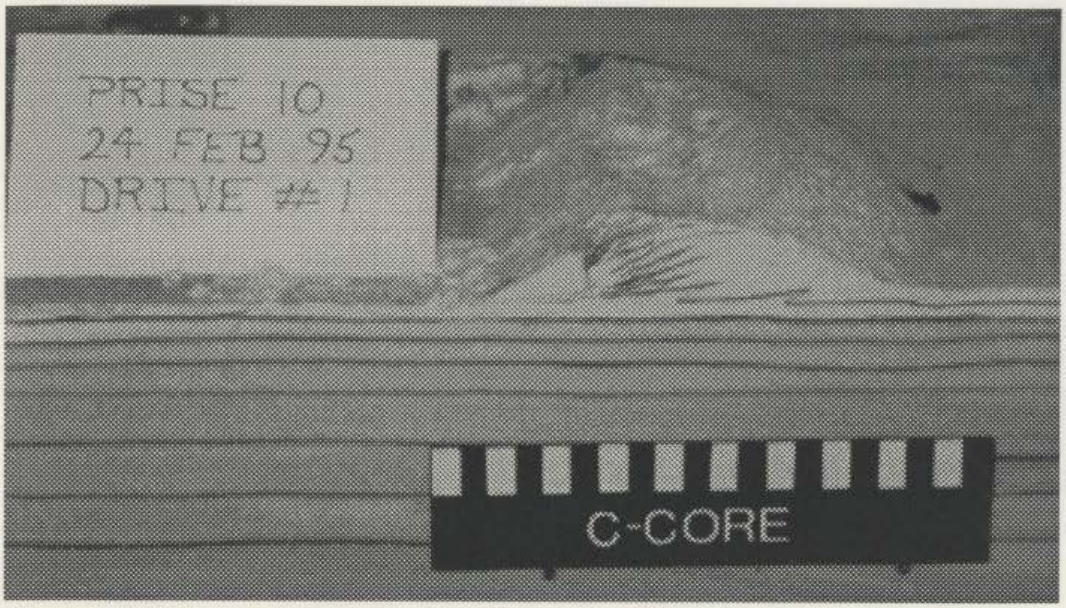

Figure 7.11 (a) **Scour G - Surcharge Profile**

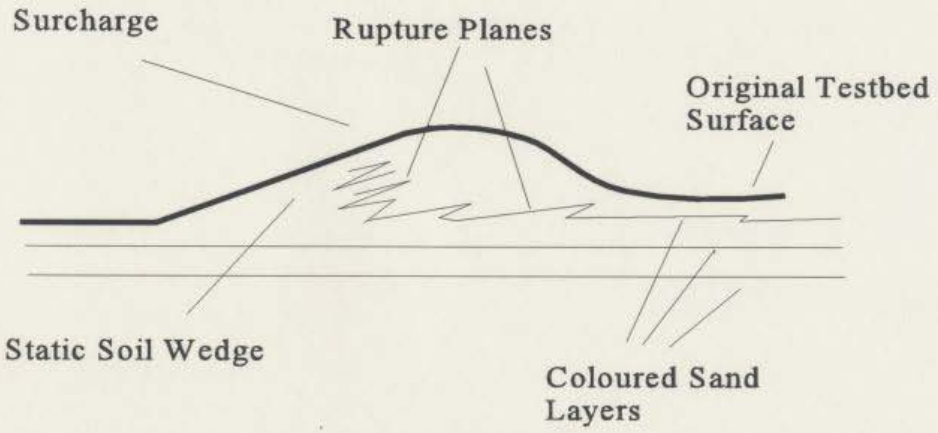

Figure 7.11 (b) **Schematic of Figure 7.11 (a) Showing The Presence of a Static Soil Wedge and Failure Planes In the Frontal Surcharge Mound**

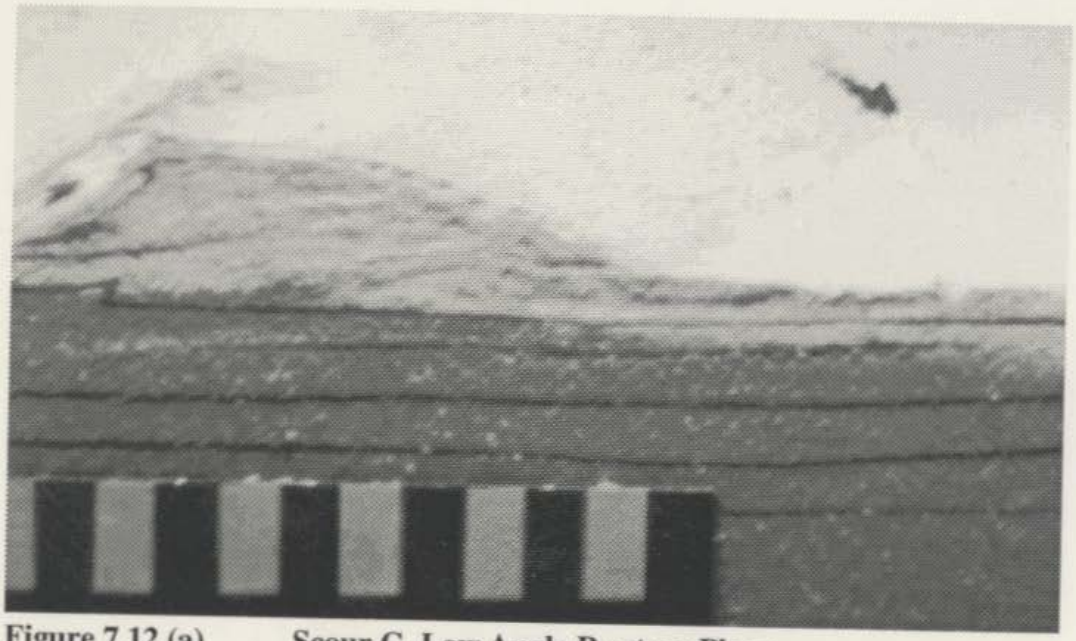

Figure 7.12 (a) Scour G, Low Angle Rupture Plane

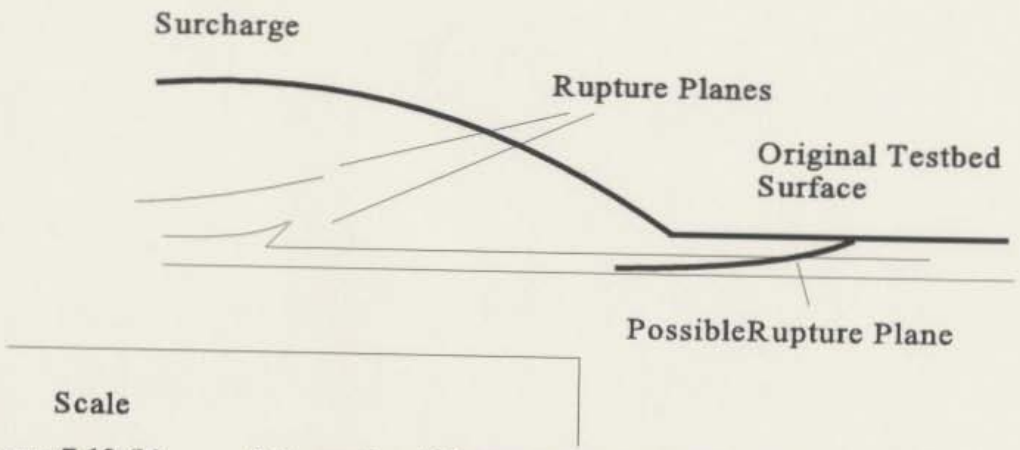

Figure 7.12 (b) Schematic of Figure 7.12 (a) Showing A Low Angle Rupture Plane as Defined by a Distorted Coloured Sand Layer

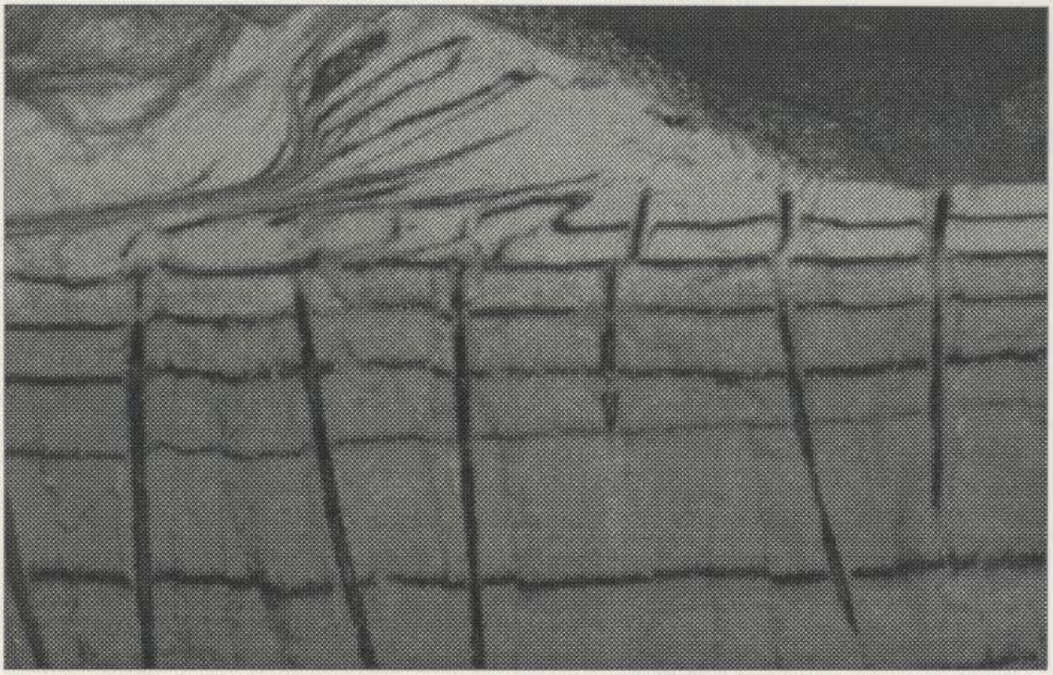

Figure 7.13 (a) **Scour G, Subscour Deformation**

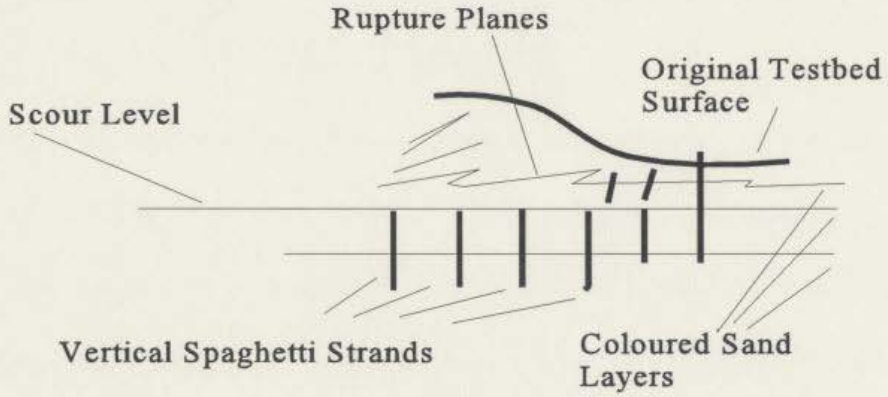

Figure 7.13 (b) **Schematic of Figure 7.13 (a) Showing Subscour Deformation and Horizontal Shear Beneath The Surcharge Mound**

Subscour soil deformations beneath each scour mark were identified by the horizontal deformation of the vertical spaghetti strands and to a lesser extent by the vertical compression of the sand layers. The subscour horizontal soil deformation data set consists of data from Scours B, C, D, E and F. There are no subscour deformation data available from Scours G and H. The five scour events used in the documentation of the subscour soil deformations represent three test configurations, i.e. 15° dense, 15° loose and 30° loose. Analysis of the documented subscour soil deformation was complicated by the variation in scour depths.

As illustrated in Figure 7.14 (a) and (b), determination of the horizontal soil displacement involved measuring the horizontal displacement (j) of the vertical spaghetti strands placed along the centerline of the scour with depth below the scour, (d). The acquired data, as presented in Figure 7.15 and Table 7.10 is semi-qualitative due to possible deviation of the spaghetti strands from vertical during placement, and therefore subject to uncertainty. The vertical subscour deformation was documented in terms of the volumetric reduction of the individual sand layers versus cumulative depth beneath the scour as shown in Figure 7.16. The percentage of vertical compaction of the individual sand layers was determined through a comparison of the average thickness of a sand layer beneath the ice keel scour (b) with the average thickness of the corresponding sand layer outside of the scour influence (a). The acquired data is presented in Figure 7.17 and Tables 7.11 through 7.15.

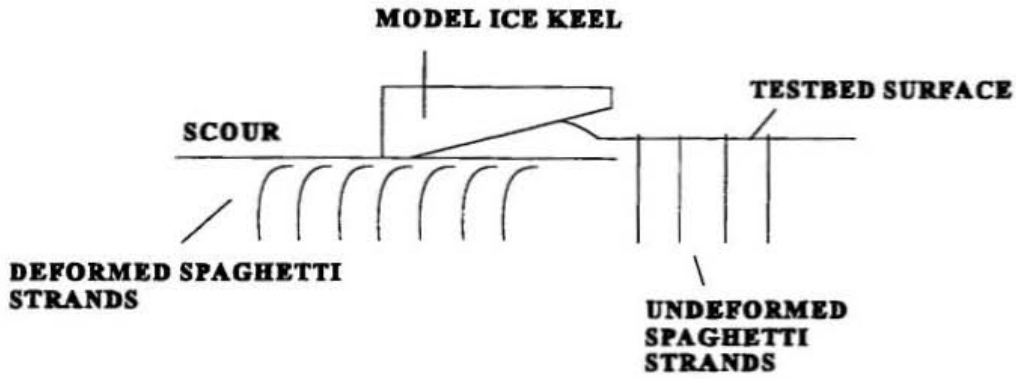

Figure 7.14 (a) Schematic Diagram Showing Deformed Spaghetti Strands

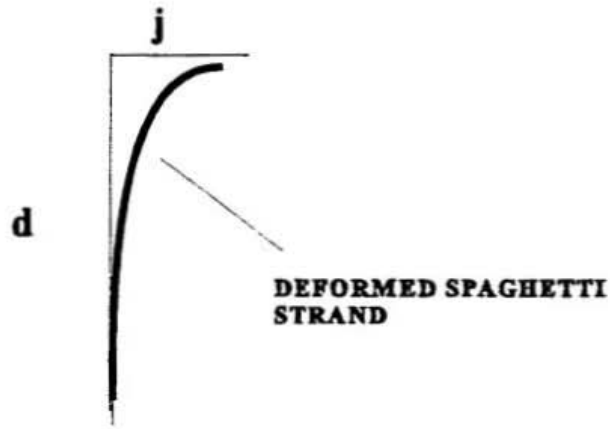

Figure 7.14 (b) Schematic Diagram Showing Deformed Strand of Spaghetti Illustrating Horizontal Deformation. j = Horizontal Displacement, d = Depth Below Scour Surface

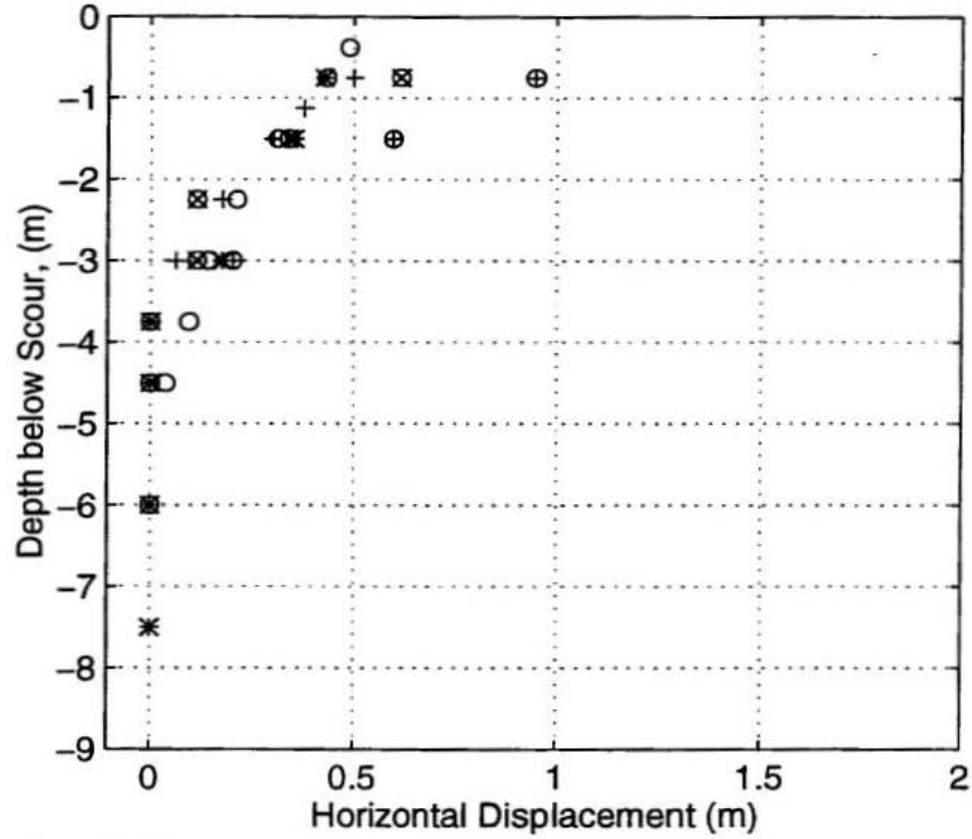

Figure 7.15 **Subscour Deformation Results Obtained For Scours B Through F Showing Horizontal Displacement in The Direction of The Scouring Ice Keel. Scour Influence is Given In Terms of Depth Below Scour Mark**

Table 7.8 **Legend - Subscour Soil Deformation**

Scour	Equivalent Scour Depth (m)	Attack Angle (°)	Initial Soil State	Symbol
B	1.70	15	Loose	*
C	0.98	30	Loose	+
D	1.10	15	Loose	o
E	1.20	15	Dense	⊗
F	2.14	15	Dense	⊖

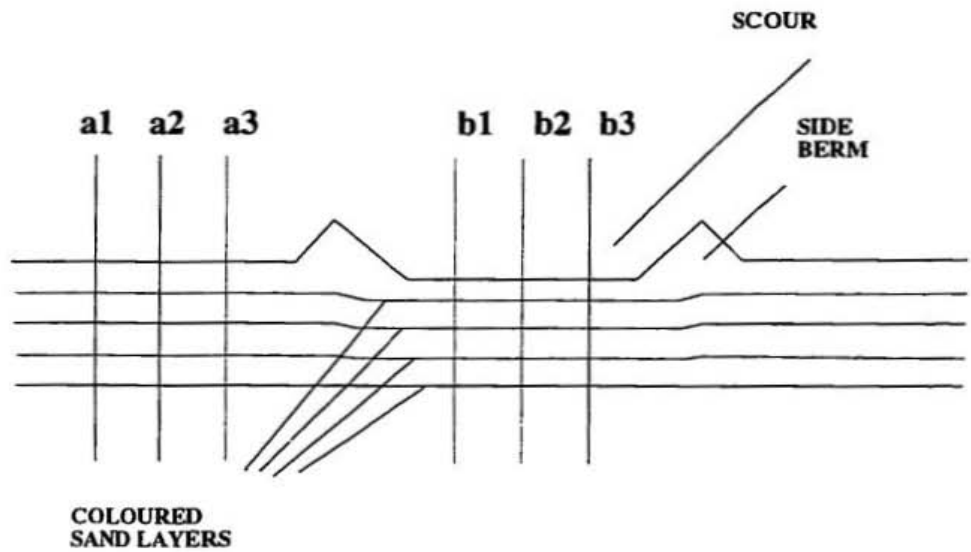

Figure 7.16 **Schematic Diagram Showing Methodology Used In Quantifying Vertical Subscour Soil Deformation**

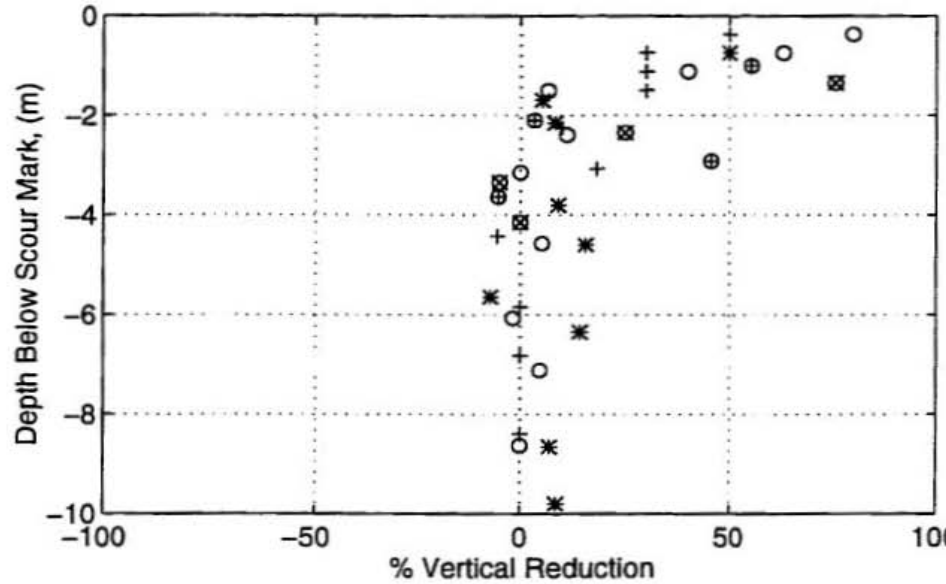

Figure 7.17 **Figure Showing Percent Vertical Reduction Versus Depth Below Scour In Equivalent Prototype Scale**

Table 7.9 **Legend - Subscour Soil Deformation**

Scour	Equivalent Scour Depth (m)	Attack Angle (°)	Testbed Description	Symbol
B	1.70	15	Loose	*
C	0.98	30	Loose	+
D	1.10	15	Loose	o
E	1.20	15	Dense	⊗
F	2.14	15	Dense	⊕

Table 7.10 Horizontal Subscour Soil Deformation Data

Scour B		Scour C		Scour D		Scour E		Scour F	
d	j	d	j	d	j	d	j	d	j
0.75	0.42	0.75	0.50	0.75	0.49	0.75	0.62	0.75	0.95
1.50	0.35	1.13	0.38	1.13	0.44	1.50	0.35	1.50	0.60
3.00	0.18	1.50	0.30	1.50	0.31	3.00	0.12	3.00	0.20
4.50	0.00	2.25	0.17	2.25	0.21	4.50	0.12	4.50	0.00
6.00	0.00	3.00	0.06	3.00	0.14	6.00	0.00	6.00	0.00
7.50	0.00	3.75	0.00	3.75	0.09	7.50	0.00	7.50	0.00
9.00	0.00	4.50	0.00	4.50	0.04	9.00	0.00	9.00	0.00
10.50	0.00	5.25	0.00	5.25	0.00	10.50	0.00	10.50	0.00
12.00	0.00	6.00	0.00	6.00	0.00	12.00	0.00	12.00	0.00
13.50	0.00	6.75	0.00	6.75	0.00	13.50	0.00	13.50	0.00

** Data plotted in Figure 7.15. Measurements based on methodology presented in Figure 7.14 (a) and (b). For reference, d = depth below scour mark, j = horizontal displacement.
** Measurements expressed in prototype units, (m)

Table 7.11 Vertical Subscour Soil Deformation Data, Scour B

a	b	delta	Vertical Reduction (%)	Cumulative Depth Below Scour (m)
0.75	0.38	0.37	50	0.75
0.95	0.90	0.05	5	1.70
0.45	0.42	0.03	8	2.15
1.65	1.50	0.15	9	3.80
0.80	0.68	0.12	16	4.50
1.05	1.13	-0.08	-7	5.66
0.71	0.60	0.11	14	6.35
2.30	2.15	0.15	7	8.66
1.16	1.05	0.11	9	9.80
1.50	1.50	0.00	0	11.33

** Data plotted in Figure 7.17. Measurements based on methodology presented in Figure 7.16. For reference, a = thickness of sand layer outside scour influence, b = thickness of sand layer beneath scour mark.

Table 7.12 Vertical Subscour Soil Deformation Data, Scour C

a	b	delta	Vertical Reduction (%)	Cumulative Depth Below Scour (m)
0.38	0.19	0.19	50	0.38
0.38	0.26	0.12	30	0.75
0.38	0.26	0.12	30	1.13
0.38	0.26	0.12	30	1.50
0.75	0.68	0.07	10	2.25
0.83	0.68	0.15	20	3.08
1.35	1.43	-0.08	-5	4.43
1.43	1.43	0.00	0	5.85
0.98	0.98	0.00	0	6.83
1.58	1.58	0.00	0	8.40

** Data plotted in Figure 7.17. Measurements based on methodology presented in Figure 7.16. For reference, a = thickness of sand layer outside scour influence, b = thickness of sand layer beneath scour mark.

Table 7.13 Vertical Subscour Soil Deformation Data, Scour D

a	b	delta	Vertical Reduction (%)	Cumulative Depth Below Scour (m)
0.38	0.08	0.30	80	0.38
0.38	0.14	0.24	63	0.75
0.38	0.23	0.15	40	1.13
0.38	0.35	0.03	7	1.50
0.90	0.80	0.10	11	2.40
0.75	0.75	0.00	0	3.15
1.43	1.35	0.08	5	4.58
1.50	1.52	-0.02	-1	6.08
1.05	1.00	0.05	5	7.13
1.50	1.50	0.00	0	8.63

** Data plotted in Figure 7.17. Measurements based on methodology presented in Figure 7.16. For reference, a = thickness of sand layer outside scour influence, b = thickness of sand layer beneath scour mark.

Table 7.14 **Vertical Subscour Soil Deformation Data, Scour E**

a	b	delta	Vertical Reduction (%)	Cumulative Depth Below Scour (m)
0.45	1.02	0.57	56	1.02
1.05	1.10	0.05	3	2.12
0.45	0.83	0.38	45	2.93
0.75	0.72	-0.03	5	3.65

** Data plotted in Figure 7.17. Measurements based on methodology presented in Figure 7.16. For reference, a = thickness of sand layer outside scour influence, b = thickness of sand layer beneath scour mark.

Table 7.15 **Vertical Subscour Soil Deformation Data, Scour F**

a	b	delta	Vertical Reduction (%)	Cumulative Depth Below Scour (m)
1.35	0.33	1.02	76	1.35
1.00	0.75	0.25	25	2.36
1.00	1.05	-0.05	-5	3.36
0.80	0.80	0.00	0	4.16

** Data plotted in Figure 7.17. Measurements based on methodology presented in Figure 7.16. For reference, a = thickness of sand layer outside scour influence, b = thickness of sand layer beneath scour mark.

Chapter Eight

Analysis and Discussion of Results

Analysis of the acquired data was focused on the measured vertical and horizontal load displacement data. The analysis involved giving consideration to the magnitude of the scour loads, the cyclic component of the load displacement data and the ratio of vertical to horizontal loads. A discussion of the general trends present in the measured load displacement data was augmented by a review of the pressure transducer and total stress cell data. The analysis of the data also takes into consideration scour attributes highlighted by the passive markers incorporated in the model testbed. Although semi-qualitative, the passive markers (in the form of coloured spaghetti strands and coloured sand layers) provide meaningful insight into the failure mechanisms operating during the passage of an ice keel in sand. It is felt that the understanding of ice keel scour gained from these experiments has important implications in terms of bearing stress and subscour soil deformation.

Table 8.1 Vertical and Horizontal Scour Loads

Scour	B	C	D	E	F	G	H
Angle (°)	15	30	15	15	15	30	15
Scour Depth (m)	1.70	0.98	1.10	1.20	2.14	1.19	1.16
Scour Width (m)	15	15	15	15	15	30	30
Model Testbed	Loose	Loose	Loose	Dense	Dense	Dense	Dense
F_V	38.3	10.9	19.9	25.9	49.5	39.4	56.3
F_H	33.8	9.8	16.9	23.6	43.9	38.3	49.5
F_V / F_H Ratio	1.10	1.11	1.18	1.10	1.13	1.03	1.14

8.1 Load Displacement Data

A review of the vertical load displacement data, as presented in Table 7.4, Table 8.1 and Figure 8.1, was used to illustrate relationships present in the acquired data set. For example, the effect of the scour depth in terms of the measured vertical load was determined through a comparison of Scours E and F. As presented in Table 8.1, both scours were created using a keel configuration with an equivalent prototype scour width of 15 m and an attack angle of 15° to the horizontal. Scours E and F were also completed in the same model testbed. The equivalent prototype scour depths for Scours E and F were 1.20 m and 2.14 m respectively. The measured peak vertical load expressed in equivalent scale was 25.9 MN for Scour E and 49.5 MN for Scour F. The increase in scour depth from 1.20 m to 2.14 m resulted in an approximate twofold increase in the measured vertical load.

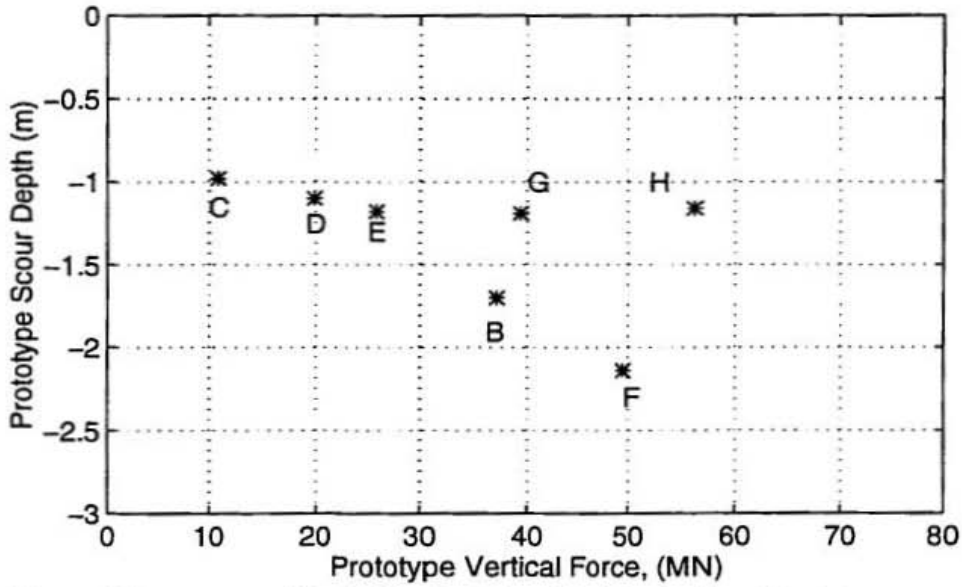

Figure 8.1 **Peak Vertical Load In Equivalent Prototype Scale Versus Scour Depth Expressed in Equivalent Prototype Scale For Scour Events B Through H.**

The effect of scour width on the measured vertical load was observed through a comparison of Scours E and H. Both scour events were created using a keel configuration with an attack angle of 15° to the horizontal. Both scours were also created in a model testbed with similar strength profiles (Figure 7.10). The equivalent scour depth for Scours E and H were established as 1.20 m and 1.16 m respectively. Scour E with an equivalent scour width of 15 m had an equivalent vertical load of 25.9 MN while Scour H with an equivalent scour width of 30 m had an equivalent vertical load of 56.3 MN. The increase in scour width from 15 m to 30 m caused an approximate twofold increase in the peak vertical load.

The effect of varying the attack angle of the model ice keel from 30° to 15° on the measured vertical load was observed through a comparison of Scours G and H. Both scours were created using a model keel with an equivalent prototype scour width of 30 m. The equivalent scour depths for Scours G and H were established as 1.19 m and 1.16 m respectively while the measured vertical load in equivalent scale were 39.4 MN and 56.3 MN respectively. The measured vertical load for Scour G with an attack angle of 30° to the horizontal was approximately 70% that of the measured vertical load obtained for Scour H with an attack angle of 15° to the horizontal. The effect of varying the attack angle of the model ice keel from 30° to 15° on the measured vertical load was also observed through a comparison of Scours C and D. Both scours were created using a model ice keel with an equivalent scour width of 15 m. The equivalent scour depths for Scours C and D were

0.98 m and 1.10 m while the measured vertical load in equivalent scale was 10.9 MN and 19.9 MN respectively. The measured vertical load for Scour C with an attack angle of 30° to the horizontal was approximately 55% that of the measured vertical load obtained for Scour D with an attack angle of 15° to the horizontal. The observed difference in the percentage of load between Scours G and H (i.e. 70%) and Scours C and D (i.e. 55%) is attributed to the slight increase in the measured scour depth for Scour D as compared to Scour C.

In terms of the relative density used in describing the model testbed, the test configuration used in Scour B was repeated in Scours E and F. However, Scour B was created in loose sand whereas Scours E and F were created in dense sand. Scour B had an equivalent peak vertical load of 38.3 MN corresponding to an equivalent scour depth of 1.70 m whereas Scours E and F had an equivalent peak vertical load of 25.9 MN and 49.5 MN and corresponding equivalent scour depths of 1.20 m and 2.14 m respectively. Based on the close similarity between the ratio of equivalent vertical load to equivalent scour depth for each of these scours, it is concluded that Scour B data is representative of a scour event in dense not loose sand. It is difficult to confirm this since there is no record of the soil strength profile for Scour B due to mechanical difficulties encountered with the cone penetrometer during the centrifuge test. However, a comparison of the measured peak vertical loads for Scours B and D as presented in Figure 8.1 serves to support the above conclusion. Both scours were created using a model ice keel possessing an equivalent prototype scour width

of 15 m and an attack angle of 15° to the horizontal. As shown in Table 8.1, the model testbed for each scour was initially characterized as loose. Scour B had an equivalent peak vertical load of 38.3 MN and a corresponding equivalent scour depth of 1.70 m while Scour D had an equivalent peak vertical load of 19.9 MN and a corresponding equivalent scour depth of 1.10 m. In comparing the two scour events, it is apparent that the equivalent peak vertical load for Scour B is approximately 190% that of the equivalent peak vertical load obtained for Scour D . It has been observed previously that an increase in the scour depth from 1.20 m to 2.14 m resulted in an approximate twofold increase in the measured vertical load. It is therefore contradictory that an approximate 30% increase in scour depth from 1.1 to 1.7 m should yield a twofold increase in the measured vertical load. This contradiction also serves to validate the conclusion that Scour B was representative of a scour event in dense sand.

The "modelling of models" attempt (Scours A and D) was not successful for the sand tests due to the lack of data corresponding to Scour A. However, from the data presented in Table 8.1 and Figure 8.1, insight into possible scale effects is possible. For example, Scours D and E were created using a model keel with a scour width of 15 m and an attack angle of 15° to the horizontal. Scour E was completed at an acceleration of 150g in dense sand while Scour D was completed at an acceleration of 75g in a loose sand. Scour E had an equivalent vertical load of 25.9 MN corresponding to an equivalent scour depth of 1.20 m while Scour D had an equivalent vertical load of 19.9 MN corresponding to an equivalent scour depth of

1.10 m. The 30% increase in the vertical load for Scour E as compared to Scour D is explained by the slight increase in scour depth for Scour E as compared with Scour D and the higher relative density of the model testbed in which Scour E was formed.

The manipulation of the vertical load data such that it is expressed in terms of load per unit width versus scour depth serves to semi-normalize the effect of scour width. The manipulated vertical load data is presented in Figure 8.2. Subsequent analysis determined that it was possible to project a straight line through the points associated with Scours B, E, F and H, as shown in Figure 8.3. Scours B, E, F and H are representative of a scour event formed by a model ice keel with an attack angle of 15° to the horizontal in dense sand (e.g. 15° dense).

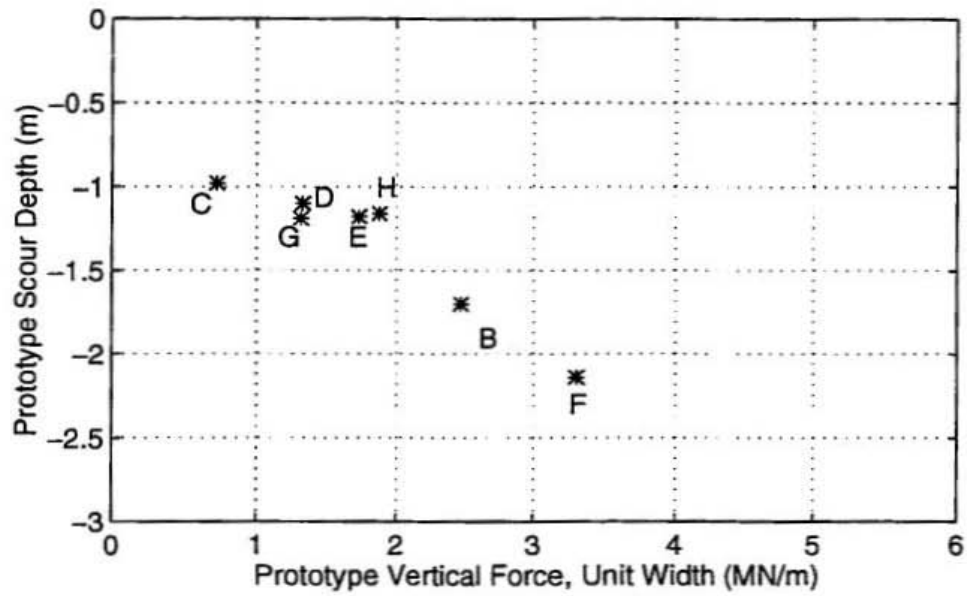

Figure 8.2 **Vertical Load Expressed In Terms of Equivalent Prototype Load Per Unit Width Versus Scour Depth Expressed in Equivalent Prototype Scale**

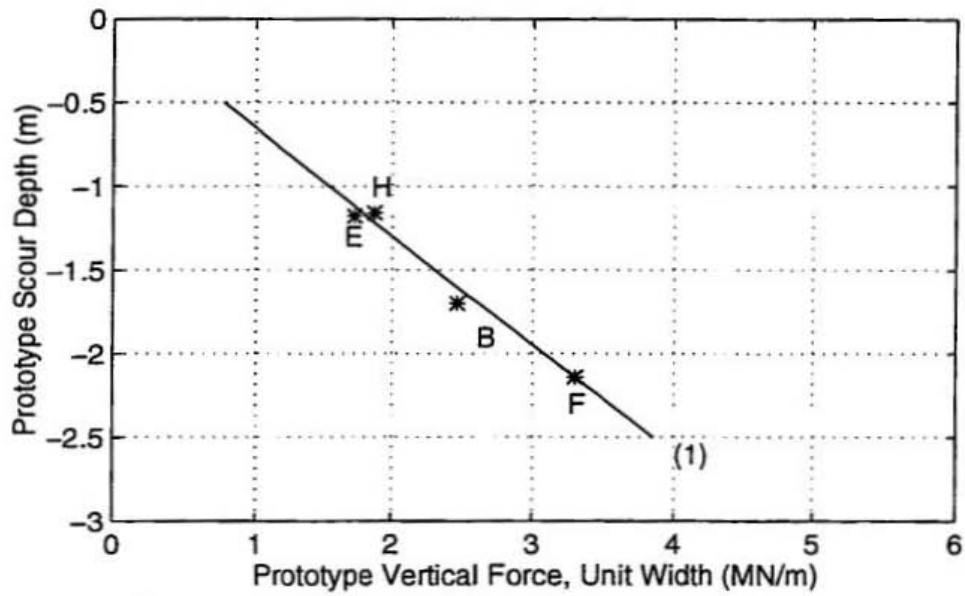

Figure 8.3 **Vertical Load In Equivalent Prototype Scale Versus Scour Depth in Equivalent Prototype Scale Showing Linear Relationship**

8.2 Passive Markers

The incorporation of passive markers in the form of coloured spaghetti strands and coloured sand layers proved useful. For example, the vertical spaghetti strands located along the centerline of the scour were effective in defining horizontal subscour deformation beneath the scour mark. In a similar manner, the coloured sand layers were instrumental in identifying the presence of a static soil wedge beneath the model ice keel as well as the presence of distinctive rupture planes located in the surcharge mound. The coloured sand layers were also instrumental in defining the magnitude of vertical subscour deformation beneath the scour mark.

The documented rupture planes identified in the surcharge mound helped to establish the probable sequence of events associated with the passage of an ice keel in sand. The features shown in Figure 8.4, and Figures 8.5 (a) and (b) are interpreted to represent the initiation of a low angle passive earth pressure failure in front of the model ice keel and subsequent translation of the model ice keel relative to the soil being displaced upward along the rupture plane. The displacement of the soil upward would result in additional loading and the initiation of a new rupture plane.

The suggested failure mechanism serves to explain the cyclic variation observed in both the horizontal and vertical load displacement plots. For example, the additional resistance

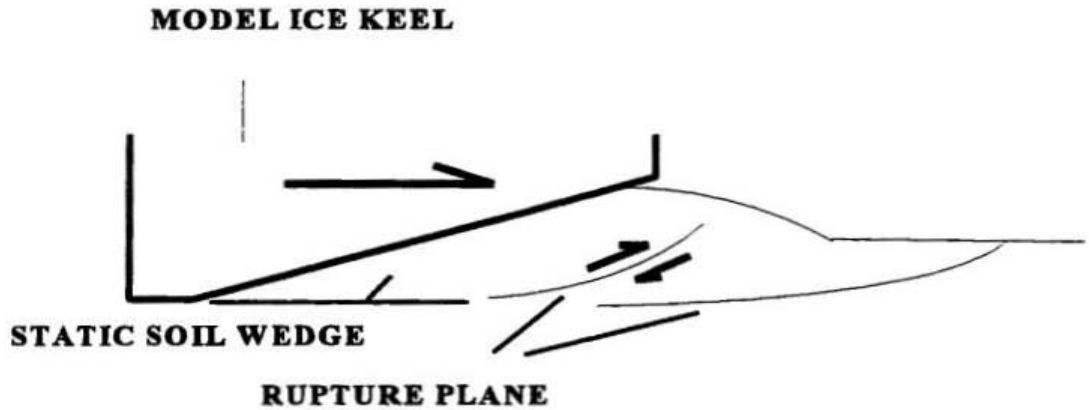

Figure 8.4 **Schematic Diagram Showing Proposed Scour Failure Mechanism With Loading Superimposed**

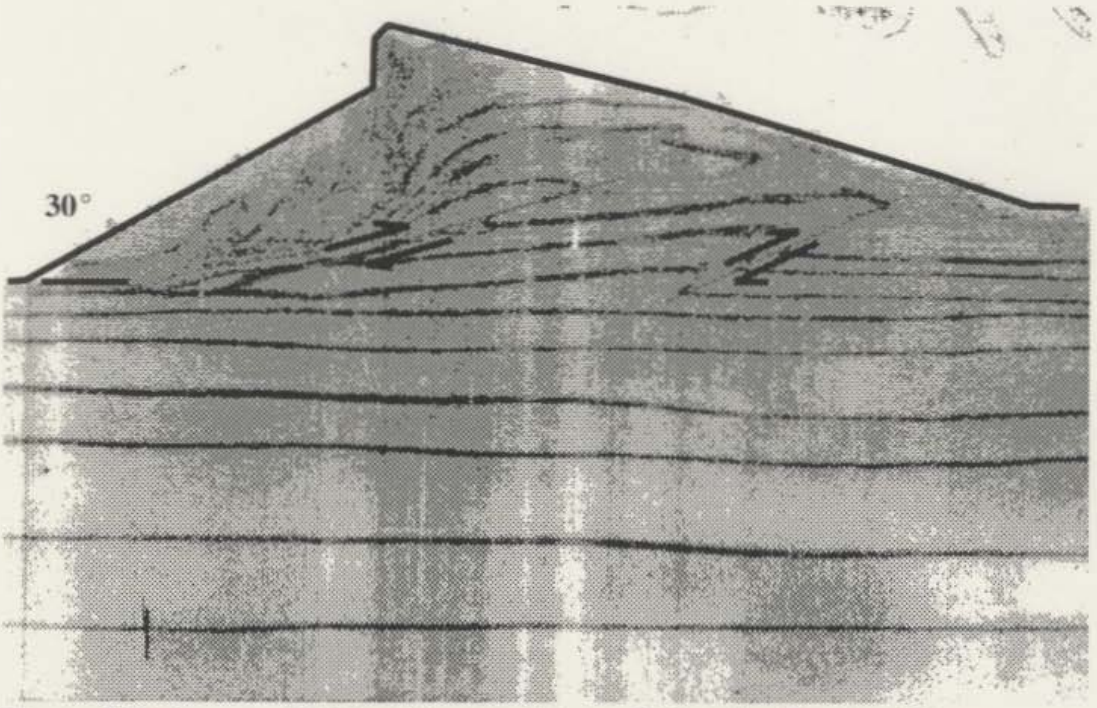

Figure 8.5 (a) Digitized Image of Scour C Showing Rupture Planes

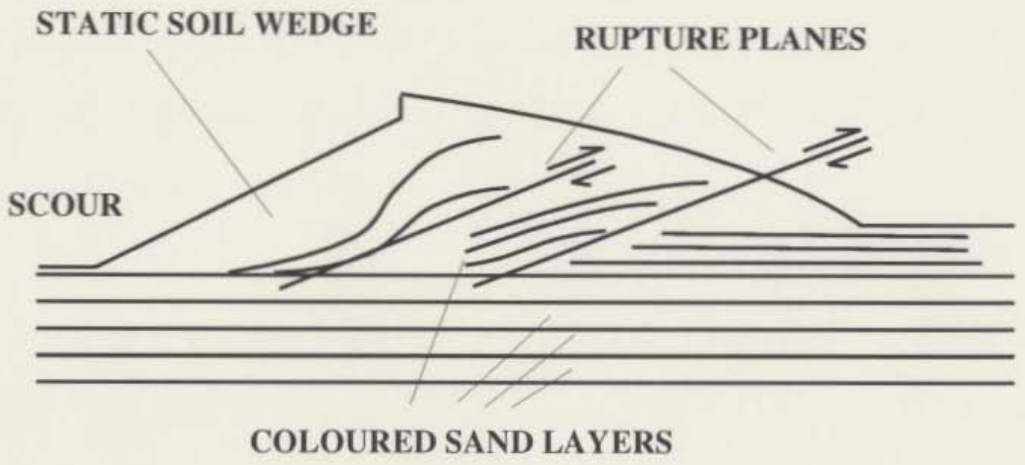

Figure 8.5 (b) Schematic of Figure 8.5 (a)

encountered by the soil body being displaced upward relative to the surcharge mound and the model ice keel is reflected in an increase in the measured vertical load. The increase in the measured vertical load applied to the rupture plane results in an increase in the measured horizontal load.

The interpretation that the cyclic behaviour of the horizontal and vertical load displacement plots is associated with the formation of a passive earth pressure failure in front of the advancing ice keel is confirmed through a comparison of the cyclic variation of the horizontal load displacement plot as presented in Figure 7.3, with the calculated passive earth pressure in front of the advancing model ice keel. The results of this comparison is presented in Table 8.2. The passive earth pressure was determined using Rankine passive earth pressure theory. It should be noted that the Rankine passive earth pressure was determined assuming a surcharge force as defined by the maximum measured height of the surcharge in front of the model ice keel. An effective unit weight of 500 kN/m^3 and 600 kN/m^3 was used for the loose and dense sand respectively.

From the data presented in Table 8.2, there is good agreement between the calculated Rankine passive earth pressure in front of the advancing ice keel and the cyclic variation in the horizontal load displacement plots. The observed correlation is significant because it provides an experimental measurement of the passive earth pressure in front of the advancing ice keel.

Table 8.2 **Comparison of Passive Earth Pressure With Cyclic Component of Horizontal Load**

Scour	B	C	D	E	F	G	H
Estimated Cyclic Component of the Measured Horizontal Load (MN)	4.0	2.0	2.0	4.0	5.0	6.0	7.0
Calculated Rankine Passive Earth Pressure (MN)	3.7	1.7	1.9	2.4	4.7	6.7	6.5

The above discussion is not meant to be a rigorous approach in quantifying the loads associated with the failure mechanism present in front of the model ice keel. Rather, it is intended to convey understanding of the failure mechanism as a whole and to assign a percentage of the measured vertical and horizontal load to the static soil wedge located beneath the model ice keel. It is emphasized that, irrespective of the actual failure mechanism, the proportion of the induced scour load associated with passive earth pressure failure in front of the model ice keel is on the order of 10% to 20% of the total scour loads.

8.3 Soil Failure Mechanisms

In addition to possible shear dragging beneath the model ice keel, it is important to take into consideration the effect of horizontal shear resistance in the vertical plane associated with the sides of the static soil wedge and model ice keel, shown in figure 8.6 (a). It was also recognized that the shear resistance along the vertical sides of the static soil wedge and

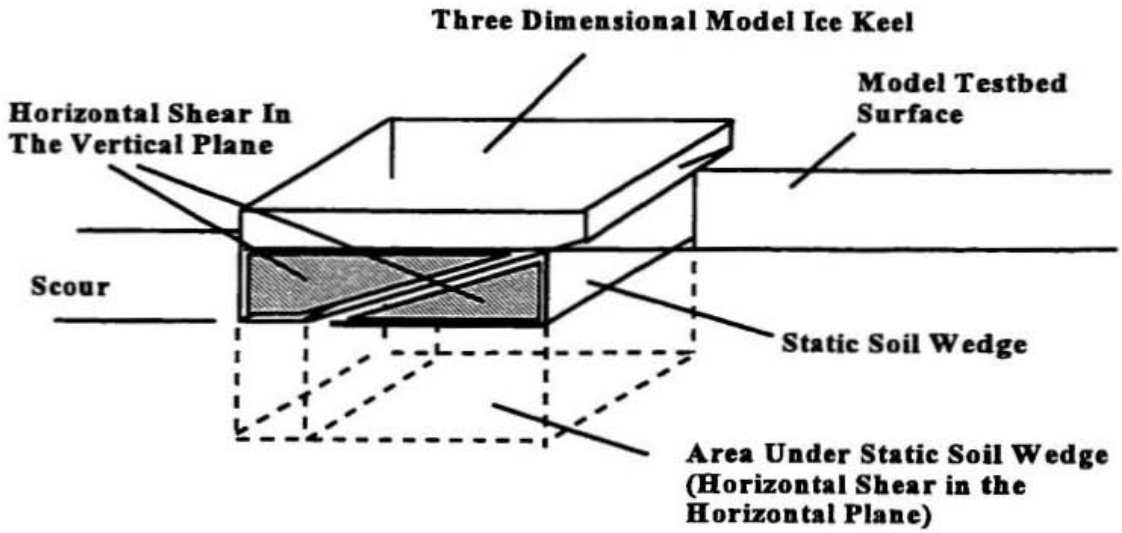

Figure 8.6 (a) Three Dimensional Schematic Diagram of Ice Keel Scour Showing Zone of Horizontal Shear in the Vertical Plane at the Edge of the Scour.

model ice keel would be absent from the vertical load displacement plot but would be present in the horizontal load displacement plot. It is therefore proposed that a more appropriate measure of the failure mechanism beneath the static soil wedge is possible through a reduction of the measured horizontal load equivalent to the horizontal shear resistance in the vertical plane located at the edges of the scour mark. In order to estimate the magnitude of this shear resistance, the empirical relationships used in determining the ultimate lateral resistance of rigid piles is used.

The ultimate lateral resistance per unit width of a rigid pile is greater than that of a corresponding wall due to the shearing resistance on the vertical sides of the failure wedges in the soil (Terzaghi, 1943). Moreover, as a means of approximating the ultimate lateral resistance on a rigid pile, a shape factor can be used. For example, Broms (1964) proposed that the lateral earth pressure which develops at failure for a pile is equal to three times the passive Rankine earth pressure on a wall. Broms (1964) also referenced the earlier efforts of Praskash (1962) who suggested that the maximum lateral earth pressure is approximately 2 to 3 times the passive earth pressure as calculated by the Rankine passive earth pressure theory.

From the profile view of a model ice keel presented in Figure 8.6(b), it can be seen that the zone of passive earth pressure failure represents approximately 10% to 15% of the total length of the model ice keel due to the influence of the attack angle. The extension of the

empirical relationships used in determining the ultimate lateral resistance of piles to the phenomenon of ice keel scour involved multiplying the shape factor used for rigid piles by the increase in the corresponding area. As presented in Table 8.3, the horizontal shear resistance in the vertical plane for a model ice keel with an equivalent prototype width of 15 m possessing an attack angle of 15° to the horizontal was approximated as 15 times the lateral passive earth pressure as determined using Rankine passive earth pressure theory. The horizontal shear resistance in the vertical plane for a 30 m wide keel possessing an attack angle of 15° to the horizontal was approximated as being 20 times the lateral earth pressure as determined using Rankine passive earth pressure theory. The reduction in the measured horizontal load corresponding to 15 times the lateral passive earth pressure for the 15 m wide keels and 20 times the lateral passive earth pressure for the 30 m wide keels resulted in the calculated F_V/F_H ratio increasing from approximately 1.1 to approximately 1.3.

Additional insight into the phenomenon of ice keel scour is provided by the vertical to horizontal load ratio. This insight is based on the premise that the measured vertical scour load and the measured horizontal scour load (minus the horizontal shear resistance in the vertical plane discussed above) are analogous to the applied normal force (σ) and measured shear force (τ) in a direct shear test. Using this assumption, it is possible to determine the internal angle of friction for the sand used in construction of the model testbed. The inverse tangent of the modified F_H/F_V ratio provides an internal angle of friction of approximately

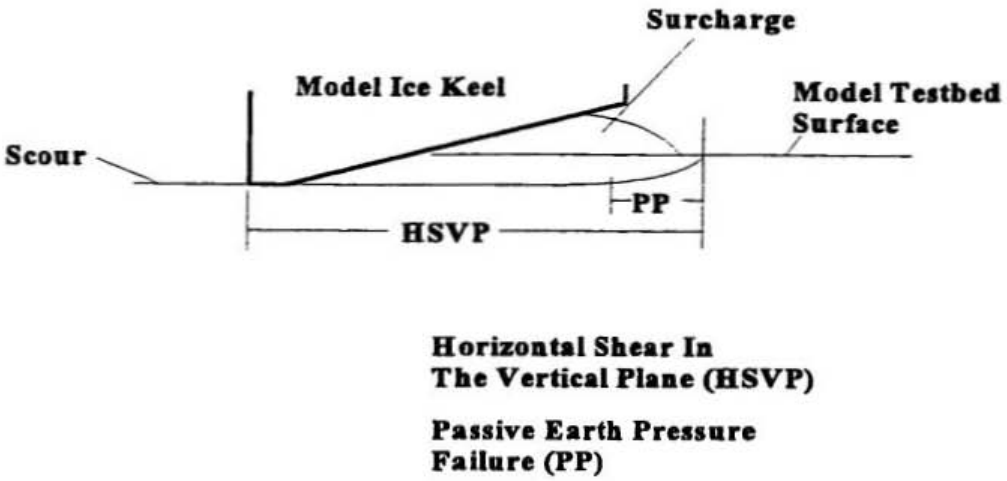

Figure 8.6 (b) Schematic Diagram of an Ice Keel Scour Event in Profile View. The Total Area Of Horizontal Shear In The Vertical Plane (HSVP) is Equal to 5 to 6 Times The Area of Horizontal Shear In The Vertical Plane Associated With The Zone of Passive Earth Pressure Failure (PP).

38.0° as shown in Table 8.3. The angle of internal friction for the quartz sand used in the construction of the model testbed as determined using undrained triaxial compression tests for loose and dense sand was 36.5°. This comparison is significant in that it supports the premise that the horizontal to vertical load ratio is directly associated with basal shear beneath the static soil wedge. An association which also serves to validate Been's (1990) shear dragging hypothesis. The ratio of vertical to horizontal force was used by Poorooshasb (1989) and Paulin (1992) as a measure of experimental repeatability.

Table 8.3 Angle of Internal Friction of the Sand

Scour	B	C	D	E	F	G	H
Attack Angle (°)	15	30	15	15	15	30	15
Scour Depth (m)	1.7	0.98	1.1	1.2	2.14	1.19	1.16
Scour Width (m)	15	15	15	15	15	30	30
Initial Soil State	Loose*	Loose	Loose	Dense	Dense	Dense	Dense
F_V(MN)	38.3	10.9	19.9	25.9	49.5	39.4	56.3
F_H(MN)	33.8	9.8	16.9	23.6	43.9	38.3	49.5
Horizontal Shear In The Vertical Plane (MN)	3.70	1.70	1.90	2.40	4.70	4.50	4.30
F_H**	30.1	8.1	15.0	21.2	39.2	33.8	45.2
F_V / F_H	1.10	1.11	1.18	1.10	1.13	1.03	1.14
F_V / F_H **	1.27	1.35	1.33	1.22	1.26	1.18	1.25
$\phi = Tan^{-1}(F_H$ **$/ F_V)$	38.2	36.6	37.0	39.3	38.4	40.2	38.8

* Interpreted as being representative of a scour in dense sand.
** Indicates modified horizontal force (total horizontal force minus horizontal shear resistance in the vertical plane).

General acceptance of this conclusion implies that the centrifuge data set involving ice keel scour in sand was representative of a three dimensional scour mechanism as opposed to a two dimensional plane strain mechanism.

8.4 Implications

The variation in the measured vertical and horizontal load displacement data with increasing scour depth and scour width can be explained in terms of basal shear beneath the static soil wedge. For example, it is observed that an increase in the scour width from 15 m to 30 m results in an approximate twofold increase in the measured vertical load. It is also observed that increasing the incision depth of the scour from 1.20 m to 2.14 m results in an approximate twofold increase in the measured vertical and horizontal loads. In an analogous manner, doubling the width or length of a direct shear box while maintaining a constant applied bearing stress would result in an approximate twofold increase in the measured vertical and horizontal loads.

The premise of a constant bearing stress with increasing scour depth was examined in reference to the static soil wedge identified beneath the inclined portion of the model ice keel. As shown in Figure 8.7, there is a corresponding increase in the area under shear due to the formation of the static soil wedge with increasing scour depth. The assumption of a relatively constant bearing stress with increasing scour depth is therefore valid since the increase in vertical load is offset by an increase in the area under shear.

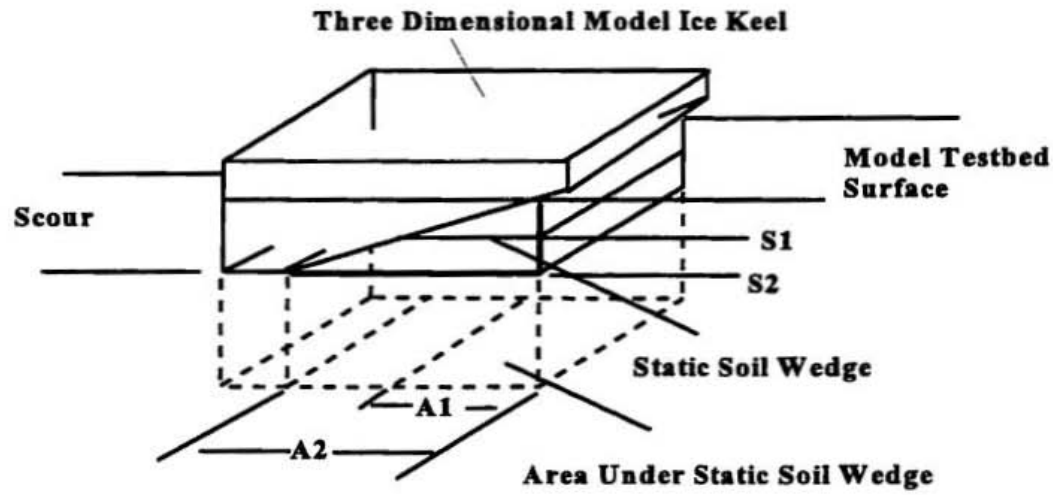

Figure 8.7 Three Dimensional Schematic Diagram of Ice Keel Scour Showing Linear Increase In Horizontal Area Under Shear (A1, A2) Beneath The Static Soil Wedge With increasing Scour Depth (S1, S2).

Based on the observed linear relationship exhibited by those scour events characterized as 15° dense in Figure 8.3, a series of four lines designated Lines #1 through #4 was superimposed on the full centrifuge data set involving sand as shown in Figure 8.8. The four lines depicted in Figure 8.8 represent four distinct scour configurations. Line #1 is representative of a scour event in dense sand formed using a model keel with a 15° attack angle to the horizontal. Line #2 is representative of a scour event in loose sand formed using a model keel with a 15° attack angle to the horizontal. Line #3 is representative of a scour event in dense sand formed using a model keel with a 30° attack angle to the horizontal. Finally, Line #4 is representative of a scour event in loose sand formed by a model ice keel with a 30° attack angle to the horizontal.

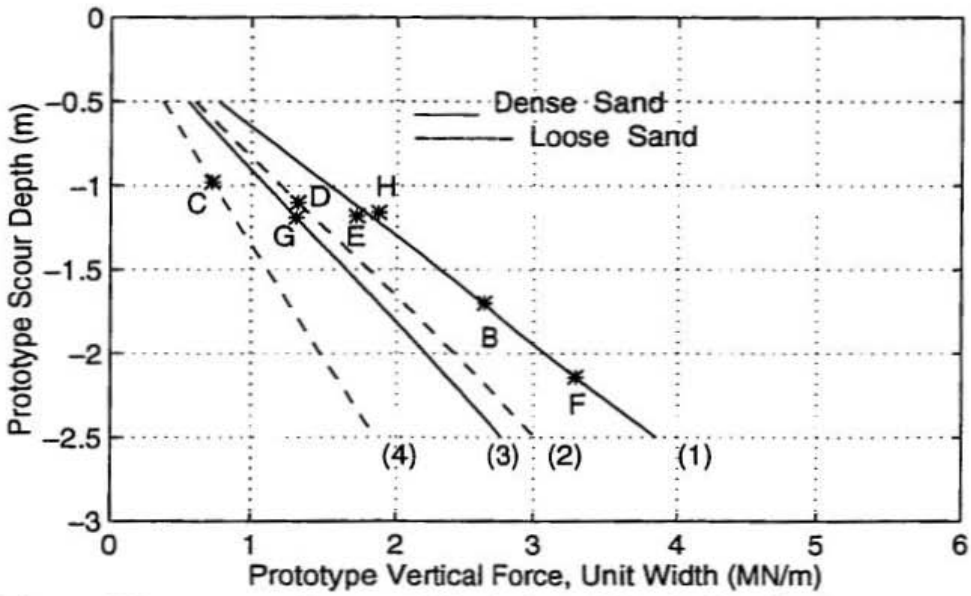

Figure 8.8 **Proposed Variation of Equivalent Prototype Vertical Scour Force Versus Scour Depth Expressed In Equivalent Prototype Scale.**

In order to validate the perceived trend in the data as presented in Figures 8.3 and 8.8, a calculated bearing stress for Scours B, D, E, F and H was determined based on the measured peak vertical load and the presence of a static soil wedge beneath the model ice keel shown schematically in Figure 8.6(a). The geometry of the static soil wedge was chosen such that its base is parallel with the base of the keel and its upper boundary is defined by the original surface of the model testbed. The above rationale was also used by Paulin (1992) to establish the worst case scenario for loading. Presented in Table 8.4, the calculated bearing stress was 330 kPa, 386 kPa, 402 kPa, 413 kPa and 430 kPa for Scours B, D, E, F and H respectively.

Table 8.4 Calculated Vertical Bearing Stress, Scours B, D, E, F and H

Scour	B	D	E	F	H
Scour Depth (m)	1.70	1.10	1.20	2.14	1.16
Scour Width (m)	15	15	15	15	30
Vertical Load (MN)	38.3	19.9	25.9	49.5	56.3
Bearing Area (m^2)	95.2	61.6	67.2	119.8	129.9
Bearing Stress (kPa)	402	323	386	413	433

In comparing the calculated vertical bearing stress for Scours E, B and F, it is noted that the three scour events are represented by a range of 27 kPa. Scours E and F represent an increase in scour depth from 1.1 m to 2.14 m and an approximate twofold increase in the measured vertical load. The 27 kPa range encompassing Scours B, E and F represents a 7% increase in the calculated bearing stress for Scour E to Scour F. Such a small change

supports the conclusion that the bearing stress is insensitive to changes in scour depth, in the scour depths investigated.

The premise that the bearing stress is insensitive to changes in scour depth is also supported by the pressure transducer data as presented in Table 7.5, Table 8.5 and in Figure 8.9. For Scours E and F, there was a difference of 39 kPa in the mean response of the pressure transducer embedded into the sloping face of the model ice keel. The 39 kPa difference represents a 24% increase in the measured contact pressure between the model ice keel and the model testbed compared to an approximate twofold increase in the measured vertical load.

Table 8.5 Pressure Transducer Response Data, Scours B, D, E, F and H

Scour	Equivalent Scour Depth (m)	Mean Response (kPa)	Peak Response (kPa)
B	1.70	196.1	282.2
D	1.10	152.7	227.5
E	1.18	160.5	312.0
F	2.14	199.5	294.6
H	1.16	116.8	201.2

In terms of the total stress cell response as presented in Table 7.7, Table 8.6 and in Figure 8.10, it should be emphasized that the observed zero shift present in the data has introduced a degree of uncertainty with respect to the quality of the data. It was therefore difficult to arrive at a meaningful comparison. An effort was made to compare the peak

total stress cell response for Scours B, D, E, F and H, with the mean pressure transducer response for the same scour events. For example, a comparison of the mean response of the pressure transducer embedded in the leading face of the model ice keel for Scour H presented in Table 8.5, with the peak response of the total stress cells for the same scour as presented in Table 8.6 would suggest good agreement between the data. However, a comparison of the mean response of the pressure transducer data with the peak response of the total stress cell data for Scour E showed large differences. In general, there were significant differences between the two data sets. The lack of agreement serves to support the previous observation made regarding the quality of the total stress data.

Table 8.6 Total Stress Cell Response, Scours B, D, E, F and H

Scour	Equivalent Scour Depth (m)	Peak Response (kPa)	Zero Offset (kPa)
B	1.70	176.7	-34.8
B	1.70	175.4	-15.5
D	1.10	111.9	-51.0
E	1.18	299.0	-7.5
F	2.14	224.5	-26.0
F	2.14	156.3	-27.2
H	1.16	121.3	0
H	1.16	105.9	30.1

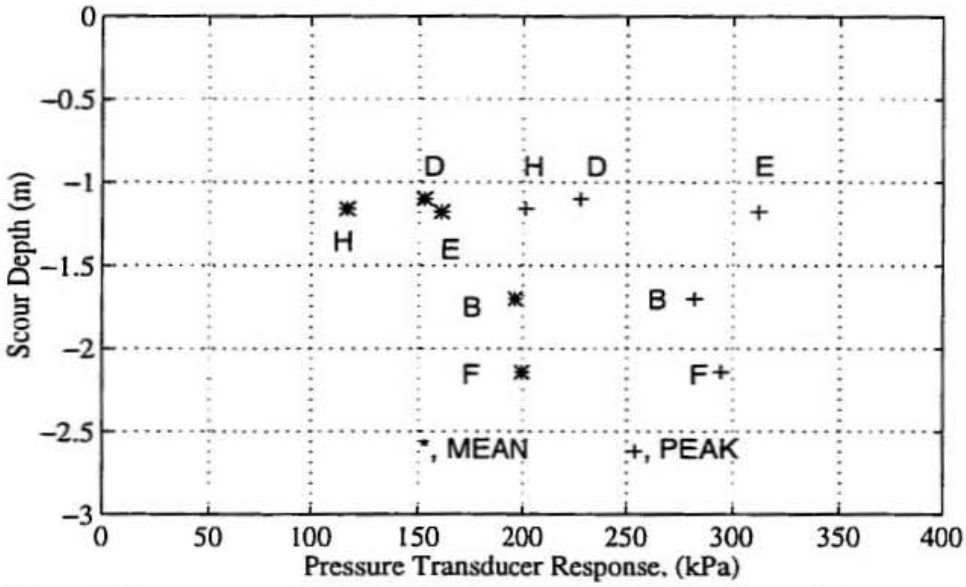

Figure 8.9 **Peak and Mean Pressure Transducer Response With Scour Depth. The Slight Increase With Increasing Scour Depth Supports The Premise That The Scour Induced Bearing Stresses Are Insensitive To Increases in Scour Depth.**

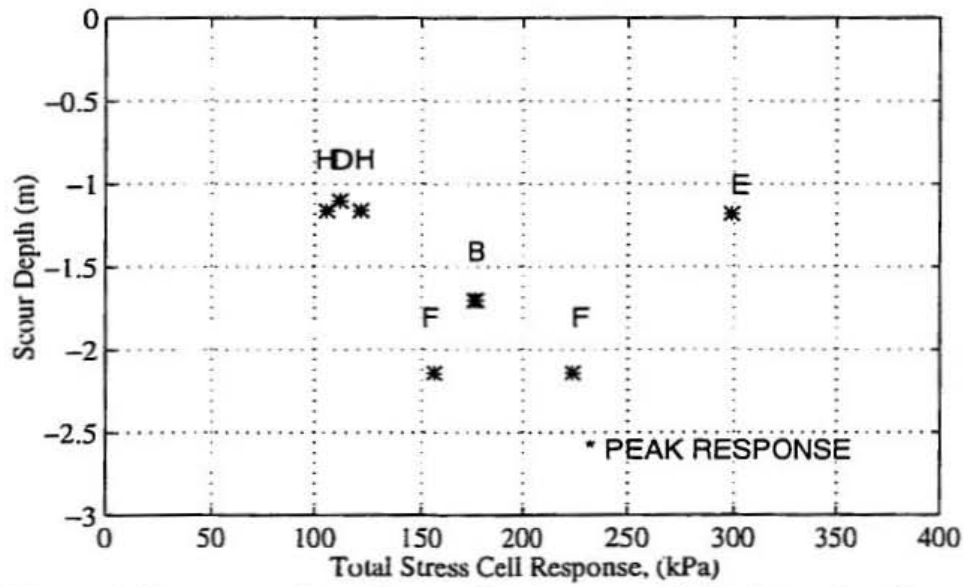

Figure 8.10 **Total Stress Cell Response With Scour Depth**

8.5 Summary

The preceding discussion has important implications in terms of understanding the mechanisms governing ice keel scour in sand. For example, it has been shown that the loads associated with scouring can be analysed in terms of basal shear beneath the base of the static soil wedge. Moreover, it is also suggested that the relationship between the horizontal and vertical scour forces is given by tan ϕ, where ϕ is the internal angle of friction of the sand. This correlation requires that the measured horizontal force be manipulated such that the horizontal shear resistance associated with the vertical sides of the static soil wedge is removed. The removal of the horizontal shear resistance in the vertical plane is based on an extension of empirical rules for calculating the ultimate lateral resistance of rigid piles. The linear relationship between vertical force expressed as load per unit scour width versus scour depth is also shown to be valid using the analogy of a direct shear box.

In terms of subscour soil displacements, the current test series confirms the potential for significant soil disturbance below the base of the scour. A more important implication arises from the validation of Been's (1990) shear dragging hypothesis. It is implicit that if the observed data can be idealised as being representative of a direct shear or direct simple shear test, then the free-field subscour displacements can also be interpreted in terms of a direct simple shear mechanism.

The observations offered have important implications for numerical analysis, particularly in terms of the prescribed boundary conditions and the idealization of ice keel scour. Previous researchers in this area (Lach, 1996; Yang *et al.* 1994; C-CORE, 1995f) have elected to model the complete keel configuration in relation to the model seabed. However, in recognition of the suggested relationship between the horizontal and vertical forces, it is felt that a more appropriate analysis would resemble that of a direct shear or direct simple shear device. It was noted that various workers (Potts et al, 1987; Budhu and Britto, 1987; Cividini and Gioda, 1992; Dounias and Potts, 1993) have examined the behaviour of soils via numerical analysis of shear devices.

Chapter Nine

Conclusions and Recommendations

As part of a larger program examining ice keel scour, the experimental program and analysis described in this thesis has yielded a large amount of quantitative and semi-quantitative data regarding ice keel scour in sand. The experimental program involved towing an instrumented model ice keel of set geometry across a model testbed at a set scour depth while under the influence of a centrifugal force. The testbed was constructed of silica sand placed according to a predetermined relative density. Transducers embedded in the model testbed provided information on scour-induced stresses and pore pressures. Instruments positioned on the model ice keel monitored keel displacement, horizontal and vertical loads and the model keel/ soil interface pressures. The experiments investigated the effect of variations in scour depth, attack angle, scour width and sand state. Passive markers, in the form of coloured sand horizons and coloured spaghetti strands, provided information regarding subscour sand displacements. Based on the test results and observations described in this thesis, the following conclusions and recommendations are offered:

(i) The development of a static soil "dead wedge" beneath the model ice keel was instrumental in defining the observed variation in scour loads and subscour soil deformation.

The static soil wedge was identified through observation of deformed passive markers placed in the model testbed.

(ii) The passive soil markers were instrumental in identification of rupture planes in the surcharge mound and the documentation of horizontal and vertical subscour soil deformations. The observed rupture planes provided insight into both the failure mechanism and the cyclic variation in the vertical and horizontal load displacement plots. With respect to the observed subscour soil deformations, the data set confirmed the potential for significant soil displacement below the base of the scour.

(iii) In assuming that the measured vertical scour load and the measured horizontal scour load (minus the horizontal shear resistance in the vertical plane) are analogous to the applied normal force (σ) and measured shear force (τ) in a direct shear test, it was determined that the ratio of vertical to horizontal scour loads is given by tan ϕ, where ϕ is the internal angle of friction of the sand This finding was significant since it implies that the ratio of horizontal to vertical load is a function of shear beneath the model ice keel. A finding which supports Been's (1990) shear dragging hypothesis.

(iv) There is a linear relationship between measured vertical load expressed as load per unit width and scour depth. This relationship was shown to be valid using the analogy of a direct shear box and the static soil wedge identified beneath the model ice keel.

(v) The increase in the area under shear due to the development of the static soil wedge beneath the model ice keel offset the increase in vertical load so that there is little net change. The bearing stress is therefore insensitive to changes in scour depth within the range of scour depths under consideration. The concept of a constant bearing stress and the validation of Been's (1990) shear dragging hypothesis has an important implication with respect to the magnitude and extent of subscour soil deformations. It is concluded that the observed subscour soil deformations were in effect direct simple shear, governed by the stress strain behaviour of the sand.

In recognition of the limited number of data points, it is recommended that further work be undertaken in order to validate the above observations and conclusions. This may be in the form of further centrifuge modelling involving extreme scour events or through numerical analysis. With respect to the latter, it is recommended that the problem of ice keel scour should be approached using the analogy of a direct or direct simple shear device.

References

Abdelnour, R., Lapp, D., Haider, S., Shinde, S.B., and Wright, B., (1981). Model Tests of Sea Bottom Scouring. Proceedings, 6th International Conference on Port and Ocean Engineering under Arctic Conditions, Québec City, Québec, pp. 688-705

Abdelnour, R. and Graham, B., (1984). Small-scale Tests of Sea Bottom Ice Scouring. Proceedings, Ice Symposium, International Association for Hydraulic Research, Hamburg, West Germany, pp. 267-279

Been, K., Palmer, A. and Comfort, G., (1990a). Analysis of Subscour Stresses and Probability of Ice Scour-Induced Damage for Buried Submarine Pipelines. Volume II, Deterministic Model of Ice-Soil-Pipe Interaction. Report Prepared by Golder Associates Ltd., Andrew Palmer and Associates Ltd., and Fleet Technology Limited for Canada Oil and Gas Lands Administration, 204p.

Been, K., Kosar, K., Hachey, J., Rogers B.T. and Palmer, A., (1990b). Ice Scour Models. Proceedings, 9th International Conference on Offshore Mechanics and Arctic Engineering, Houston, Texas, Vol. V, pp. 179-188

Been, K., (1990). Mechanisms of Failure and Soil Deformation During Scouring. Proceedings, Workshop on Ice Scouring and the Design of Offshore Pipelines. Canada Oil and Gas Lands Administration, Calgary, Alberta, pp. 179-192

Broms, B.B., (1964). Lateral Resistance of Piles in Cohesionless Soils. ASCE, Journal of the Soil Mechanics and Foundations Division, 90(SM3), pp. 123-156

Budhu, M. and Britto, A., (1987). Numerical Analysis of Soils In Simple Shear Devices. Soils and Foundations, Vol. 27, No. 2, pp. 31-41

C-CORE, (1995a). Pressure Ridge Ice Scour Experiment, Phase 3: Centrifuge Modelling of Ice Keel Scour. PRISE 01B, Data Report. Prepared by C-CORE - Centre for Cold Ocean Resources Engineering, March 1995, 8p.

C-CORE, (1995b). Pressure Ridge Ice Scour Experiment (PRISE), Phase 3: Centrifuge Modelling of Ice Keel Scour. PRISE 01C, Data Report. Prepared by C-CORE - Centre for Cold Ocean Resources Engineering, March 1995, 8p.

C-CORE, (1995c). Pressure Ridge Ice Scour Experiment (PRISE), Phase 3: Centrifuge Modelling of Ice Keel Scour. PRISE 09, Data Report. Prepared by C-CORE - Centre for Cold Ocean Resources Engineering, March 1995, 8p.

C-CORE, (1995d). Pressure Ridge Ice Scour Experiment, Phase 3: Centrifuge Modelling of Ice Keel Scour. PRISE 10, Data Report. Prepared by C-CORE - Centre for Cold Ocean Resources Engineering, March 1995, 8p.

C-CORE, (1995e). Pressure Ridge Ice Scour Experiment, PRISE: Phase 3 - Centrifuge Modelling of Ice Keel Scour: Draft Final Report. April 1995. Publication 95-C12, 52p.

C-CORE, (1995f). Pressure Ridge Ice Scour Experiment, PRISE: Phase 3 - Engineering Model Application: Draft Final Report. August 1995, Publication 95-C19, 61p.

Chari, T.R., (1975). Some Geotechnical Aspects of Iceberg Grounding. Ph.D. Thesis, Memorial University of Newfoundland, St. John's, 181p.

Chari, T.R., (1979). Geotechnical Aspects Of Iceberg Scours On Ocean Floors. Canadian Geotechnical Journal, Vol. 16, No. 2, pp. 379-390

Chari, T.R. and Muthukrisknaiah, K., (1978). Iceberg Threat to Ocean Floor Structures. Proceedings, Symposium on Ice Problems, International Association for Hydraulic Research, Luleå, Sweden, pp. 421-435

Chari, T.R. and Green, H.P., (1981). Iceberg Scour Studies in Medium Dense Sands. Proceedings, 6th International Conference on Port and Ocean Engineering under Arctic Conditions, Québec City, Québec, Vol. 2, pp. 1012-1019

Cividini, A. and Gioda, G., (1992). A Finite Element Analysis of Direct Shear Tests on Stiff Clays. International journal For Numerical and Analytical Methods in Geomechanics, Vol. 16, pp. 869-886

Craig, W.H., James R.G. and Schofield, A.N., (1988). Centrifuges in Soil Mechanics. A.A. Balkema, Rotterdam, 266p.

Cunnard, C., (1993). Pressure Ridge Ice Scour Experiment: Design and Development of a Centrifuge Model. Work Term Report, Memorial University of Newfoundland, 28p.

Dixon, J.M., (1988). Centrifuge Modelling Of Fold-Thrust Mountain Belts: Thrust Ramp Nucleation. In: Centrifuge '88, Proceedings of the International Conference on Geotechnical Centrifuge Modelling (J.F. Corte, ed.). A.A. Balkema, Rotterdam, pp. 553-562

Dounias, G.T. and Potts, D.M., (1993). Numerical Analysis of Drained Direct and Simple Shear Tests. Journal of Geotechnical Engineering, Vol. 119, No. 12, pp. 1870-1891

Dunwoody, A.B., Losch, J.A. and Been, K., (1984). Ice/Berm Interactions. Proceedings, 16th Annual Offshore Technology Conference, Houston, Texas, pp. 223-229

FENCO - Foundation of Canada Engineering Corporation Limited, (1975). An Analytical Study of Ice Scour on the Sea Bottom. Report for the Arctic Petroleum Operators Association, APOA Project No. 69, 241p.

Gilbert, G.R., (1990). Scour Shape and Subscour Disturbance Studies From The Canadian Beaufort Sea. In: Clark, J.I., Konuk, I., Poorooshasb, F., Whittick, J. and Woodworth-Lynas, C.M.T., Ice Scouring and the Design of Offshore Pipelines. Proceedings of an invited workshop, April 18-19th, Calgary, Alberta. Canada Oil and Gas Lands Administration and Centre for Cold Ocean Resources Engineering, pp. 127-144

Green, H.P., (1984). Geotechnical Modelling of Iceberg-Seabed Interaction. M.Eng. thesis, Memorial University of Newfoundland, St. John's, Newfoundland, 165p.

Hnatiuk, J. and Wright, B.D., (1983). Sea Bottom Scouring in the Canadian Beaufort Sea. Proceedings, 15th Annual Offshore Technology Conference, Houston, Texas, Vol. 3, pp. 35-40

Hodgson, G.J., Lever, J.H., Woodworth-Lynas, C.M.T. and Lewis, C.F.M. (editors), (1988). The Dynamics of Iceberg Grounding and Scouring (DIGS) Experiment and Repetative Mapping of the Eastern Canadian Continental Shelf. Environmental Studies Research Funds Report, No. 094, Ottawa, 316p.

Köenig, D., Jessberger, H.L., Bolton, M., Phillips, R., Bagge, G., Rezi, R. and Garnier J., (1994). Pore Pressure Measurement During Centrifuge Modelling Tests: Experience of Five Laboratories. Centrifuge 94, Leung, Lee, and Tan (eds), Balkema, Rotterdam, pp. 101-108

Kutter, B.L., Idriss, I.M . Khonke, T.,Lakeland, J., Li, X.S., Sluis, W., Zeng, X., Tauscher, R.C., Goto, Y. and Kubodera, I., (1994). Design of a Large Earthquake Simulator at UC Davis. Centrifuge 94, Leung, Lee, and Tan (eds), Balkema, Rotterdam, pp. 169-176

Lach, P., (1996) Centrifuge Modelling of Ice Scour in Clay, Forthcoming Ph.D. Thesis, Memorial University of Newfoundland, St. John's, Newfoundland.

Lach, P. and Clark, J.I., (1994). Ice Scouring of the Seabed. Centrifuge 94, Leung, Lee, and Tan (eds), Balkema, Rotterdam, pp. 803-808

Lewis, C.F.M., (1977). The Frequency and Magnitude of Drift Ice Groundings From Ice-Scour Tracks in the Canadian Beaufort Sea. Proceedings, 4th International Conference on Port and Ocean Engineering Under Arctic Conditions, St. John's, Newfoundland, Vol. 1, pp. 568-576

Lewis, C.F.M. and Blasco, S.M., (1990). Character And Distribution Of Sea-Ice And Iceberg Scours. In: Clark, J.I., Konuk, I., Poorooshasb, F., Whittick, J. and Woodworth-Lynas, C.M.T., Ice Scouring and the Design of Offshore Pipelines. Proceedings of an invited workshop, April 18-19th, Calgary, Alberta. Canada Oil and Gas Lands Administration and Centre for Cold Ocean Resources Engineering: pp. 57-101

Longva, O. and Bakkejord, K.J., (1990). Iceberg Deformation And Erosion In Soft Sediments, Southeast Norway. Marine Geology, 92, pp. 87-104

Lovell, S. and Schofield, A.N., (1986). Centrifuge Modelling Of Sea Ice. Proceedings of the 1st International Conference on Ice Technology, Springer-Verlag, Berlin: pp. 105-113

Mitchell, R. and Stratton, B.C., (1994). LNAPL Penetration into Porous Media. Centrifuge 94, Leung, Lee, and Tan (eds), Balkema, Rotterdam, pp. 345-350

Palmer, A., Konuk, I., Love, J., Been, K. and Comfort, G., (1989). Ice Scour Mechanisms. Proceedings, Tenth International Conference on Port and Ocean Engineering Under Arctic Conditions, Luleå, 1, pp. 123-132

Palmer, A., Konuk, I., Comfort, G. and Been, K., (1990). Ice Gouging and the Safety of Marine Pipelines. Proceedings, 22nd Annual OTC, Houston, Texas, May 7-10, OTC 6371, pp. 235-244

Palmer, A., (1990). Design of Marine Pipelines in Seabed Vulnerable to Ice Scour. In: Clark, J.I., Konuk, I., Poorooshasb, F., Whittick, J. and Woodworth-Lynas, C.M.T., Ice Scouring and the Design of Offshore Pipelines. Proceedings of an Invited Workshop, April 18-19th, Calgary, Alberta. Canada Oil and Gas Lands Administration and Centre for Cold Ocean Resources Engineering: pp. 57-101

Paulin, M.J., (1992). Physical Model Analysis Of Iceberg Scour In Dry And Submerged Sand. M.Eng. Thesis, Faculty of Engineering, Memorial University of Newfoundland, St. John's, 183p.

Pelletier, B.R., and Shearer, J.M., (1972). Sea Bottom Scouring in the Beaufort Sea Of The Arctic Ocean. Proceedings, 24th International Geological Congress, Montreal, Québec, Section 8, pp. 251-261

Peltzer, G. and Garnier, J., (1988). Experimental approach in a centrifuge of large scale continental tectonics in Asia. Centrifuge '88, Proceedings of the International Conference on Geotechnical Centrifuge Modelling (J.F. Corté, ed.), A.A. Balkema, Rotterdam: pp. 563-574

Phillips, R., Clark, J.I., Paulin, M.J., Meaney, R., Millan, D.E.L. and Tuff, K., (1994). Canadian National Centrifuge Centre With Cold Regions Capabilities. Centrifuge 94, Leung, Lee, and Tan (eds), Balkema, Rotterdam, pp. 57-62

Pilgrim, N.K. and Zeng, X., (1994). Slope Stability with Seepage In Centrifuge Model Earthquakes. Centrifuge 94, Leung, Lee, and Tan (eds), Balkema, Rotterdam, pp. 233-238

Poorooshasb, F., (1989). Large Scale Laboratory Tests Of Seabed Scour. C-CORE Contract Report No. 89-C15, 56p.

Poorooshasb, F., (1990). On Centrifuge Use For Ocean Research. Marine Geotechnology, Vol 9, pp. 141-158

Poorooshasb, F., Clark J.I. and Woodworth-Lynas C.M.T., (1989). Small-Scale Modelling of Iceberg Scouring of the Seabed. Proceedings, 10th International Conference on Port and Ocean Engineering under Arctic Conditions, Lulea, Sweden, Vol. I, pp. 133-145

Poorooshasb, F. and Clark, J.I., (1990). On Small-Scale Ice Scour Modelling. In: Clark, J.I., Konuk, I., Poorooshasb, F., Whittick, J. and Woodworth-Lynas, C.M.T., Ice Scouring and the Design of Offshore Pipelines. Proceedings of an invited workshop, April 18-19th, Calgary, Alberta. Canada Oil and Gas Lands Administration and Centre for Cold Ocean Resources Engineering: pp. 193-235

Potts, D.M., Dounias, G.T. and Vaughan, P.R., (1987). Finite Element Analysis Of The Direct Shear Box Test. Geotechnique, Vol. 37, No. 1, pp. 11-23

Prakash, S., (1962). Behaviour of Pile Groups Subject to Lateral Loads, PhD Thesis, University of Illinois, Urbana, Illinois, U.S.

Prasad, K.S.R., (1985). Analytical and Experimental Modelling of Iceberg Scours, M.Eng. Thesis, Memorial University of Newfoundland, St. John's, Newfoundland, 173p.

Schofield, A.N., (1980). Cambridge Geotechnical Centrifuge Operations. Geotechnique, 30, No. 3, pp. 227-268

Smith, C.C., (1991). Thaw Induced Settlement Of Pipelines In Centrifuge Model Tests. Ph.D. Thesis, Cambridge University: 208p.

Terzaghi, K., (1943). Theoretrical Soil Mechanics. J. Wiley, New York, N.Y., 510p.

Woodworth-Lynas, C.M.T., Christian, P., Seidel, M. and Day T., (1986). Relict Iceberg Scours on King William Island, N.W.T., In: Ice Scour and Seabed Engineering (Lewis, C.F.M., Parrott, D.R., Simpkin, P.G. and Buckley, J.T., Eds.), Environmental Studies Revolving Funds Report No. 049; pp. 64-70

Woodworth-Lynas, C.M.T., Josenhans, H.W., Barrie, J.V., Lewis, C.F.M. and Parrott, D.R., (1991). The Physical Processes Of Seabed Disturbance During Iceberg Grounding And Scouring. Continental Shelf Research, 11, pp. 939-961

Woodworth-Lynas, C.M.T., (1992). The Geology Of Ice Scour. Ph.D. Thesis, University of Wales: 269p.

Woodworth-Lynas, C.M.T. and Barrie, J.V., (1985). Iceberg Scouring Frequencies and Scour Degradation of Canada's Eastern Shelf Areas Using Sidescan Sonar Mosaic Techniques. In: Proceedings of the Eight International Conference on Port and Ocean Engineering Under Arctic Conditions. September, Narassarssuaq, Greenland, Vol. 1, pp. 419-442

Woodworth-Lynas, C.M.T. and Guigné, J.Y., (1991). Iceberg Scours In The Geological Record: Examples From Glacial Lake Agassiz. In: Glacimarine Environments: Processes and Sediments (J.A. Dowdeswell and J.D. Scourse, eds.). Geological Society Special Publication No. 53, pp. 217-233

Woodworth-Lynas, C.M.T., Phillips, R., Clark, J.I., Meaney, R., Hynes, F., and Xiao, X., (1995). PRISE - The Pressure Ridge Ice Scour Experiment: Preliminary Verification of Ice Keel Scour Centrifuge Results Against Field Data. Sea Ice Mechanics and Arctic Modelling Workshop, Anchorage, Alaska, April 25-28, 1995. Poster Presentation.

Yang, Q.S, Lach, P.R., Clark, J.I. and Poorooshasb, H.B., (1994). Finite Element Analysis of Ice Scour With Comparison to Centrifuge Test. In: Clark, J.I., Phillips, R., Woodworth-Lynas, C.M.T., Paulin, M.J., Lach, P.R., Yin, J-H., Poorooshasb, H.B., Yang, Q.S. and Blasco, S., Quantification of Seabed Damage Due to Ice Scour. Proceedings of an Invited Workshop, Calgary, Alberta, Canada, 1994, 22p.

Zelikson, A., (1995). Hydro-Geotechnical Modelling On Large Centrifuges. In: Application of Centrifuge Modelling to Geotechnical Design (W.H. Craig, ed.). A.A. Balkema, Rotterdam: pp. 155-170

Appendix A

Force and Pressure Data for Scour Events B Through H

The horizontal load measurements, expressed in kN for Scours B through H are shown in Figures A.1 to A.7 respectively. The vertical measurements, expressed in kN for Scours B through H are shown in Figures A.8 to A.14. The pressure transducer or spot pressure values, expressed in kPa for Scours B through H are shown in Figures A.15 to A.21. The response of the total stress cell (TLC) in kPa for Scours B through H are given in Figures A.21 through A.31. Finally, the response of the pore pressure transducers, expressed in kPa for Scours B through H are shown in Figures A.32 to A.45.

Horizontal (TC) Load Displacement Data

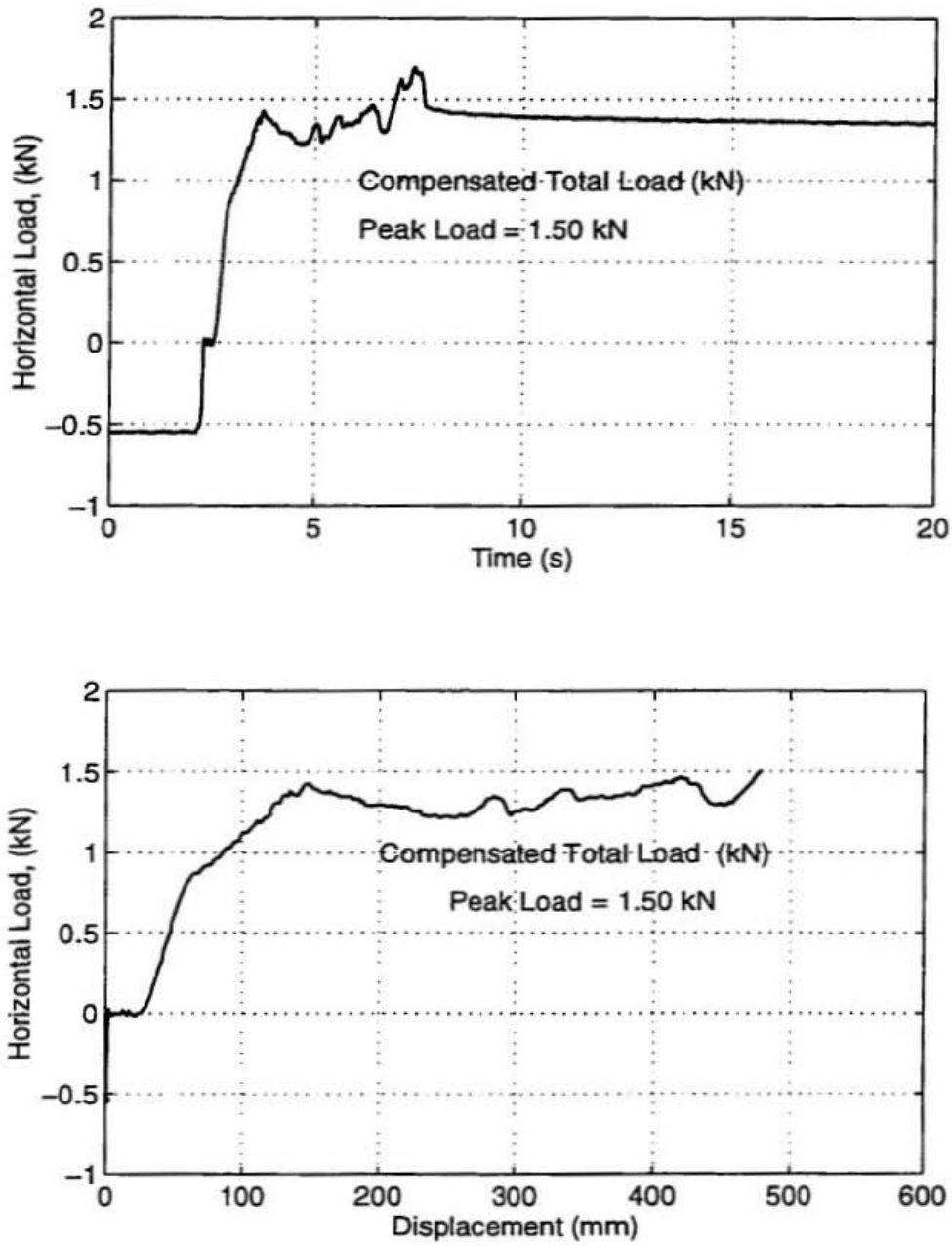

Figure A.1 **Scour B, Compensated Horizontal Load Versus Time and Displacement**

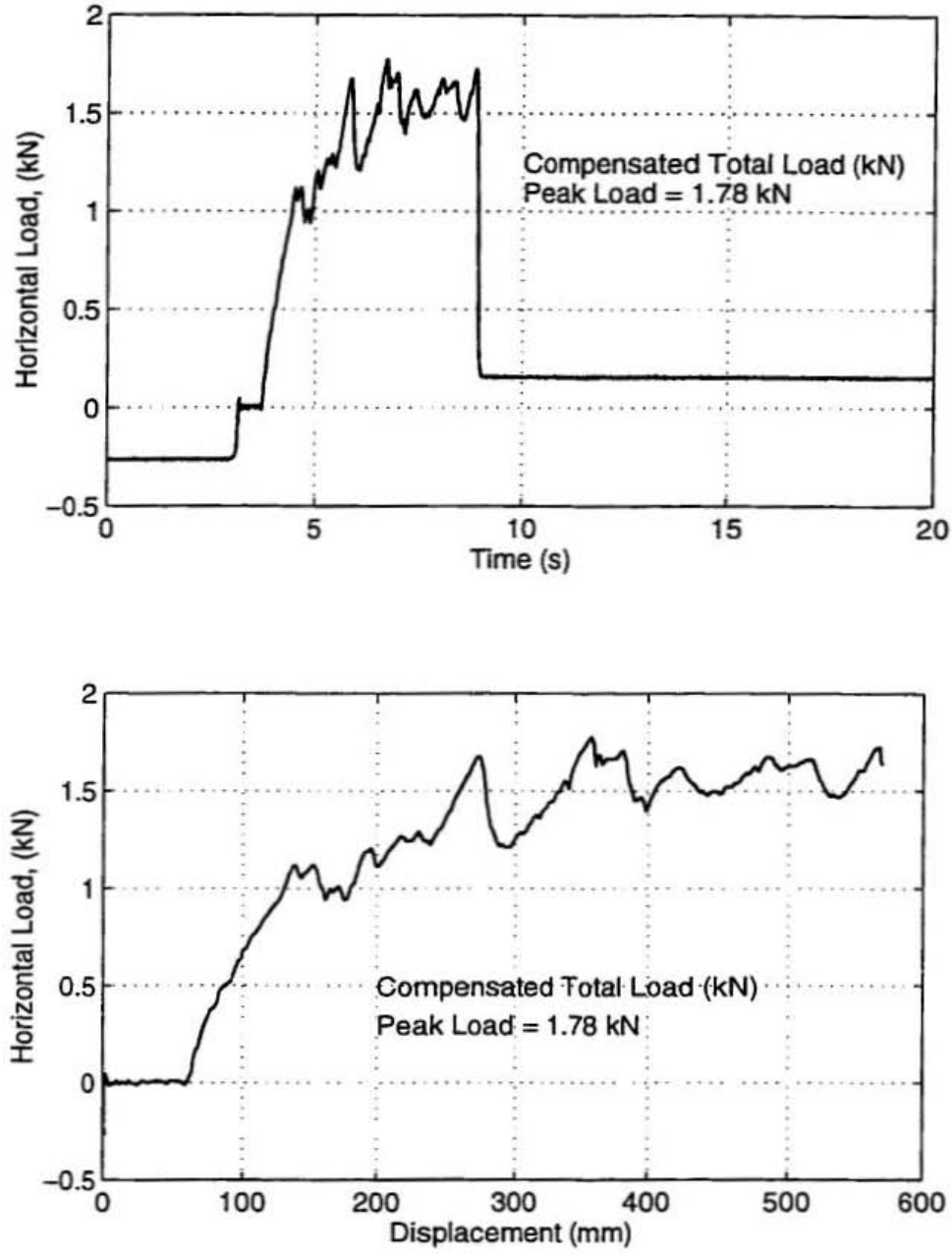

Figure A.2 **Scour C, Compensated Horizontal Load Versus Time and Displacement**

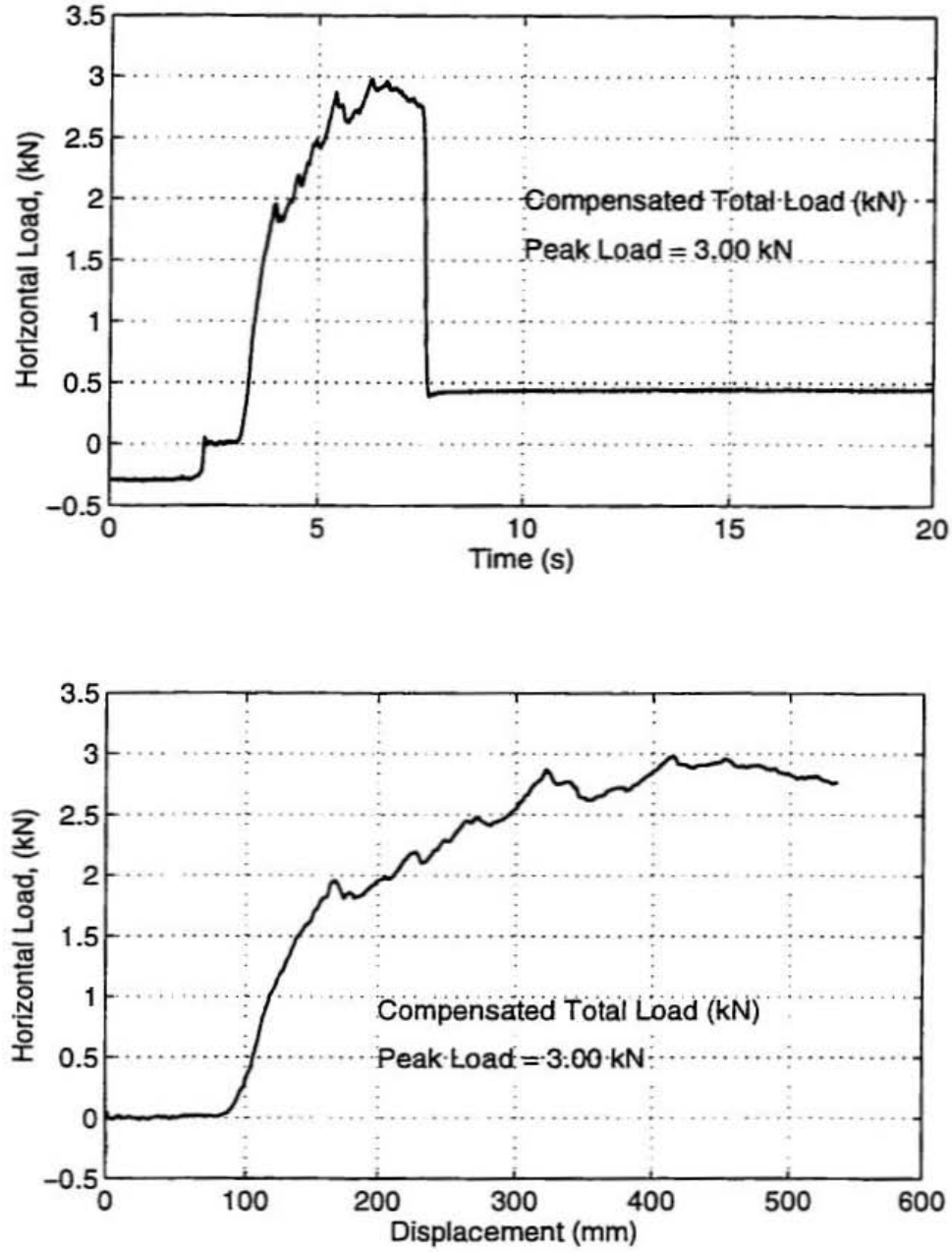

Figure A.3 **Scour D, Compensated Horizontal Load Versus Time and Displacement**

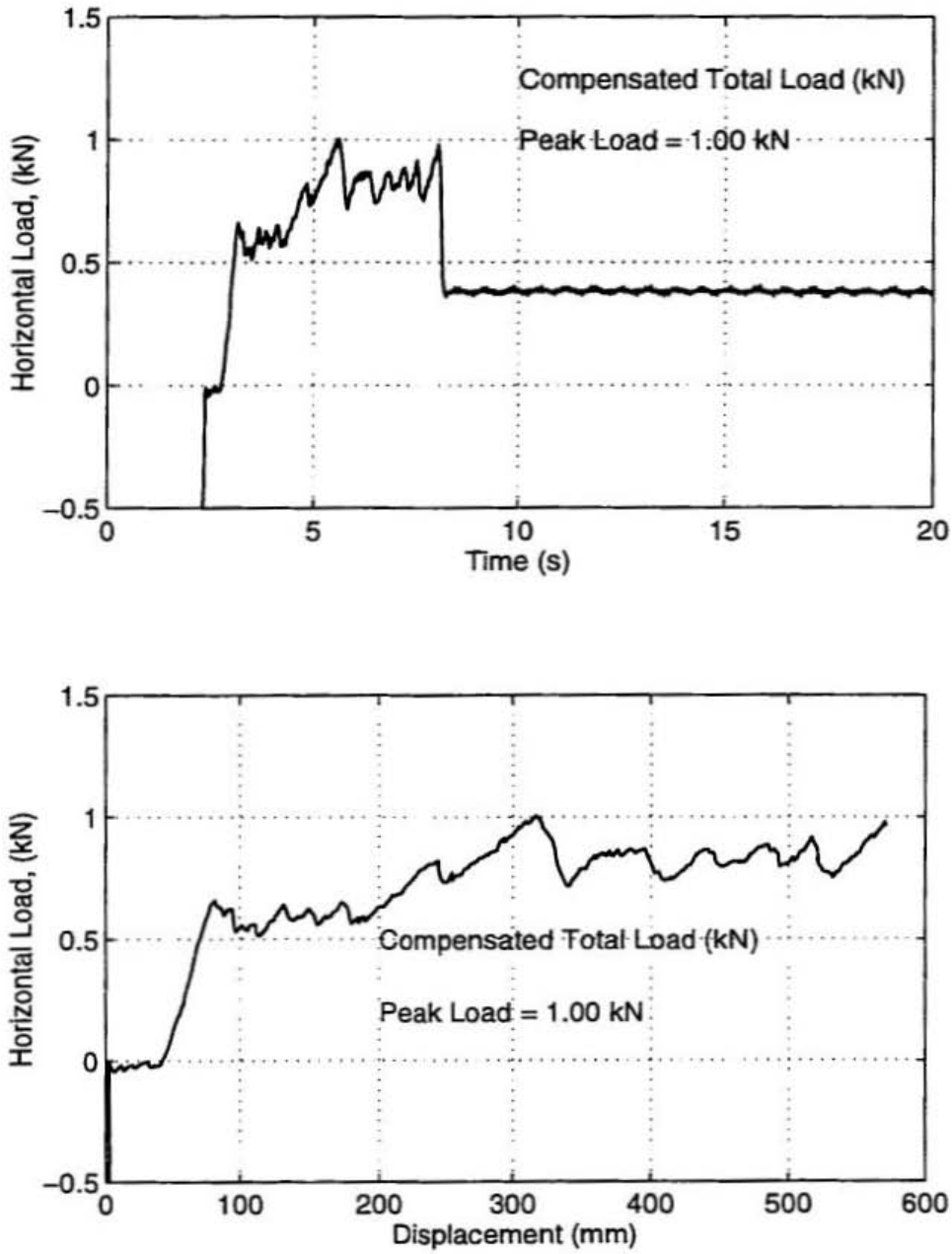

Figure A.4 **Scour E, Compensated Horizontal Load Versus Time and Displacement**

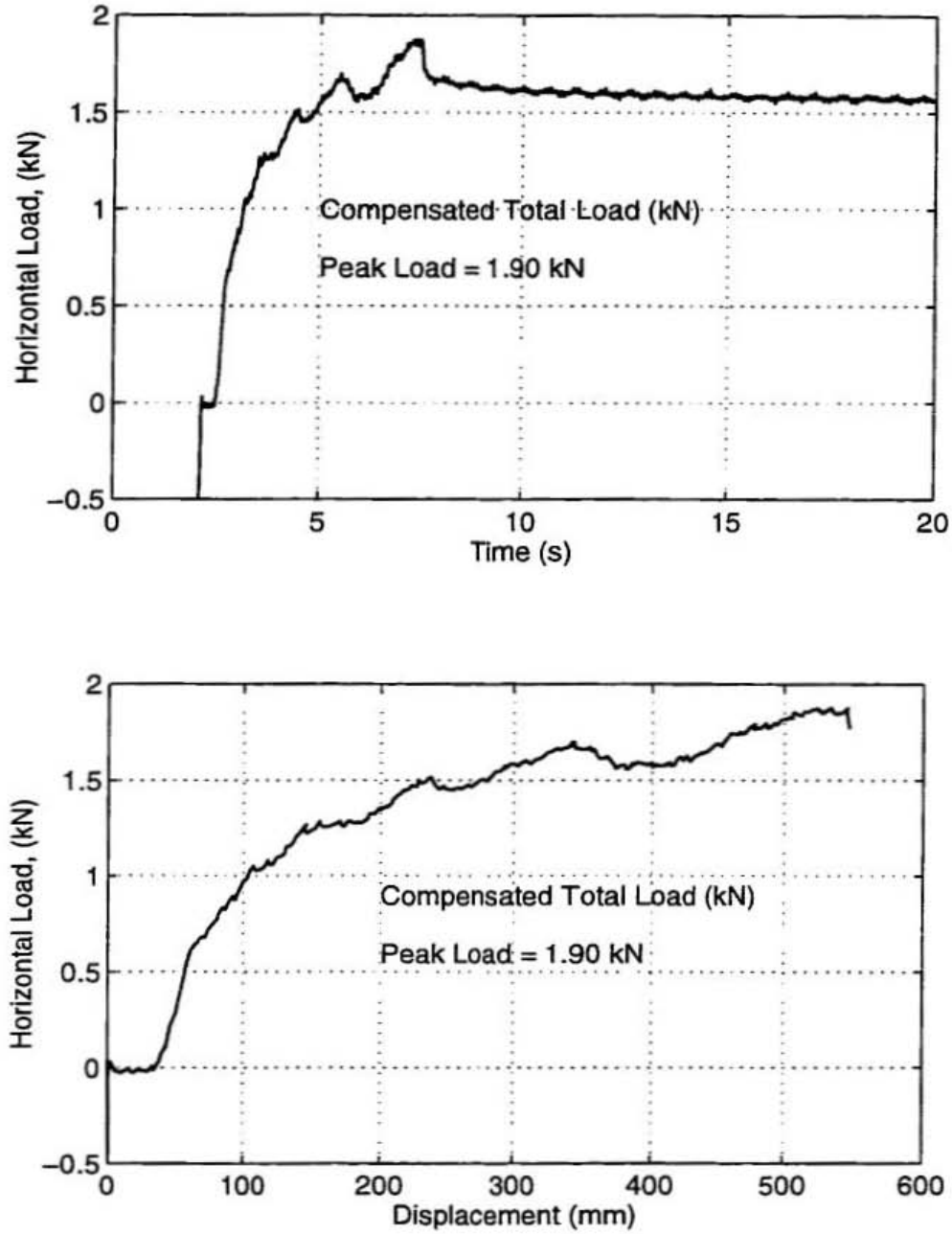

Figure A.5 **Scour F, Compensated Horizontal Load Versus Time and Displacement**

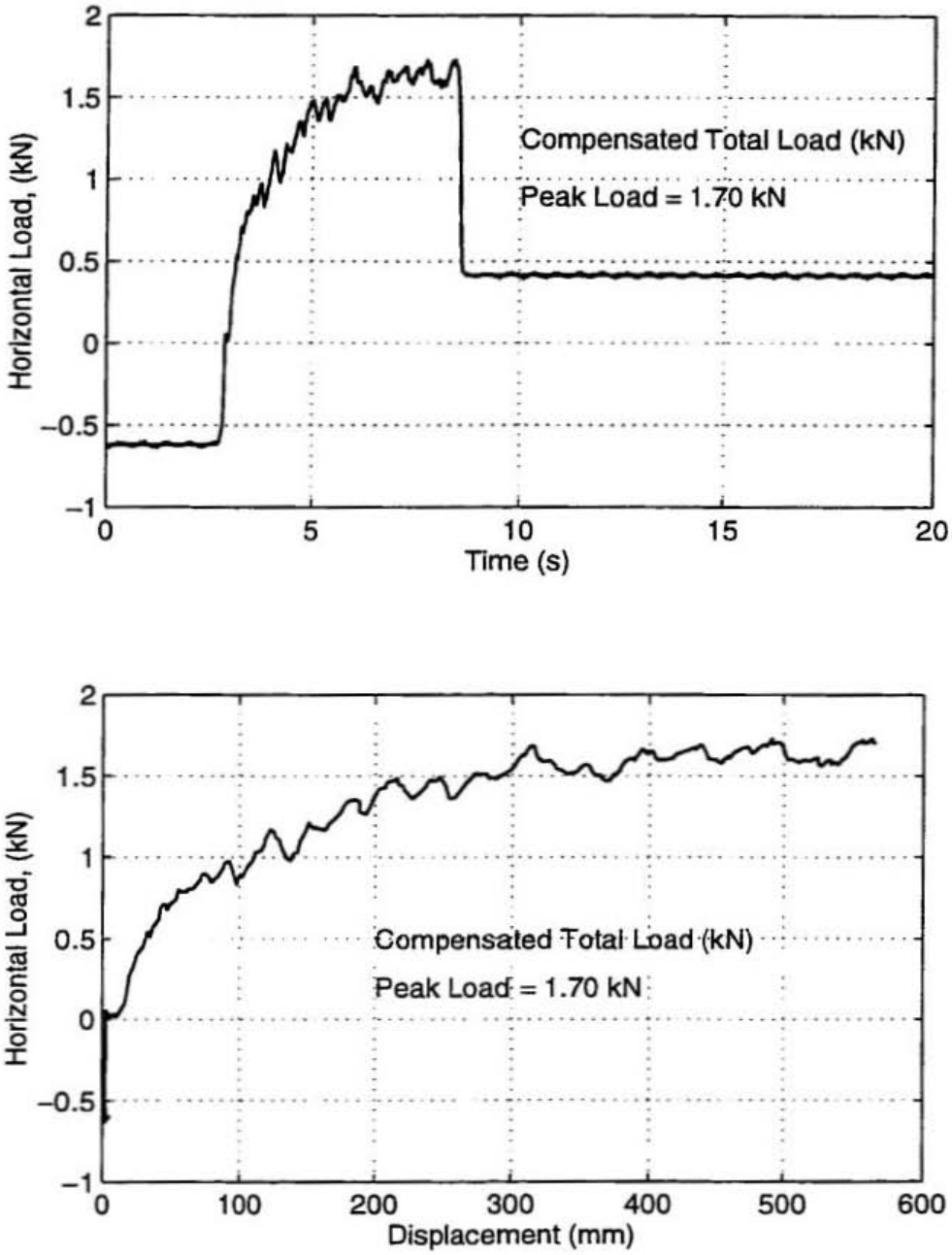

Figure A.6 **Scour G, Compensated Horizontal Load Versus Time and Displacement**

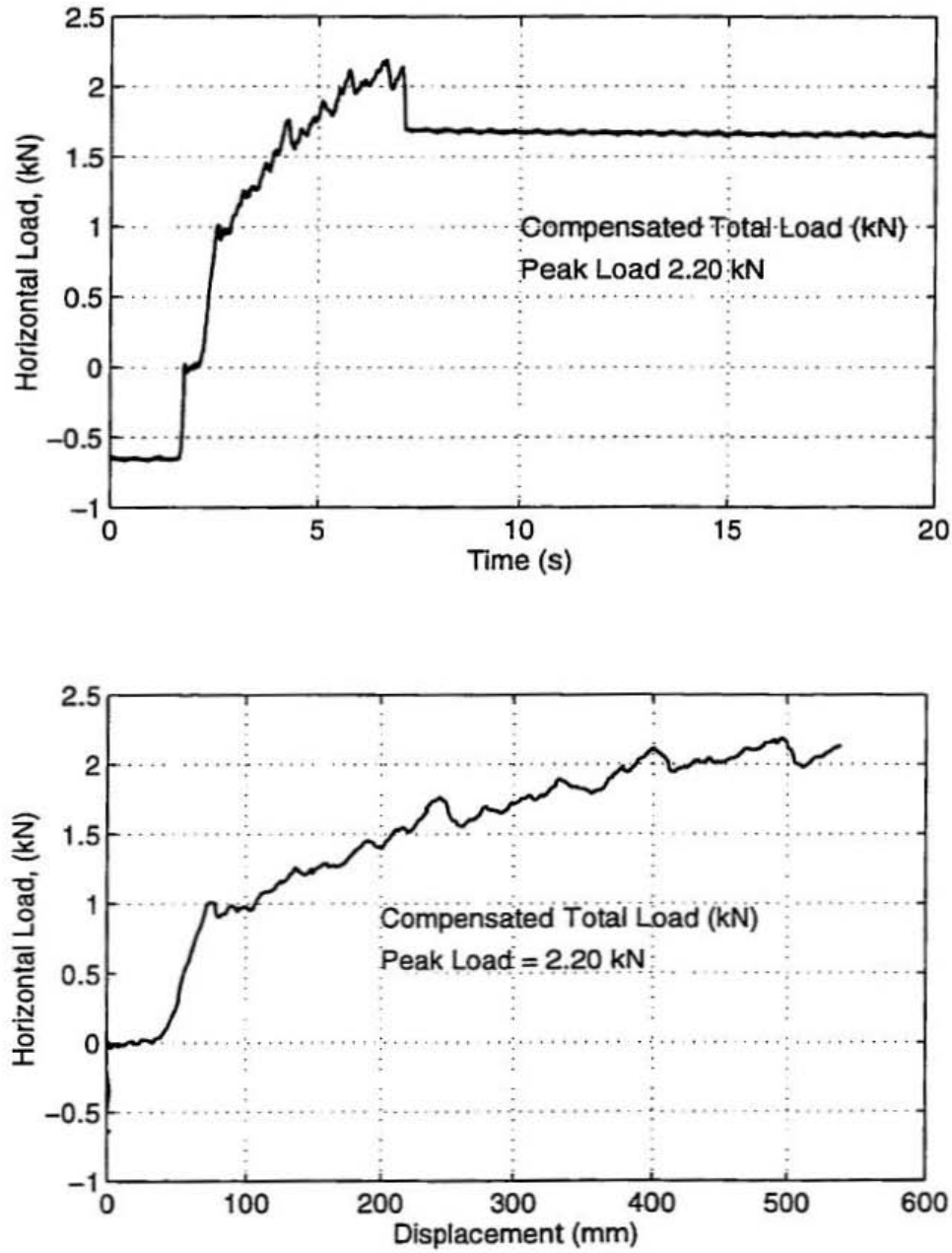

Figure A.7 **Scour H, Compensated Horizontal Load Versus Time and Displacement**

Vertical Load Displacement (LC) Data

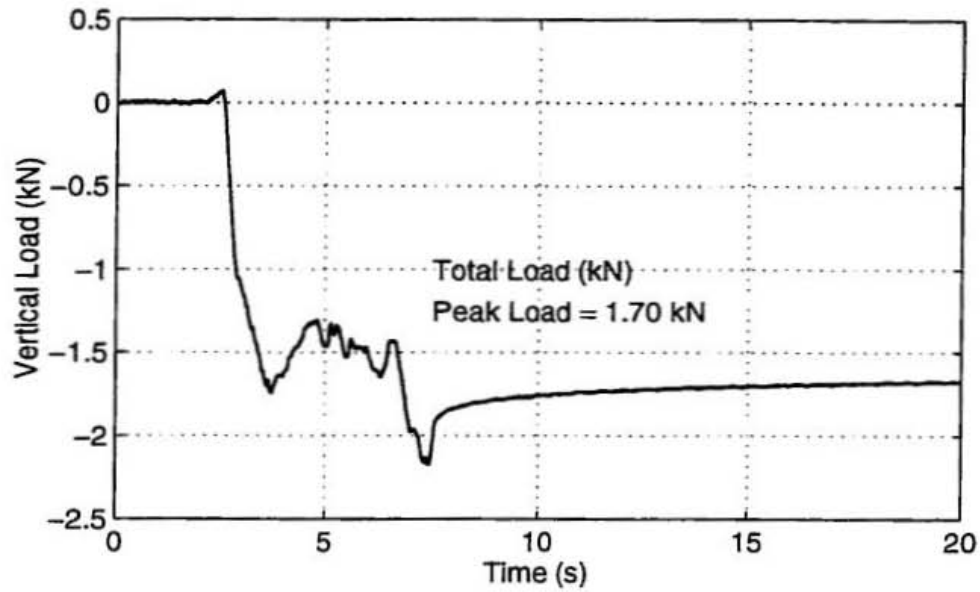

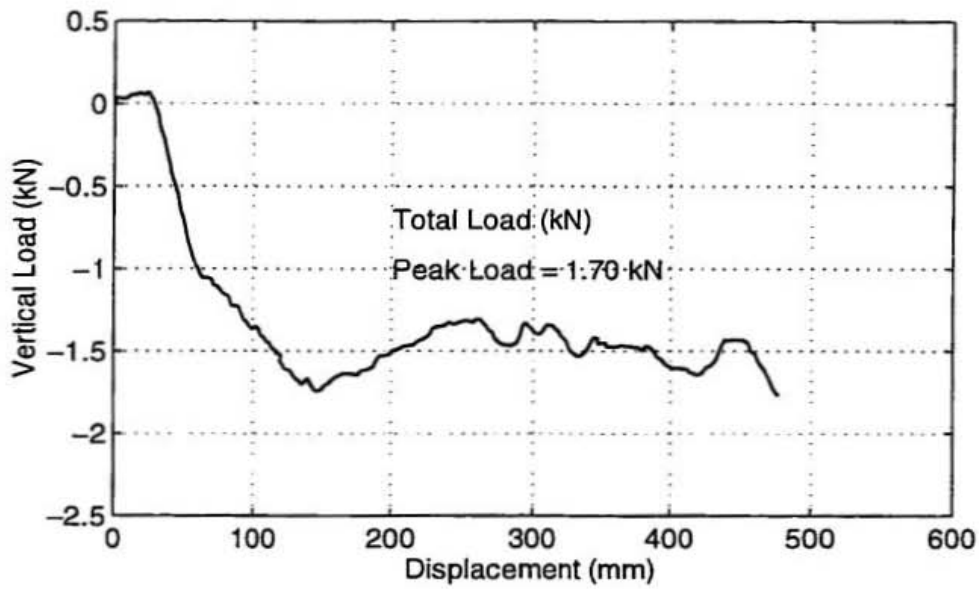

Figure A.8 **Scour B, Measured Vertical Load Versus Time and Displacement**

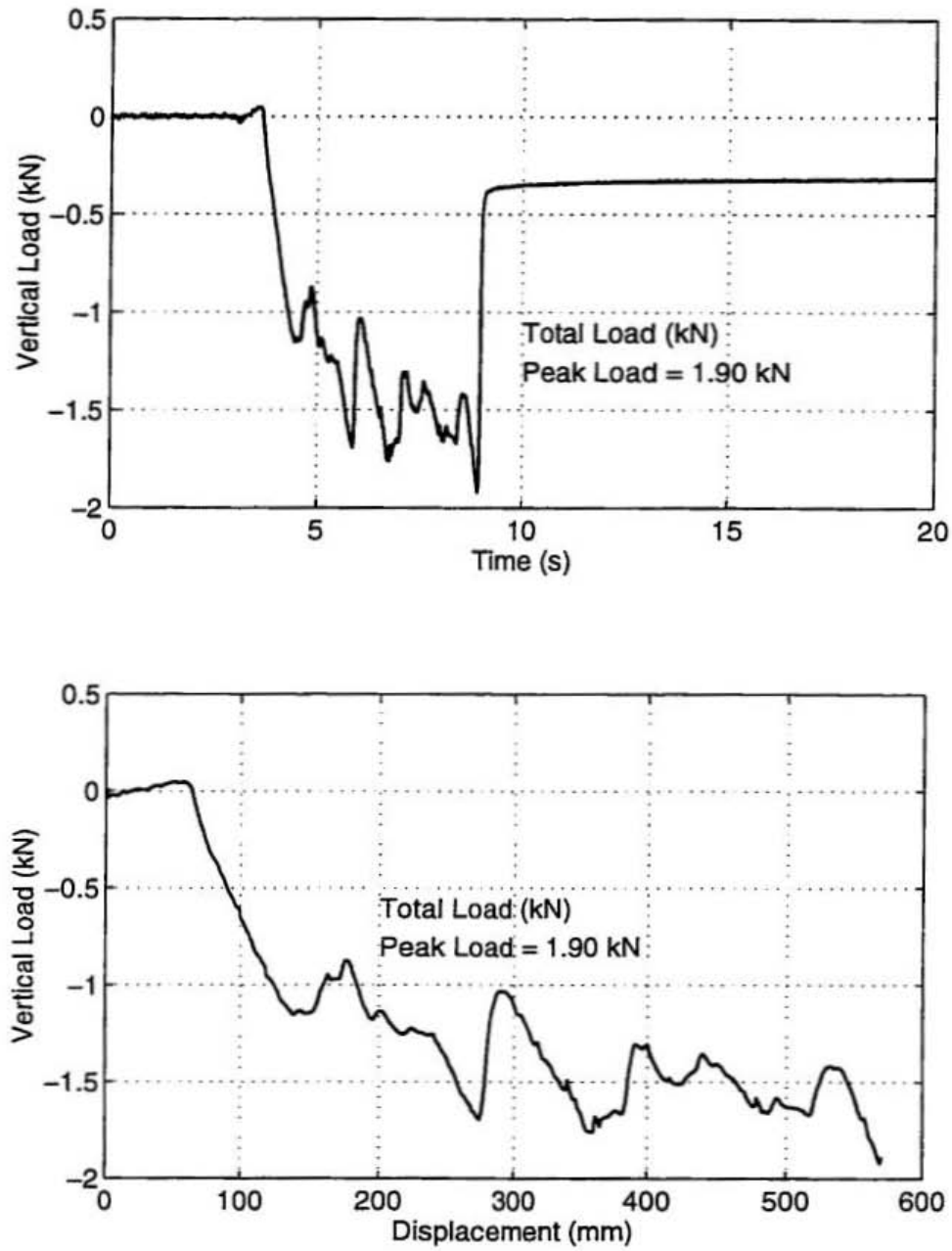

Figure A.9 **Scour C, Measured Vertical Load Versus Time and Displacement**

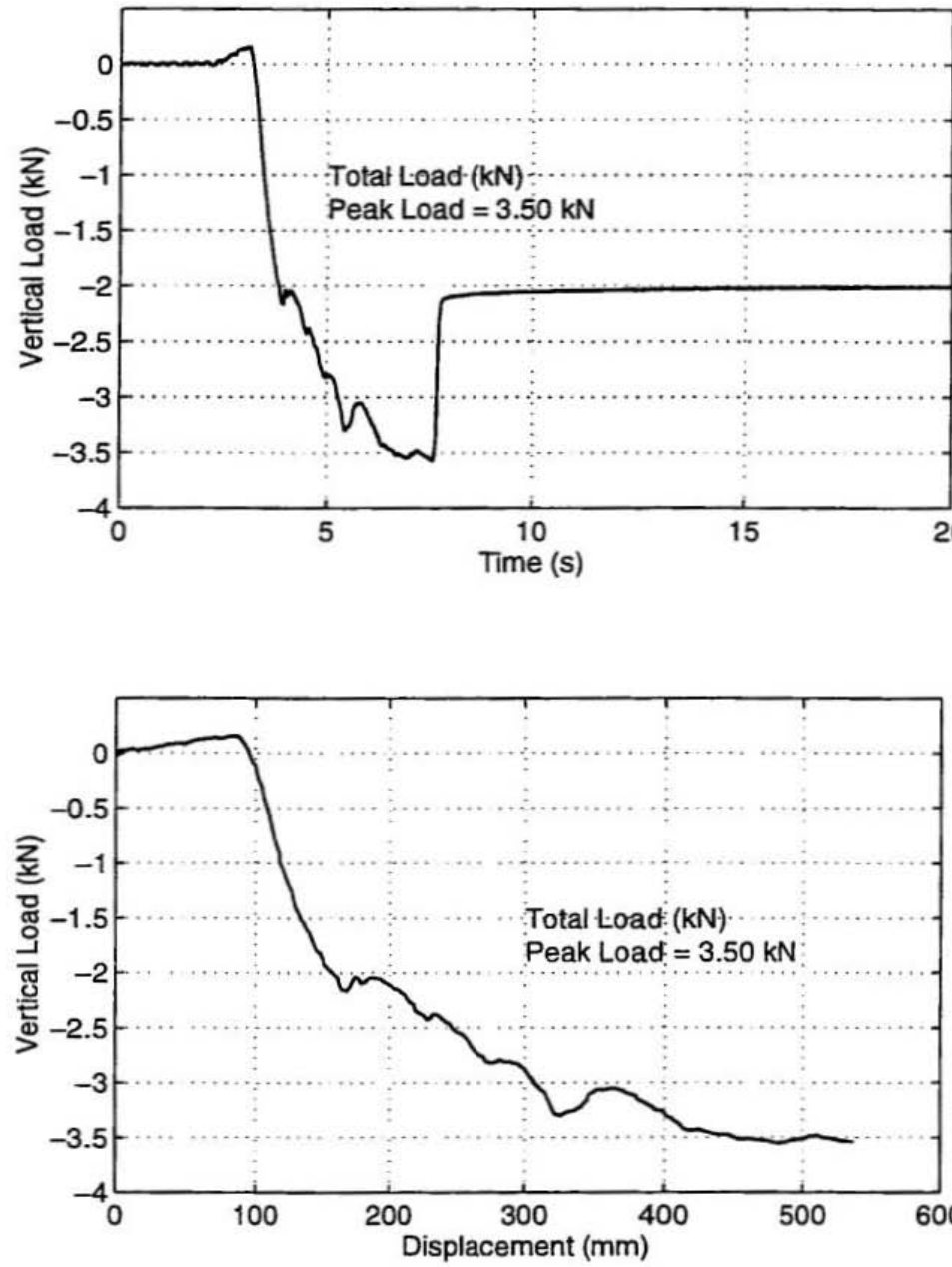

Figure A.10 **Scour D, Measured Vertical Load Versus Time and Displacement**

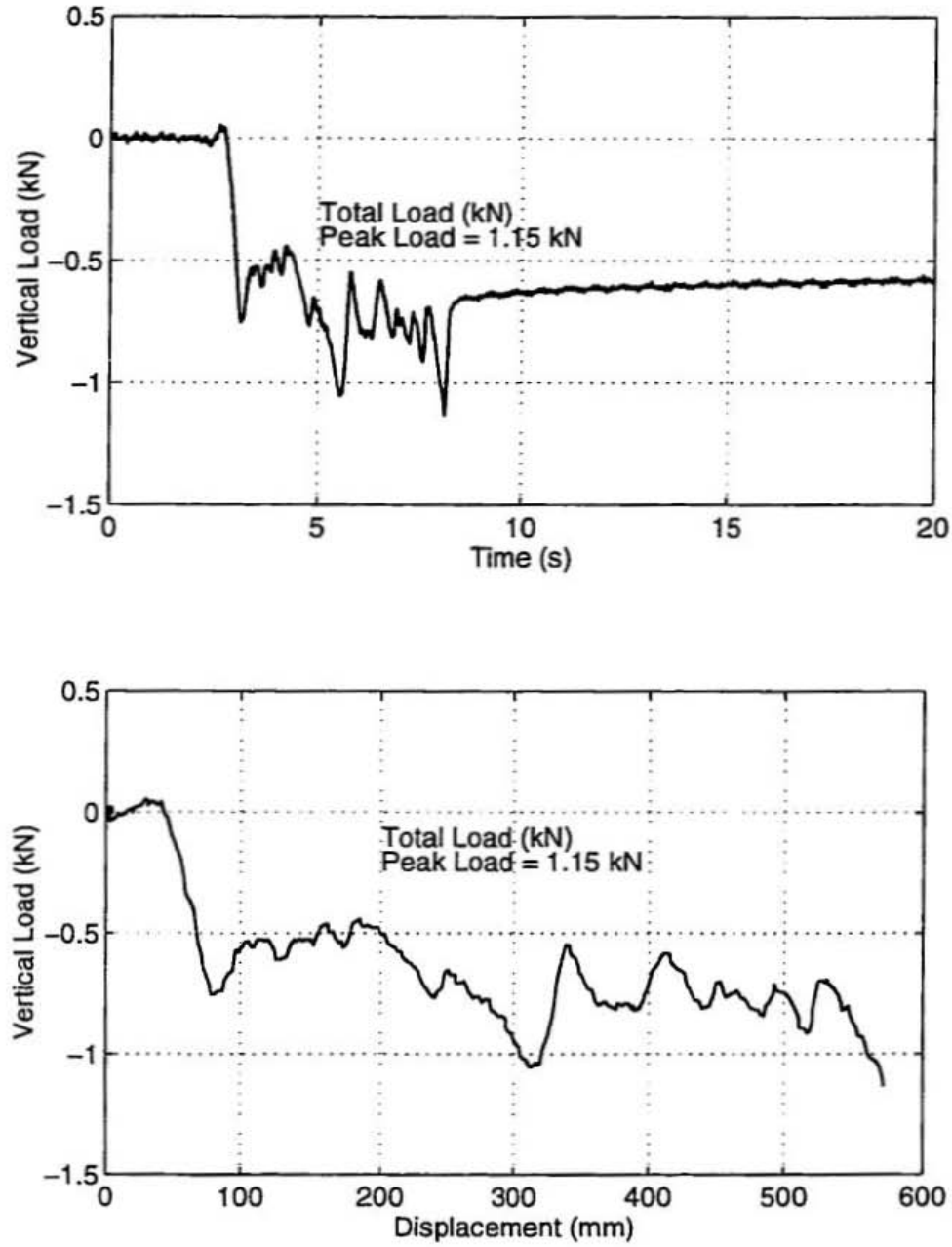

Figure A.11 **Scour E, Measured Vertical Load Versus Time and Displacement**

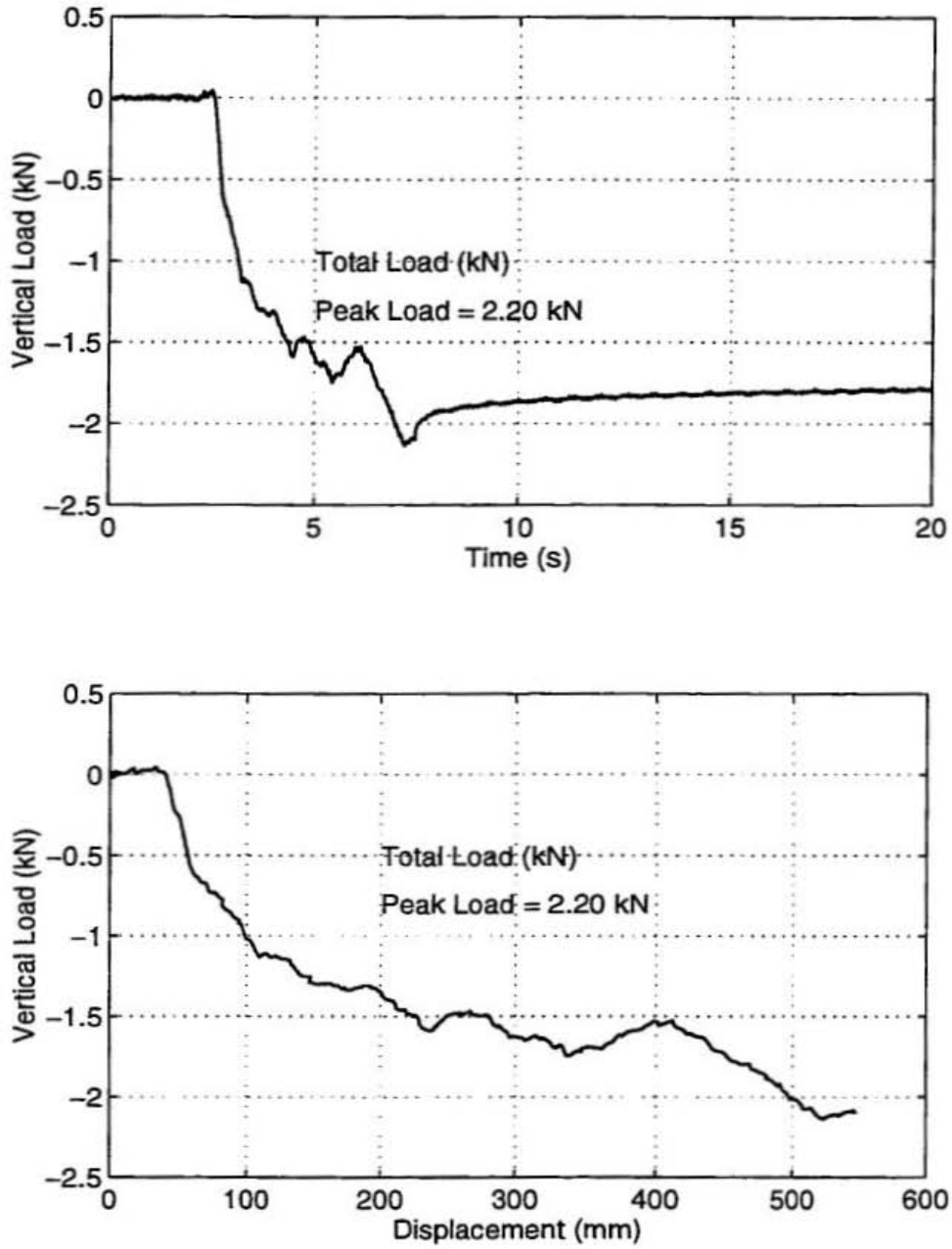

Figure A.12 **Scour F, Measured Vertical Load Versus Time and Displacement**

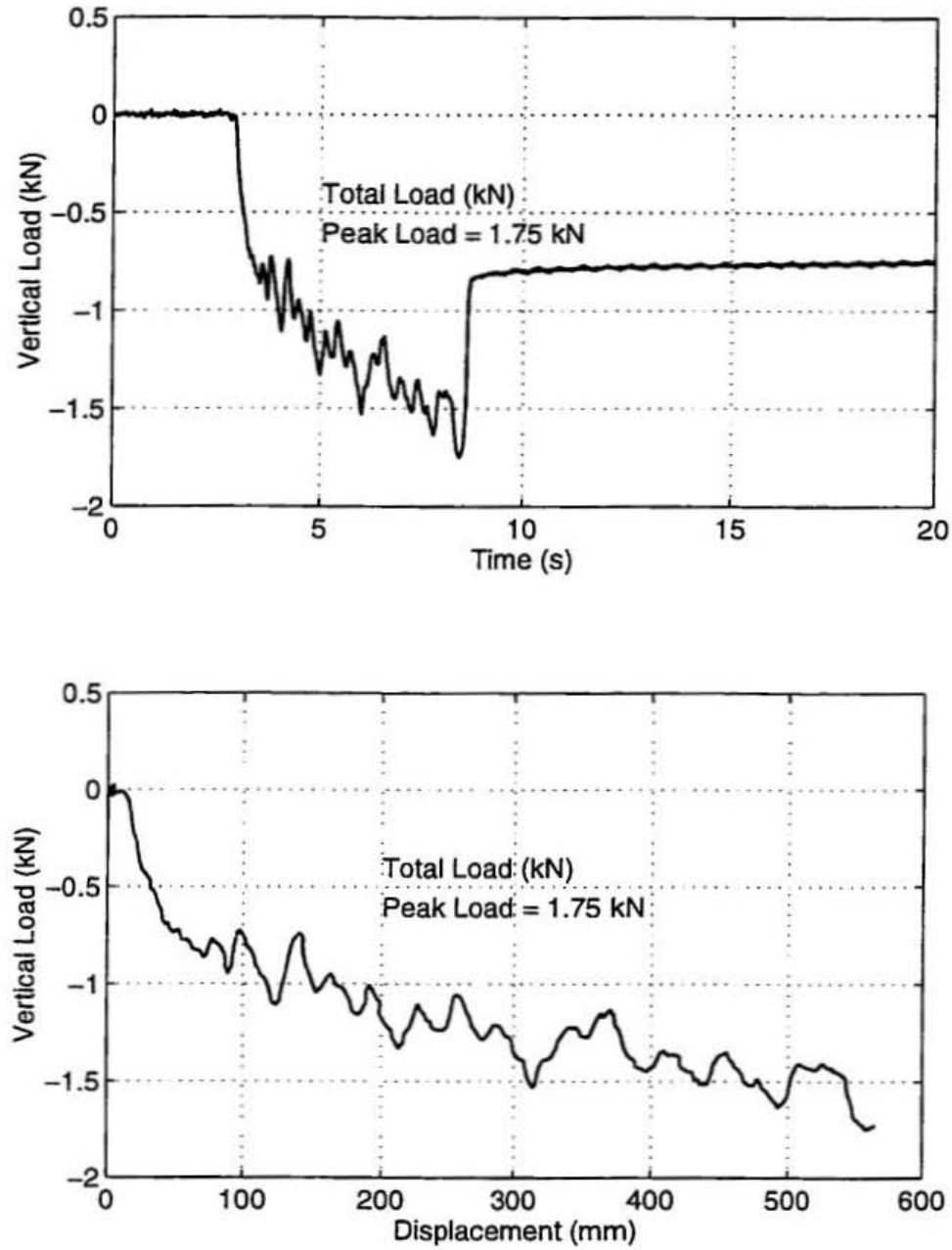

Figure A.13 **Scour G, Measured Vertical Load Versus Time and Displacement**

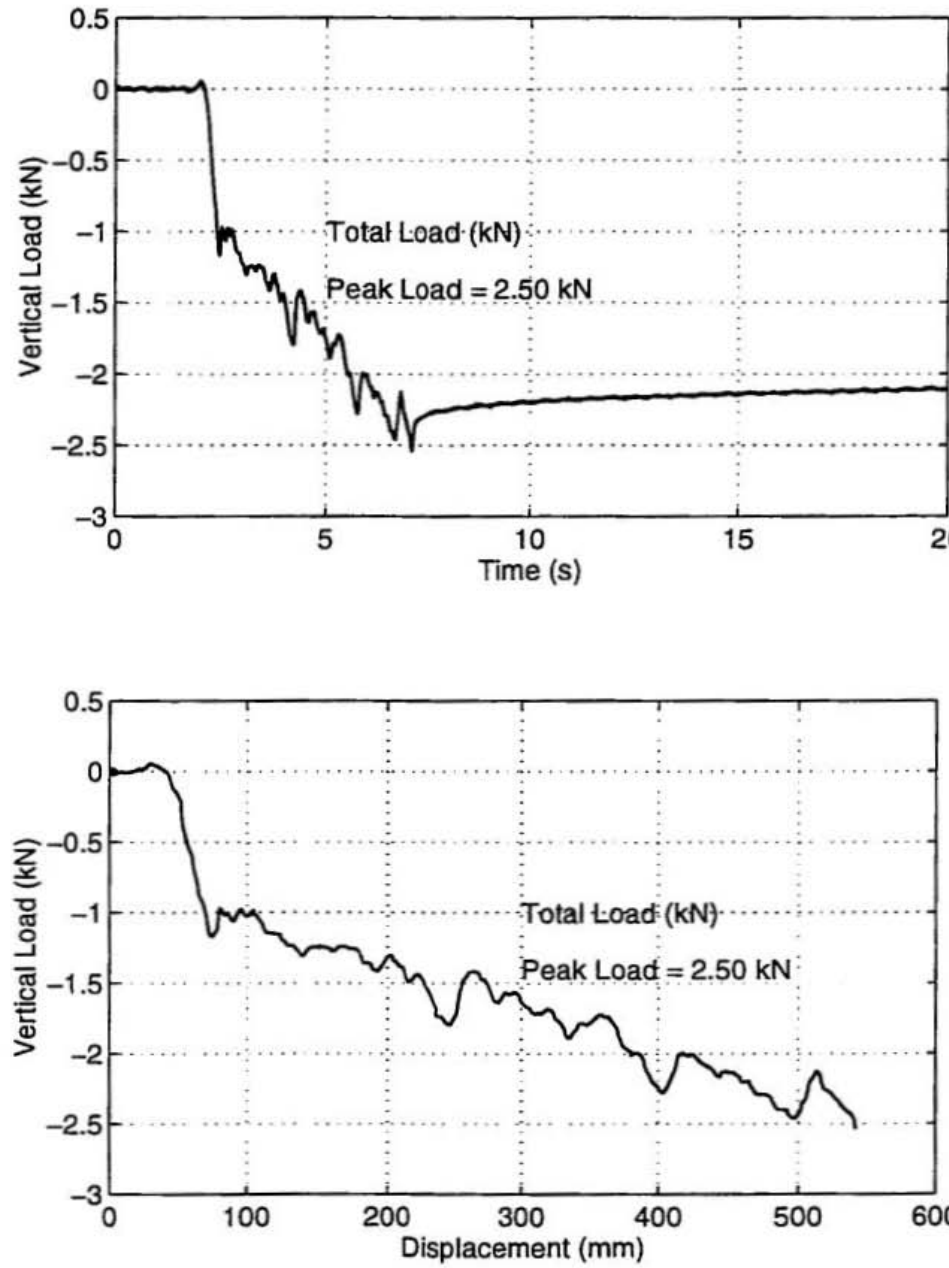

Figure A.14 **Scour H, Measured Vertical Load Versus Time and Displacement**

Pressure Transducer (PT) Data

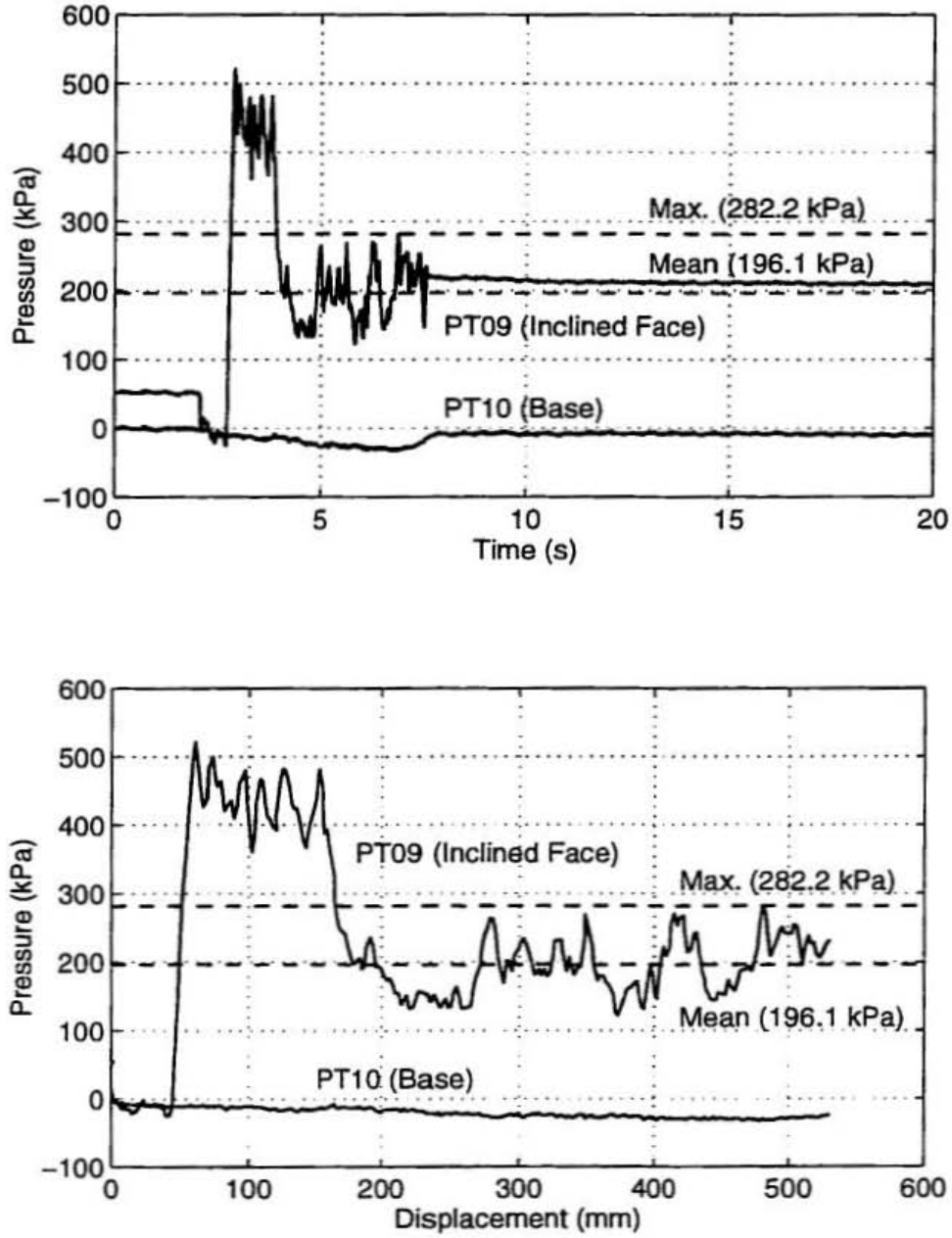

Figure A.15 **Scour B, Measured Spot Pressure Versus Time and Displacement**

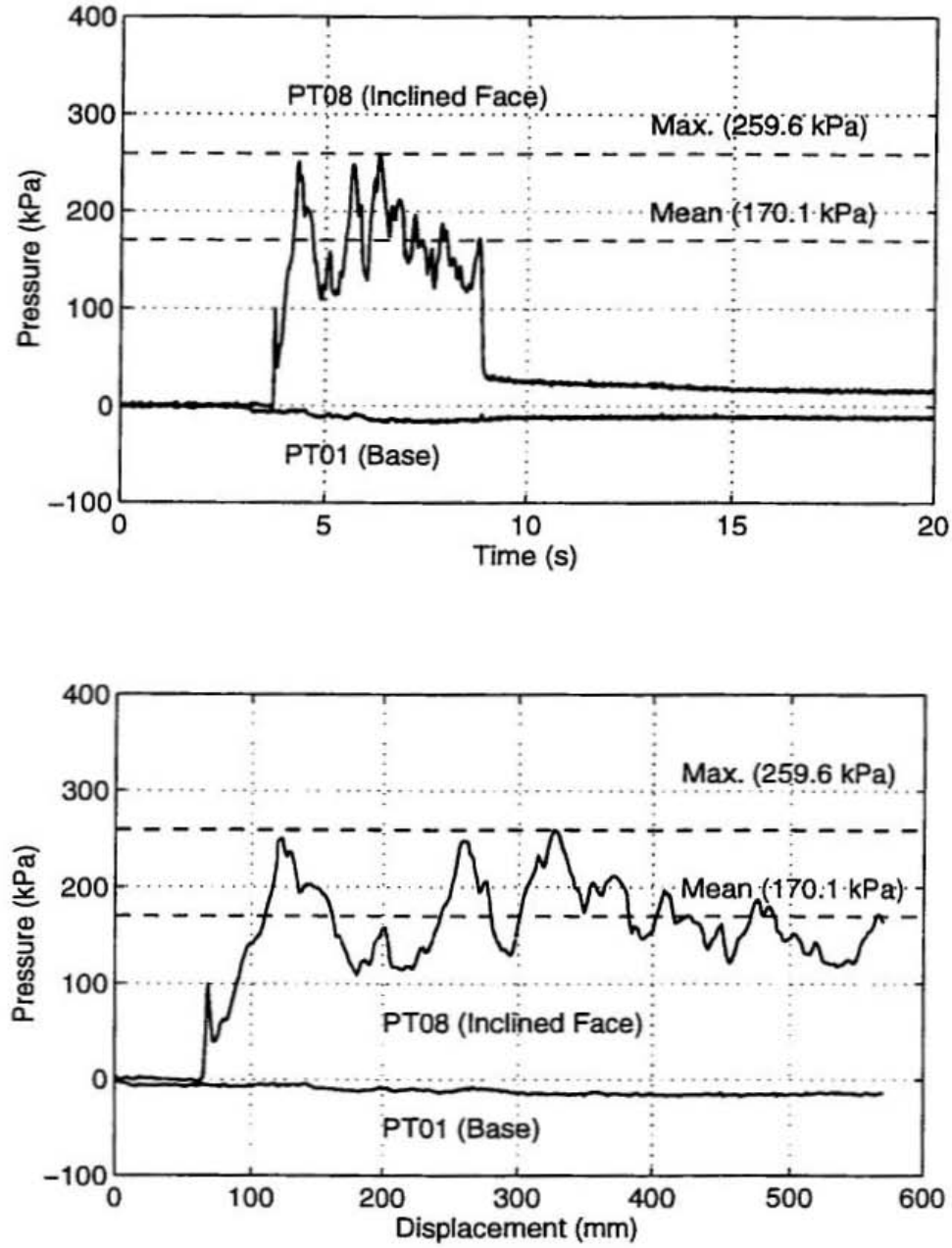

Figure A.16 **Scour C, Measured Spot Pressure Versus Time and Displacement**

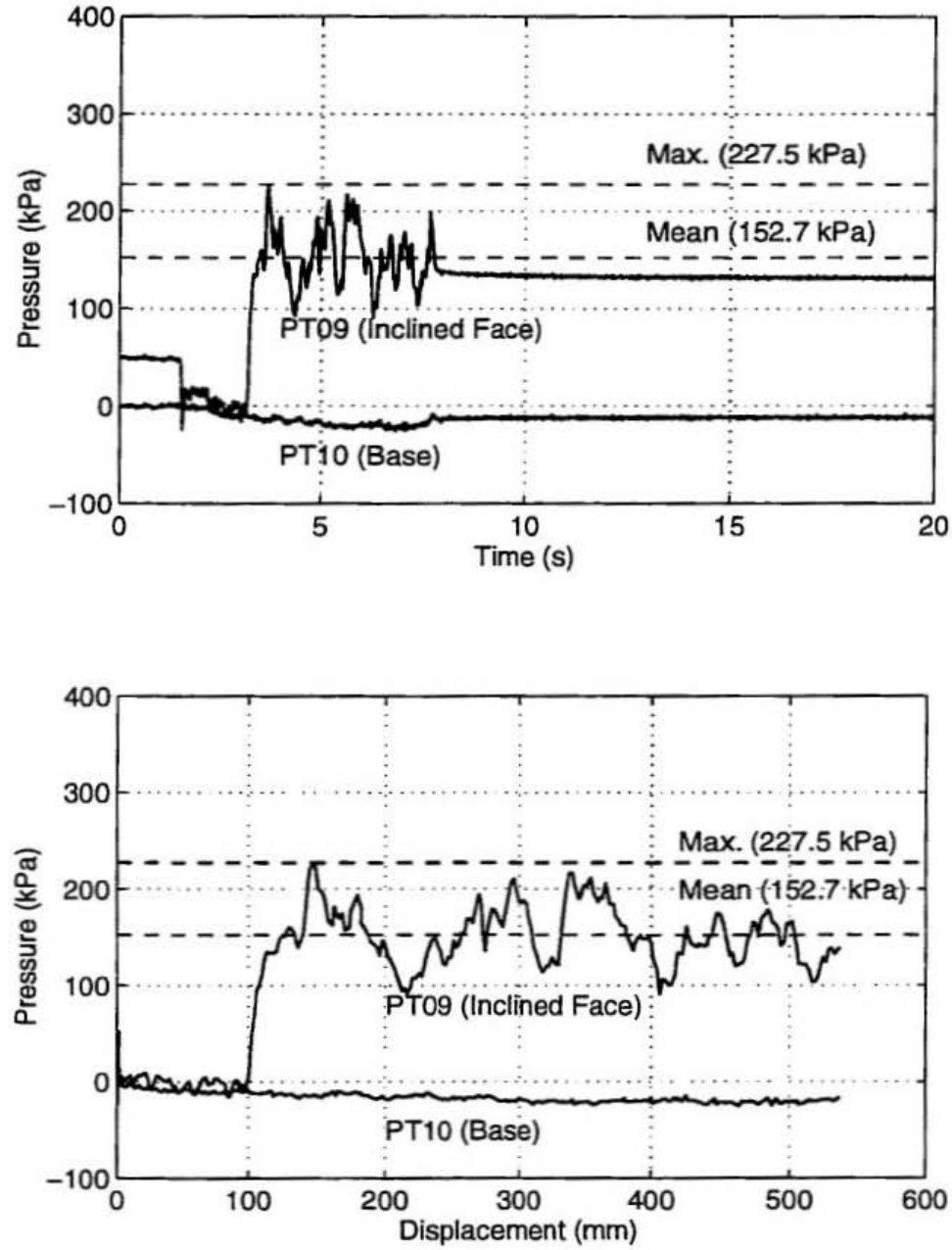

Figure A.17 **Scour D, Measured Spot Pressure Versus Time and Displacement**

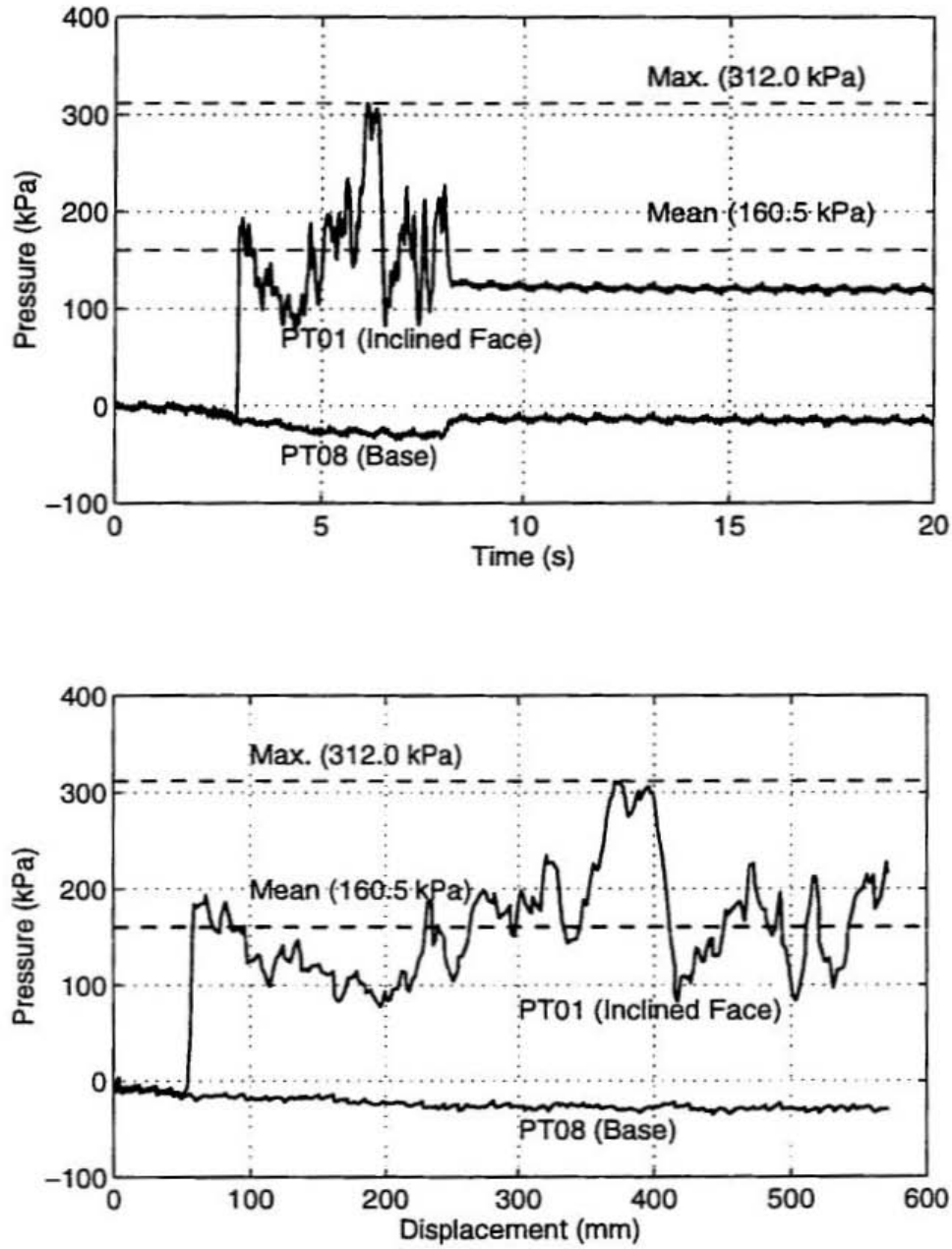

Figure A.18 **Scour E, Measured Spot Pressure Versus Time and Displacement**

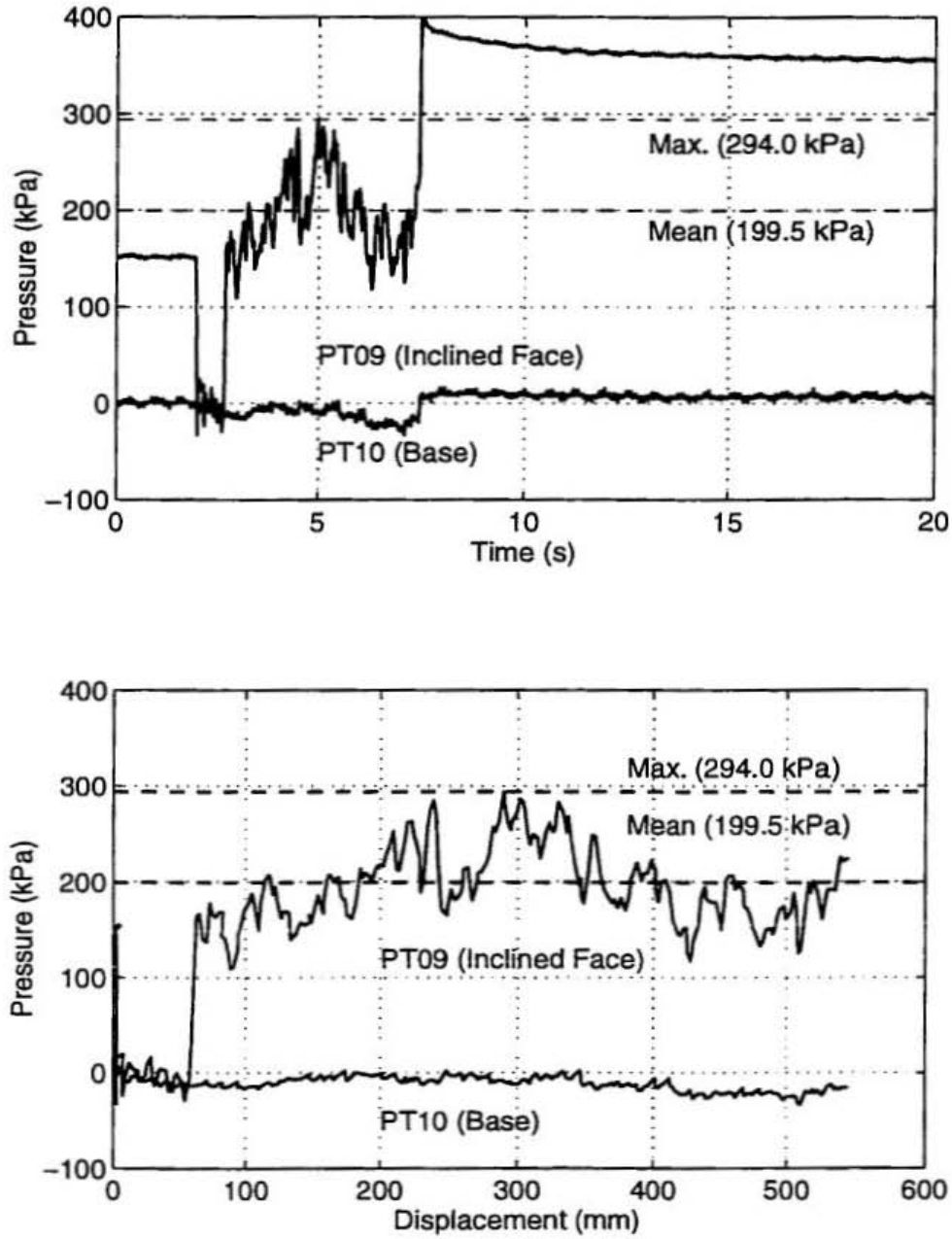

Figure A.19 **Scour F, Measured Spot Pressure Versus Time and Displacement**

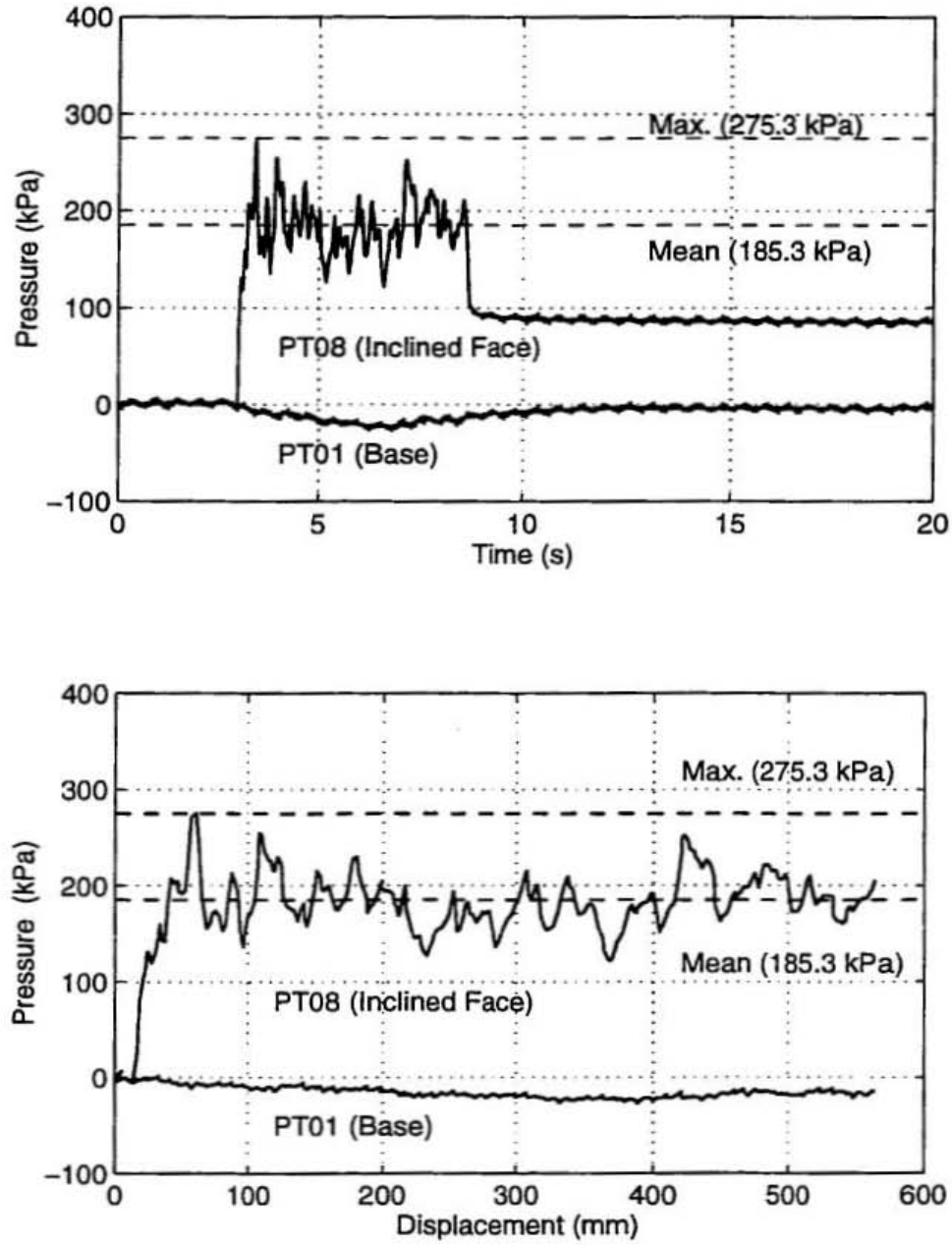

Figure A.20 **Scour G, Measured Spot Pressure Versus Time and Displacement**

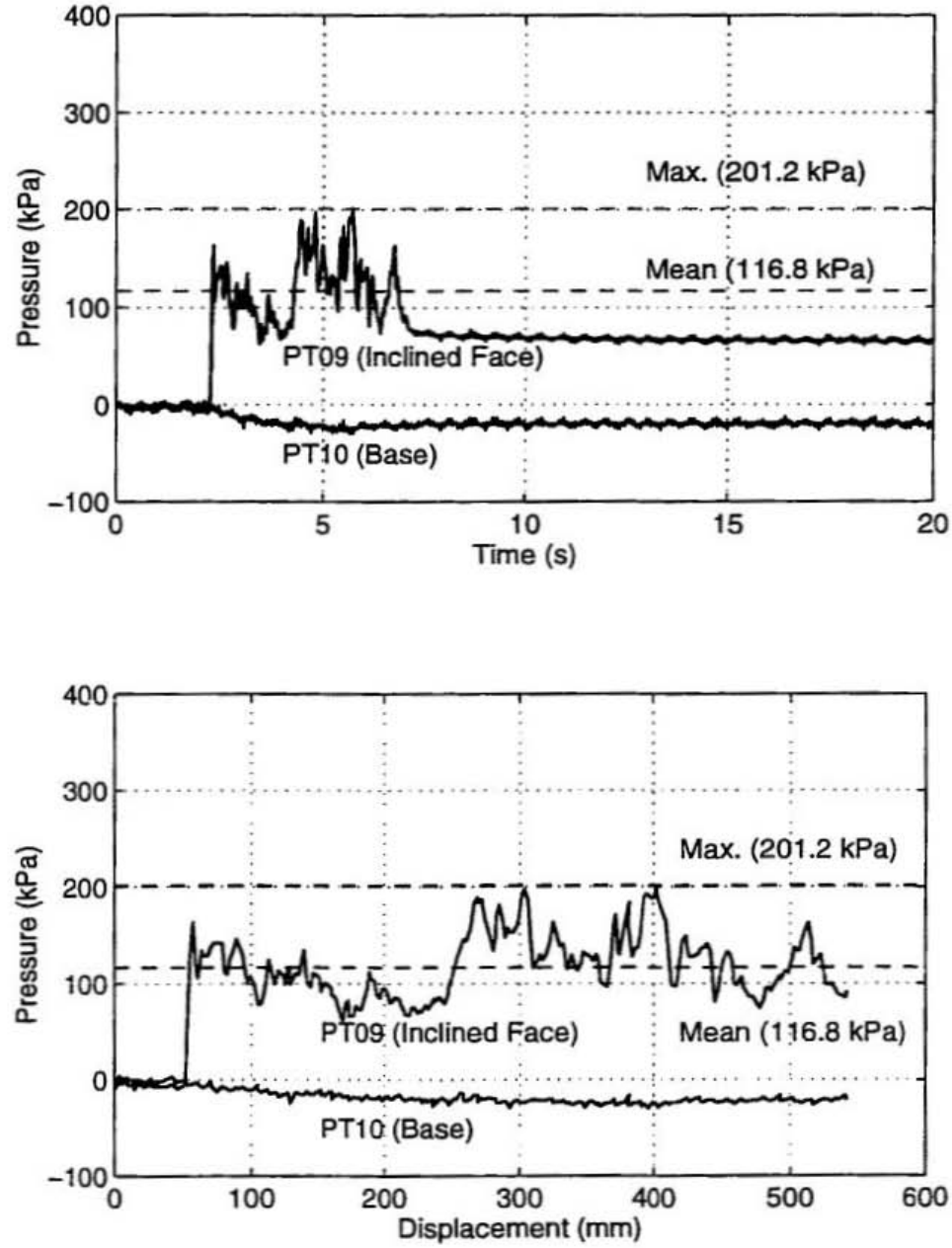

Figure A.21 **Scour H, Measured Spot Pressure Versus Time and Displacement**

Total Stress Cell (TLC) Data

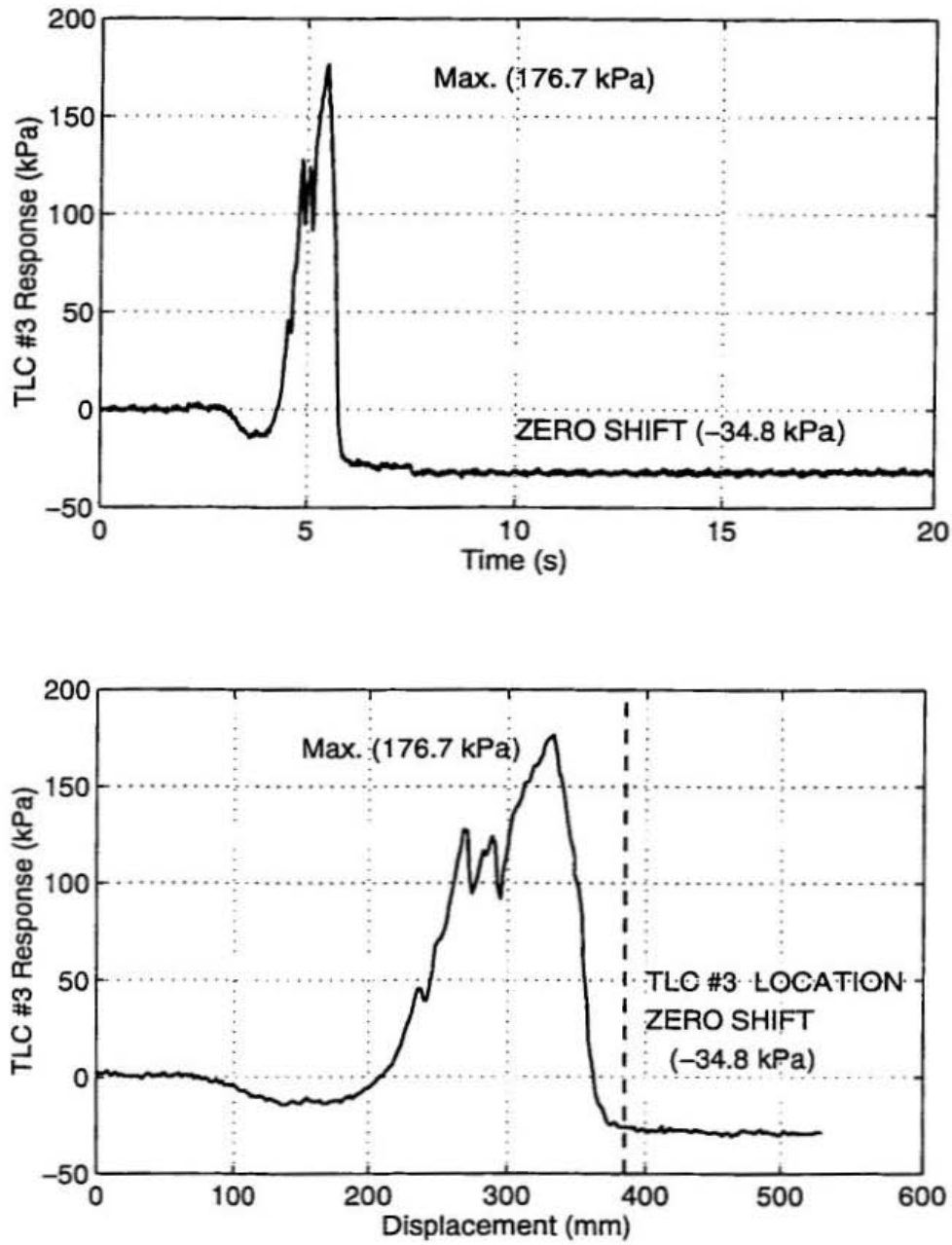

Figure A.22 **Scour B, TLC #3 Response Versus Time and Displacement**

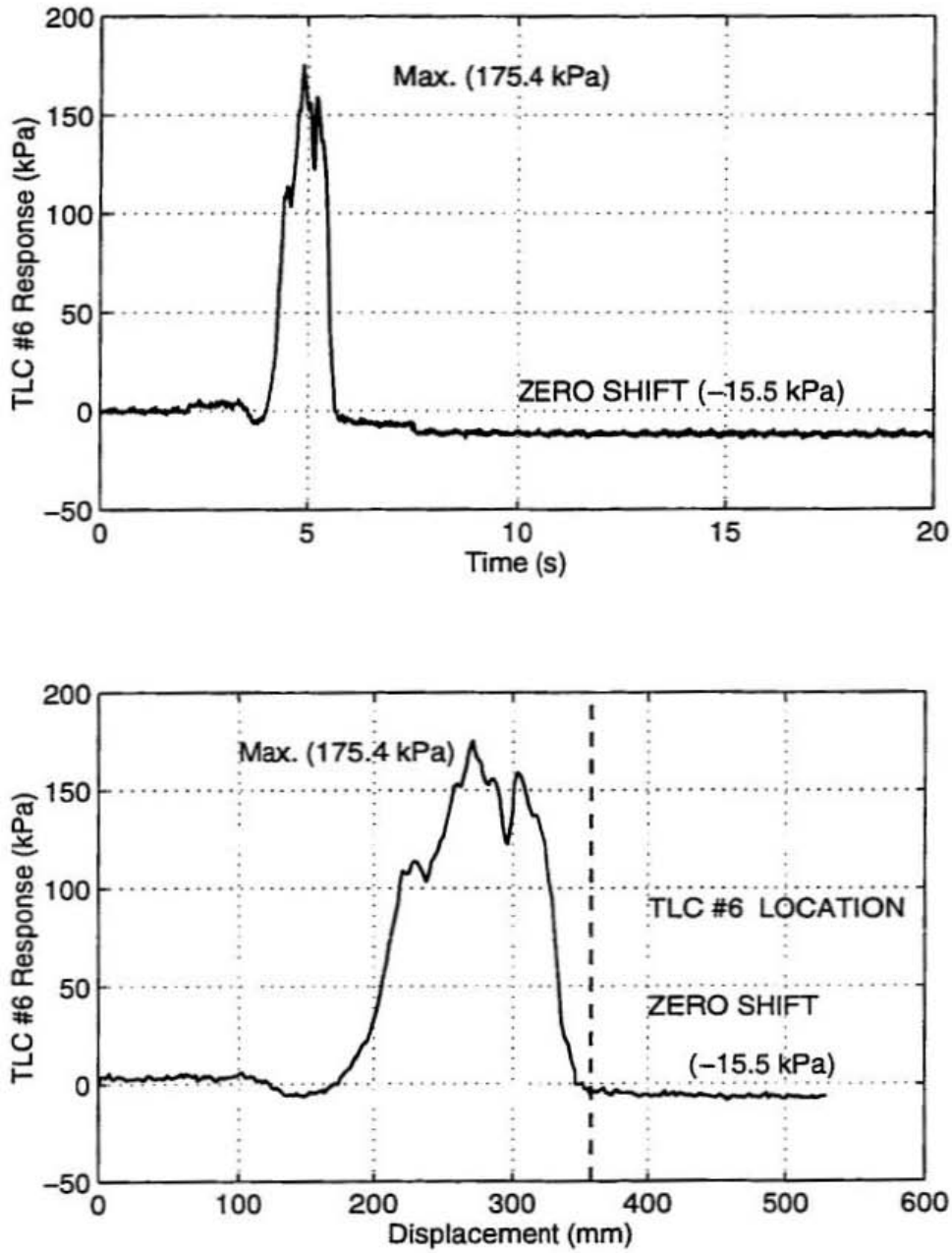

Figure A.23 **Scour B, TLC #6 Response Versus Time and Displacement**

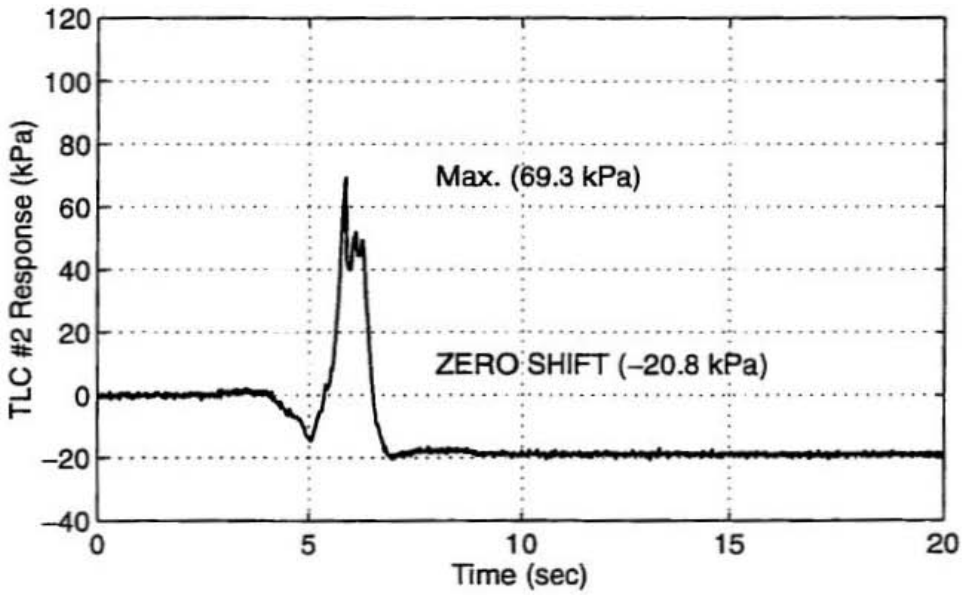

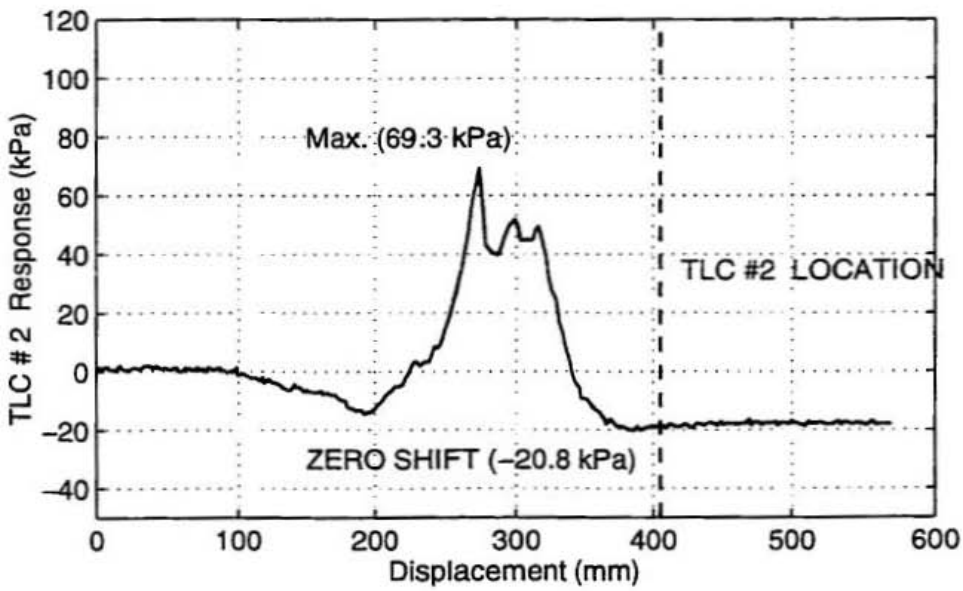

Figure A.24 **Scour C, TLC #2 Response Versus Time and Displacement**

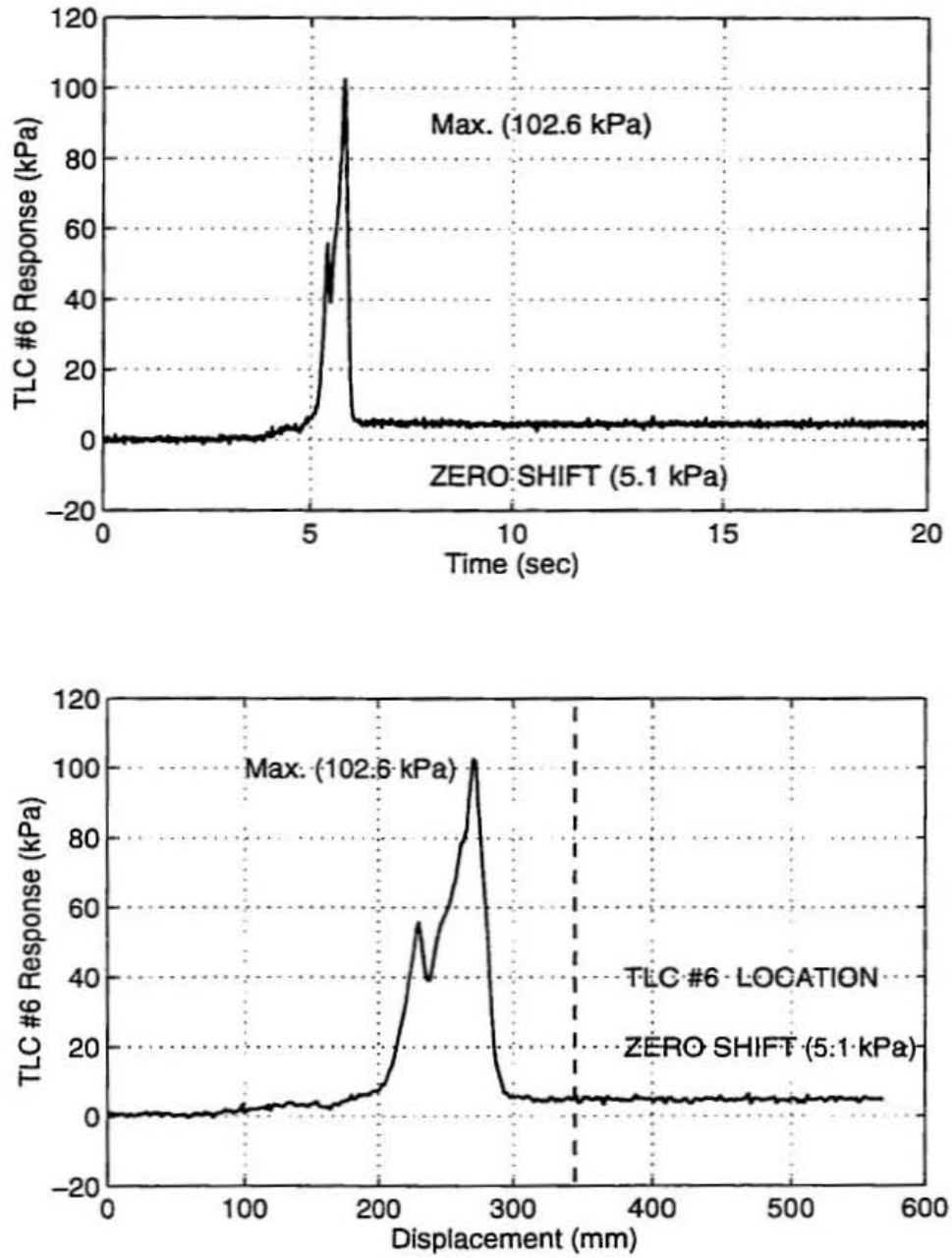

Figure A.25 **Scour C, TLC #6 Response Versus Time and Displacement**

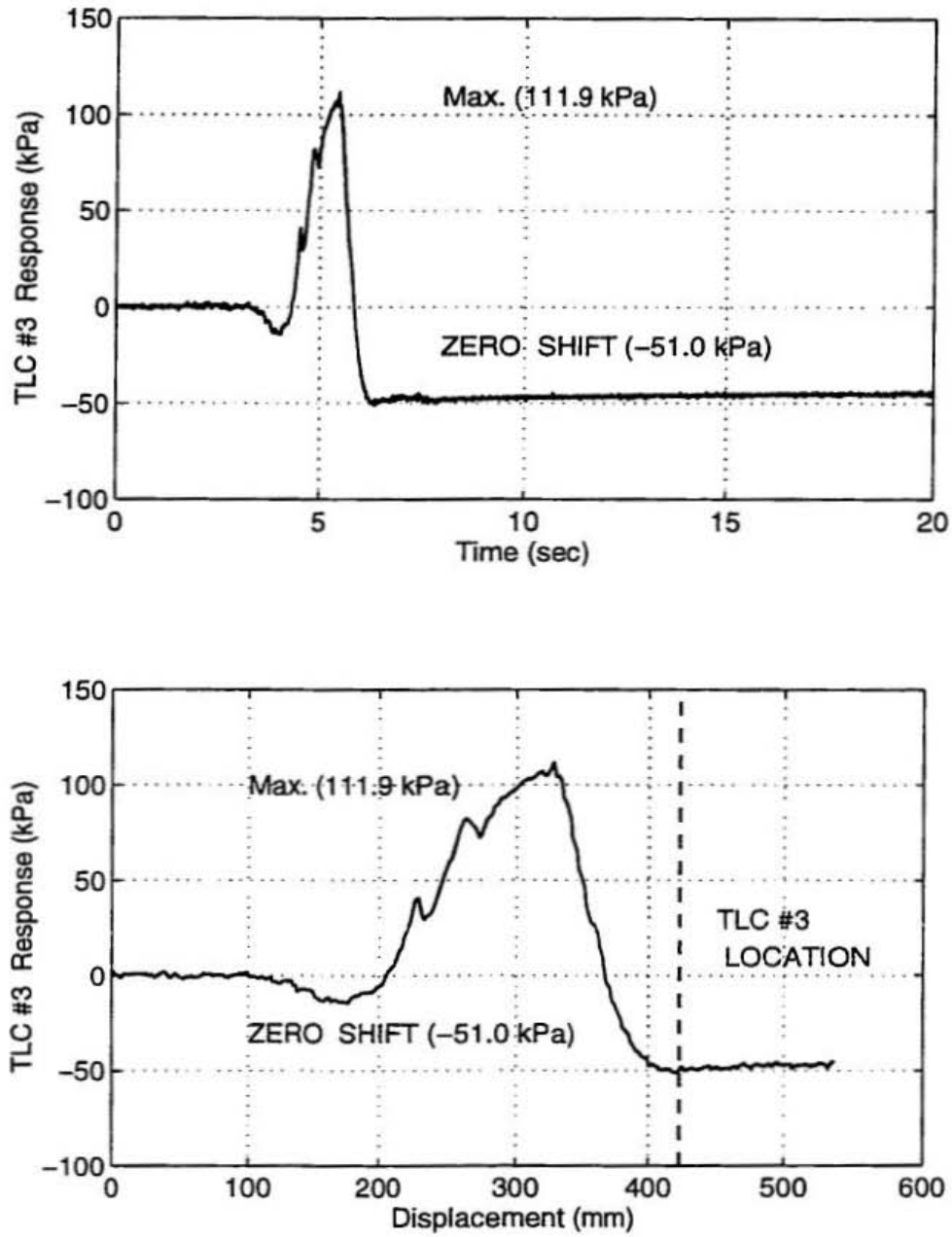

Figure A.26 **Scour D, TLC #3 Response Versus Time and Displacement**

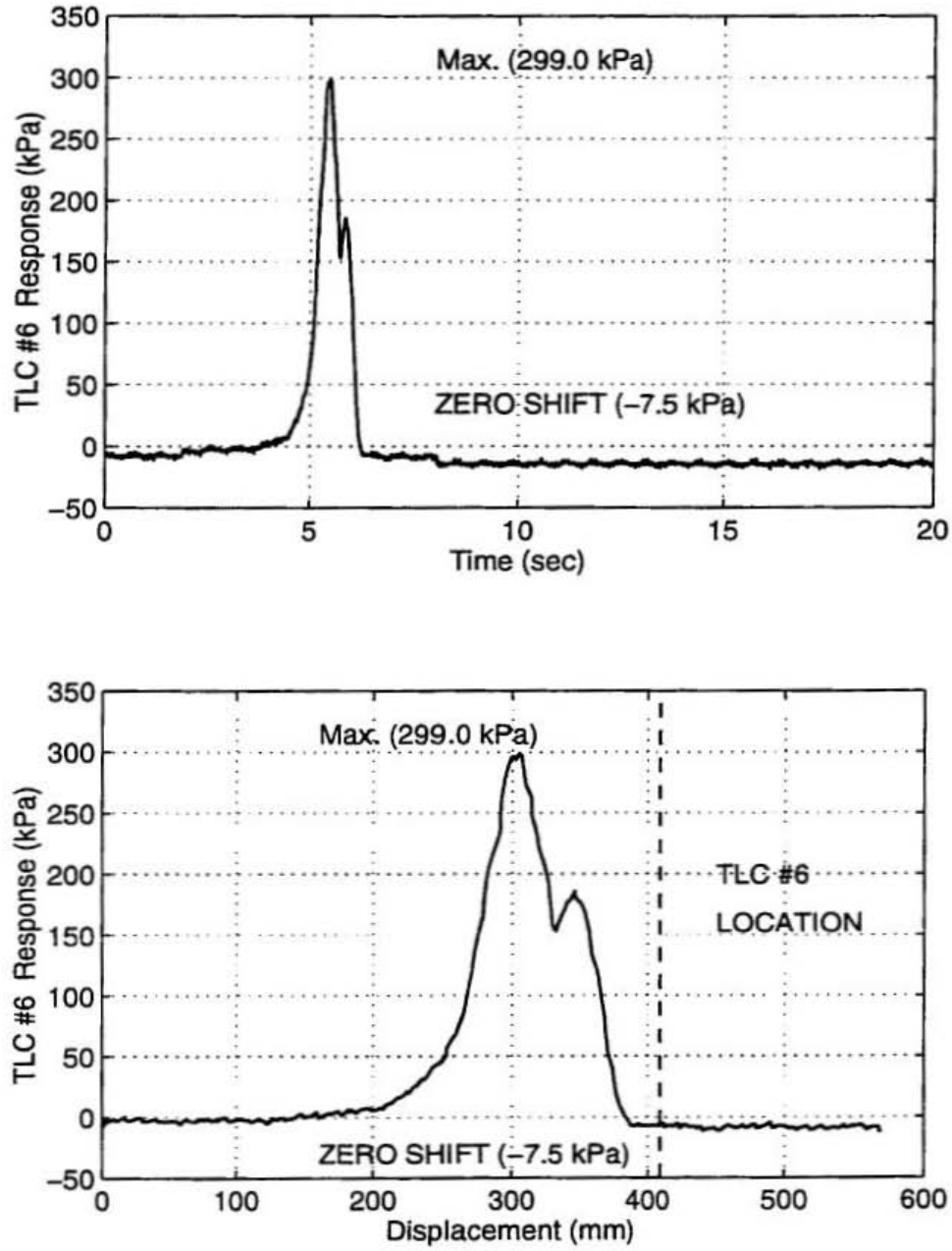

Figure A.27 **Scour E, TLC #6 Response Versus Time and Displacement**

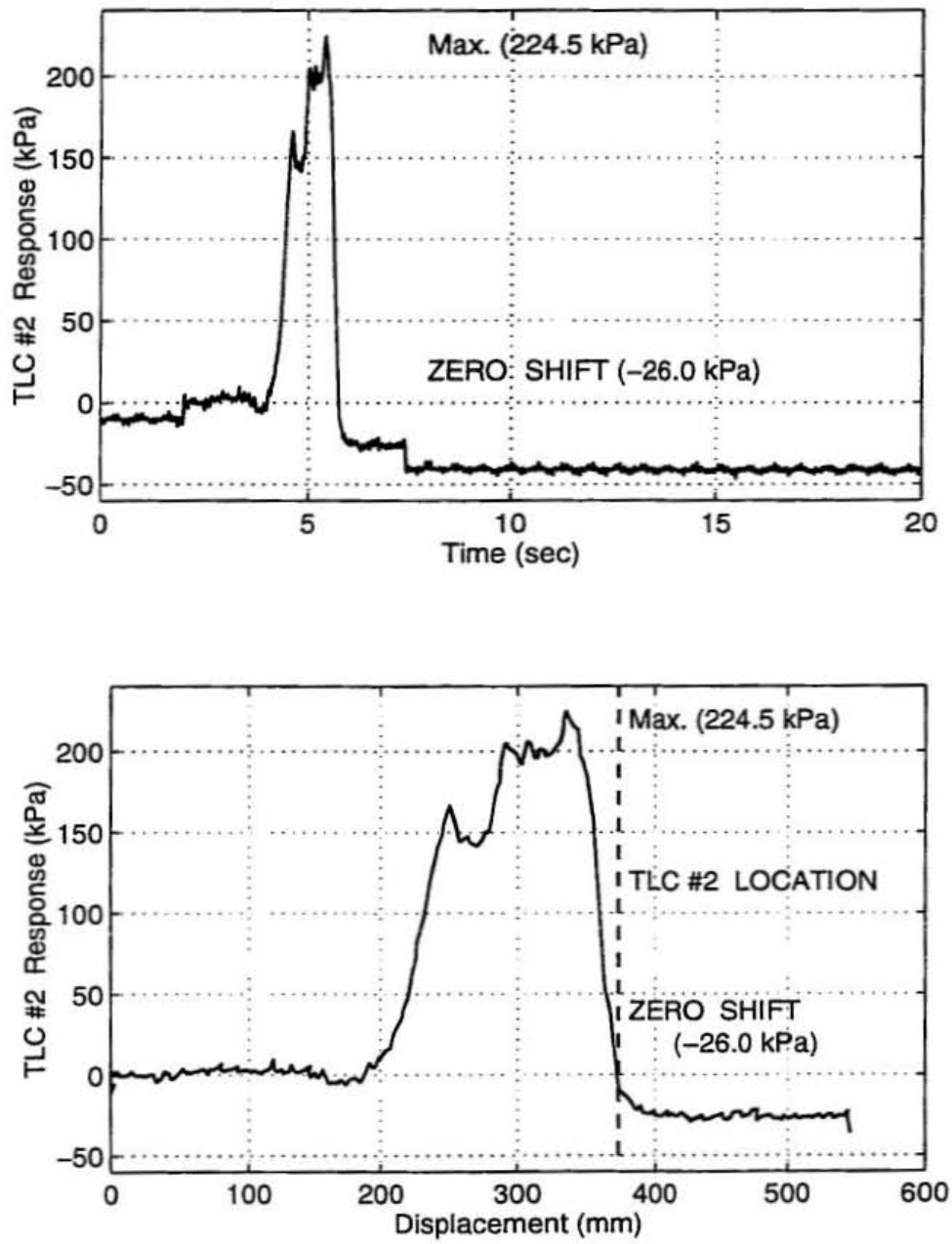

Figure A.28 **Scour F, TLC # 2 Response Versus Time and Displacement**

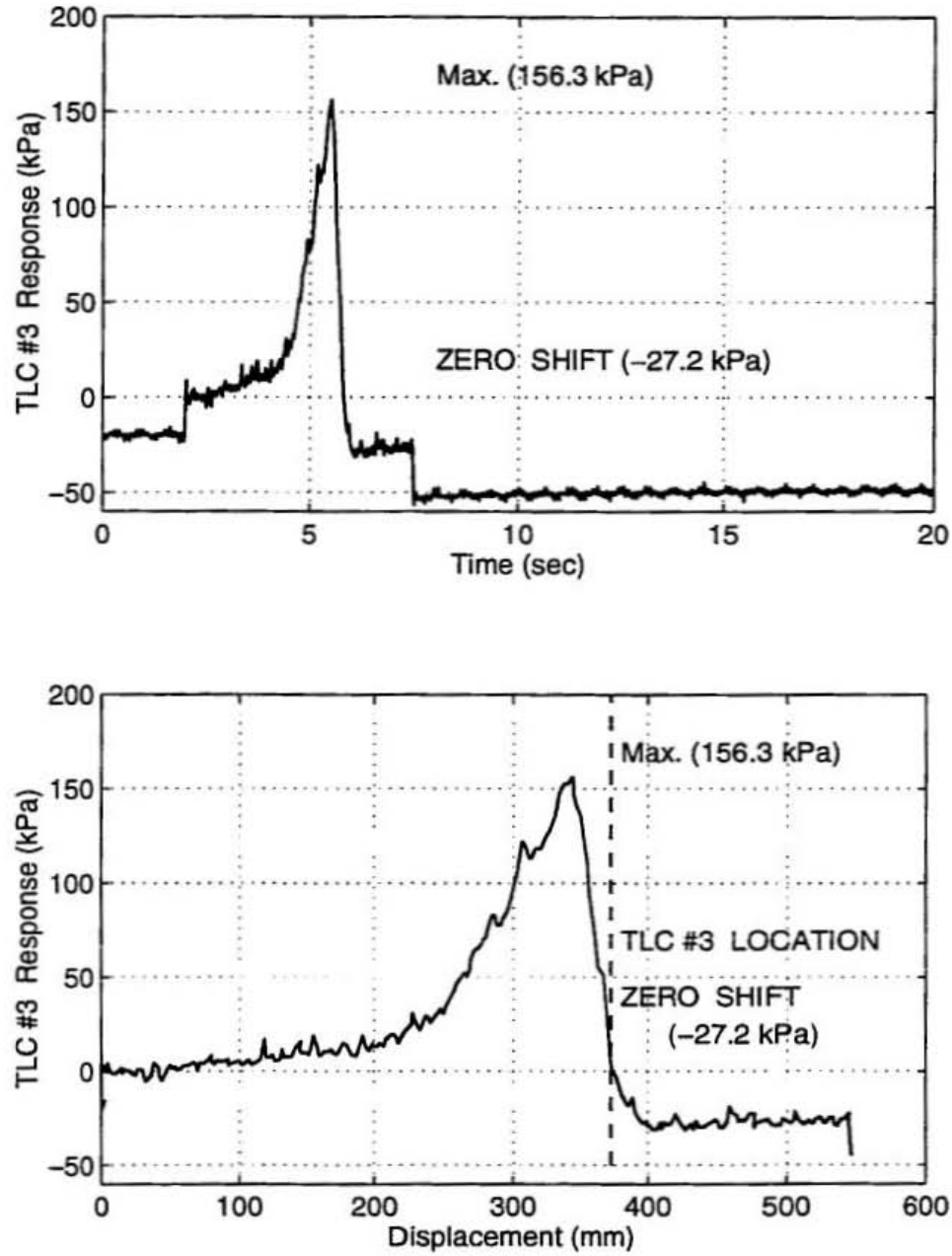

Figure A.29 **Scour F, TLC #3 Response Versus Time and Displacement**

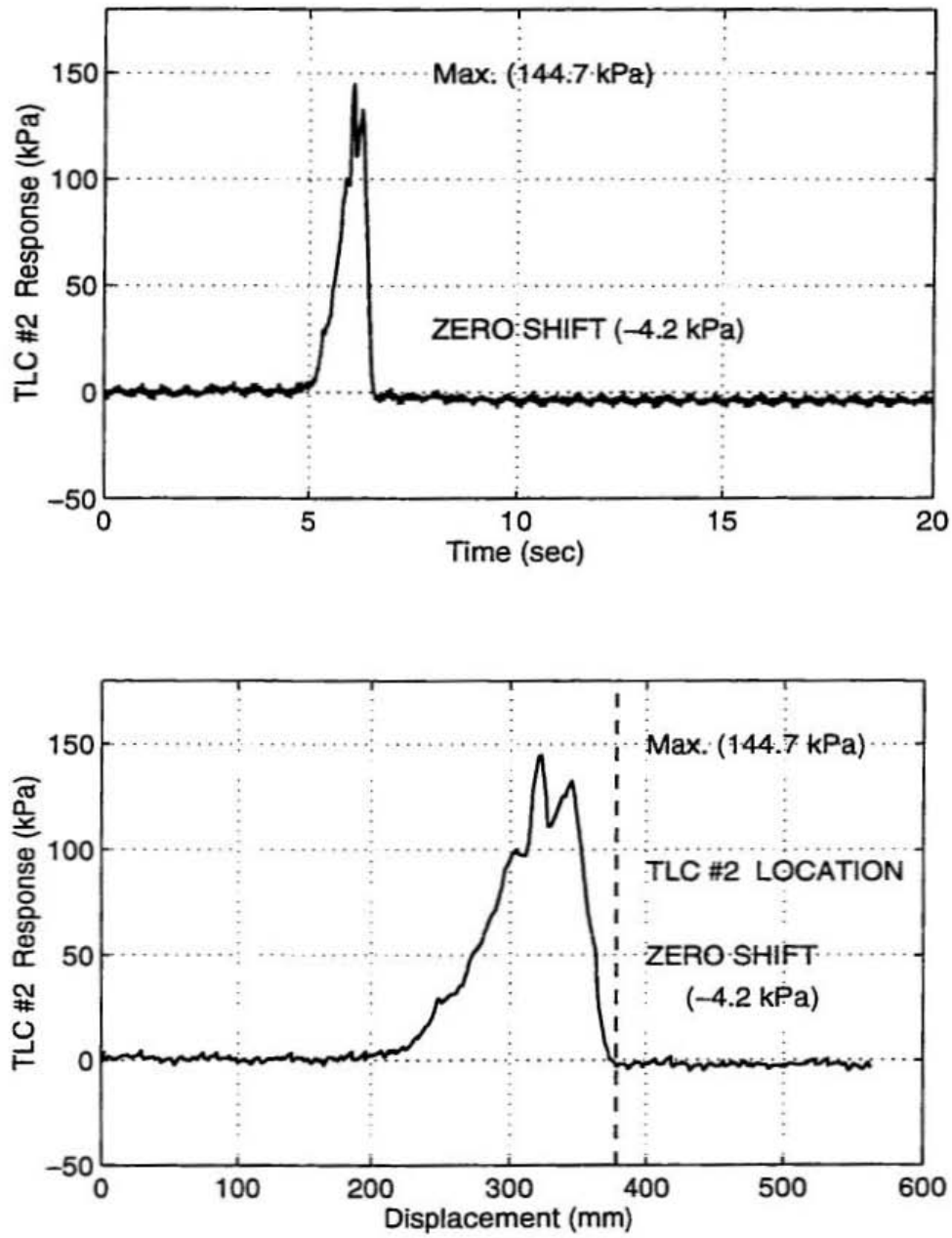

Figure A.30 **Scour G, TLC #2 Response Versus Time and Displacement**

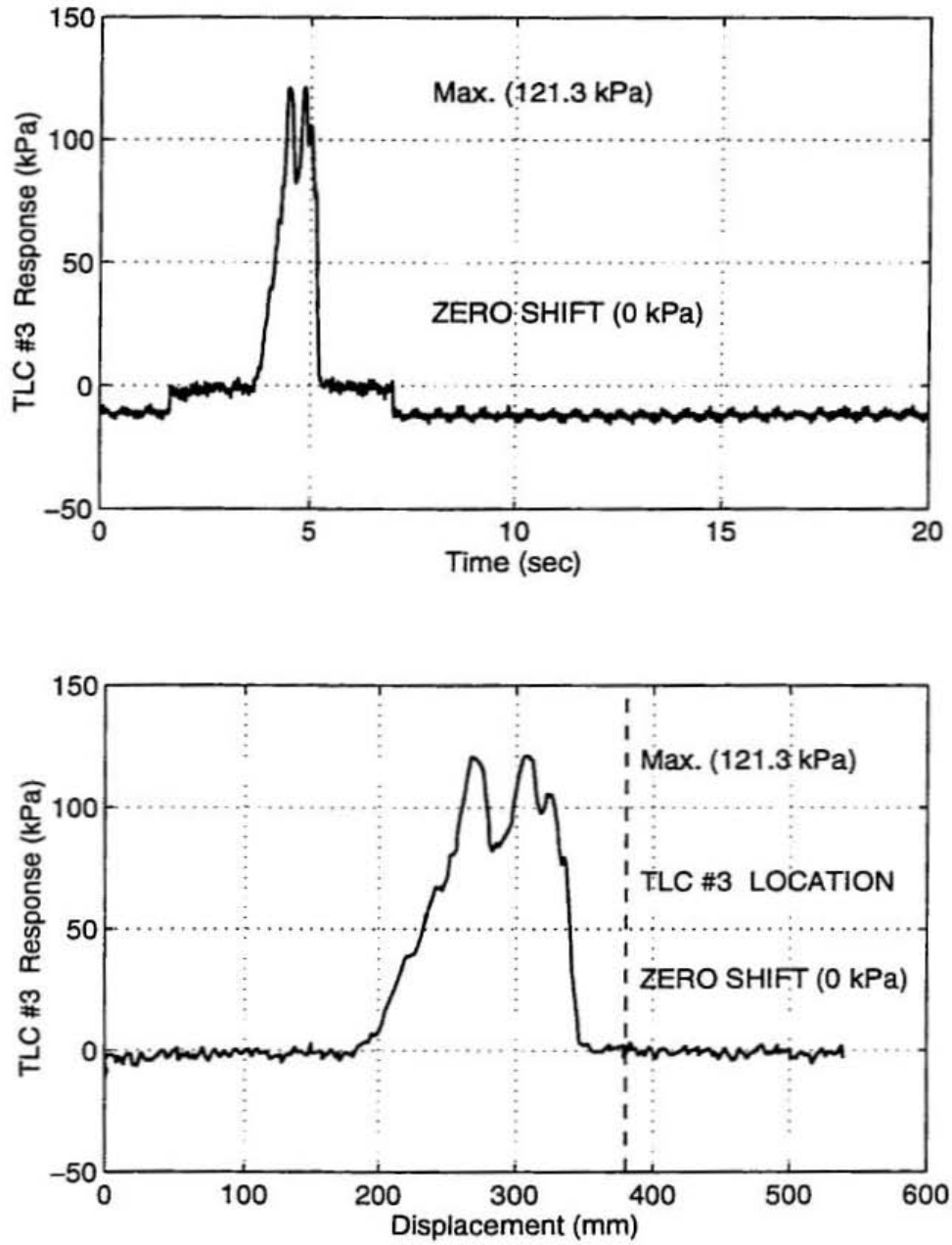

Figure A.31 **Scour H, TLC #3 Response Versus Time and Displacement**

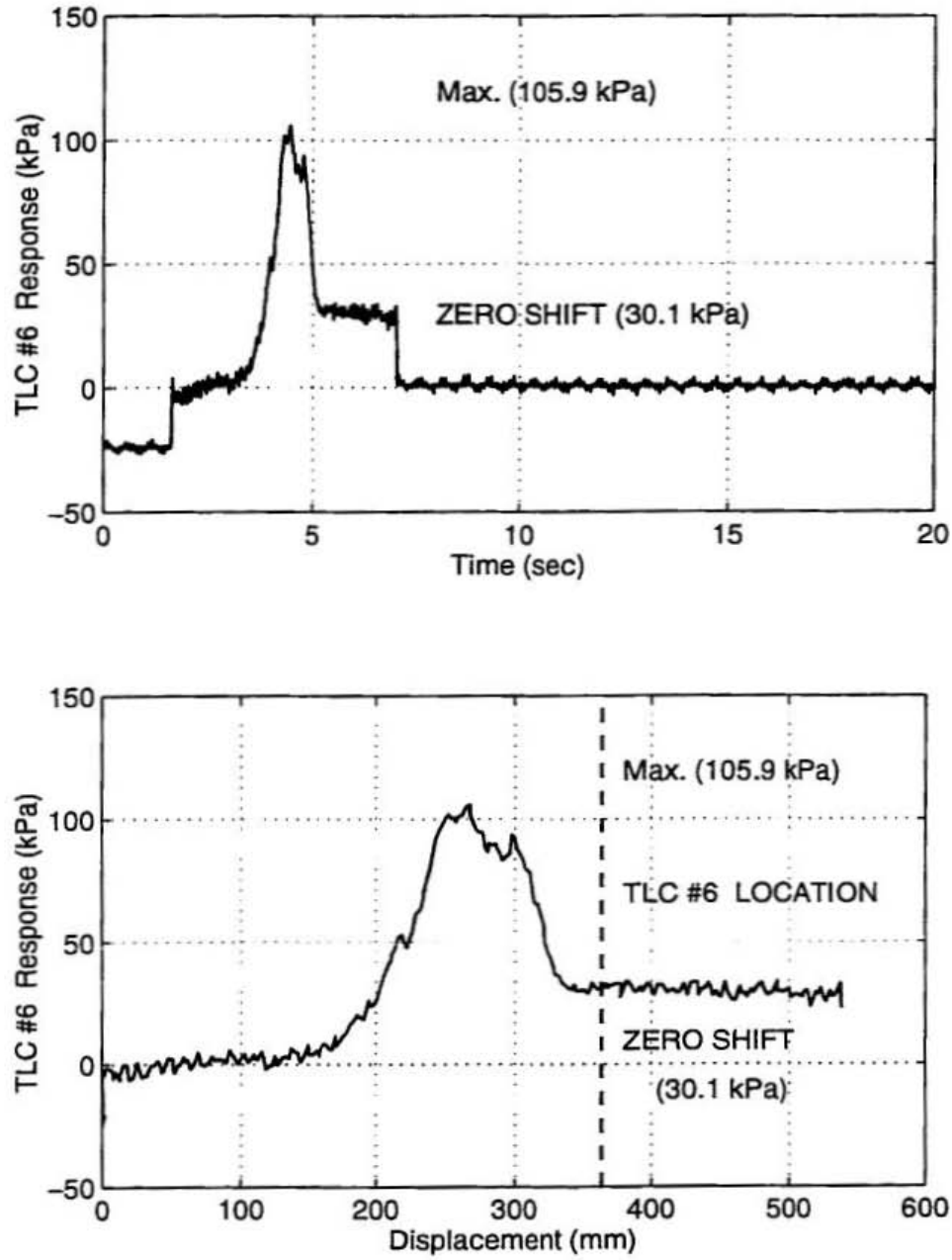

Figure A.32 **Scour H, TLC #6 Response Versus Time and Displacement**

Pore Pressure Transducer (PPT) Data

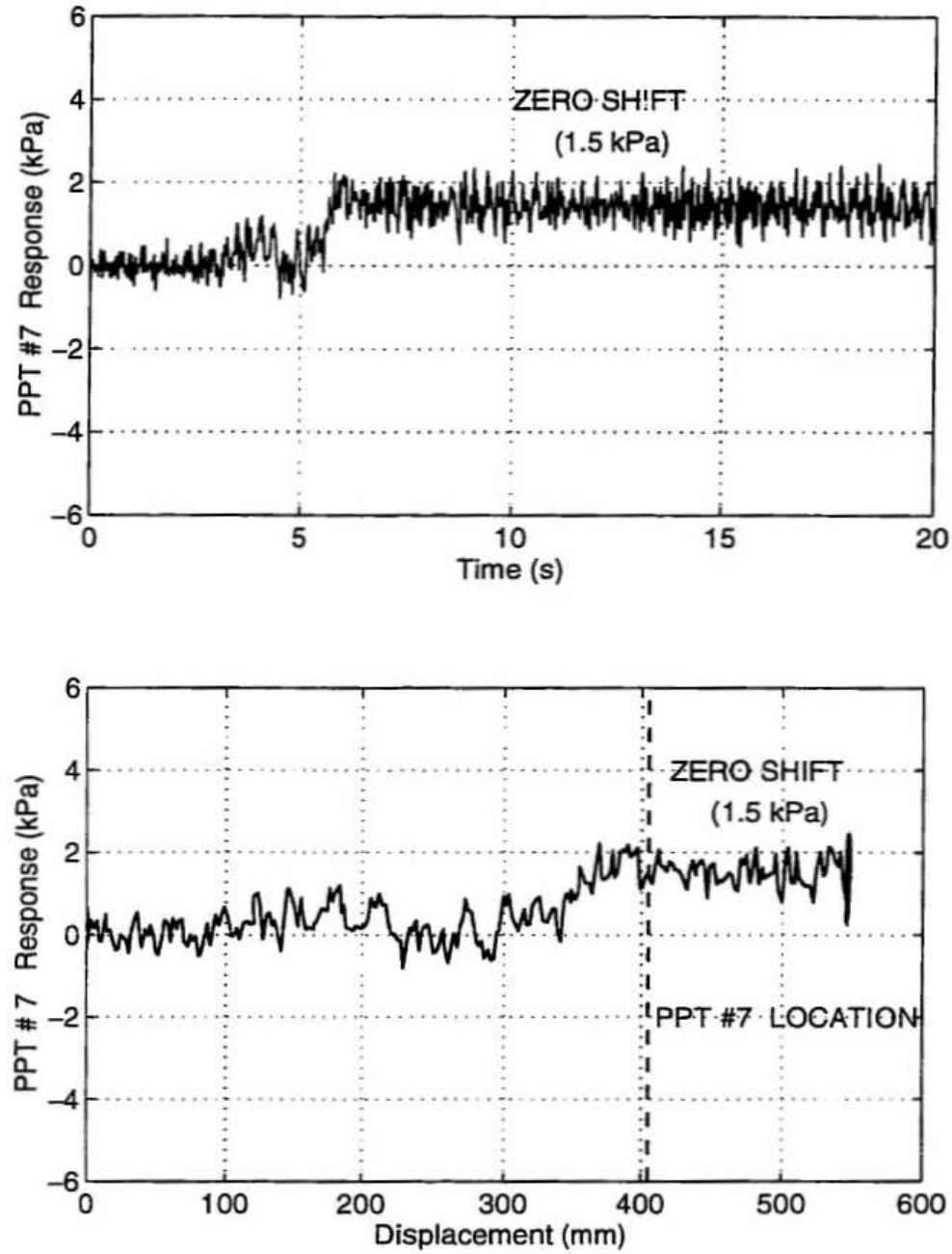

Figure A.33 **Scour B, PPT #7 Response Versus Time and Displacement**

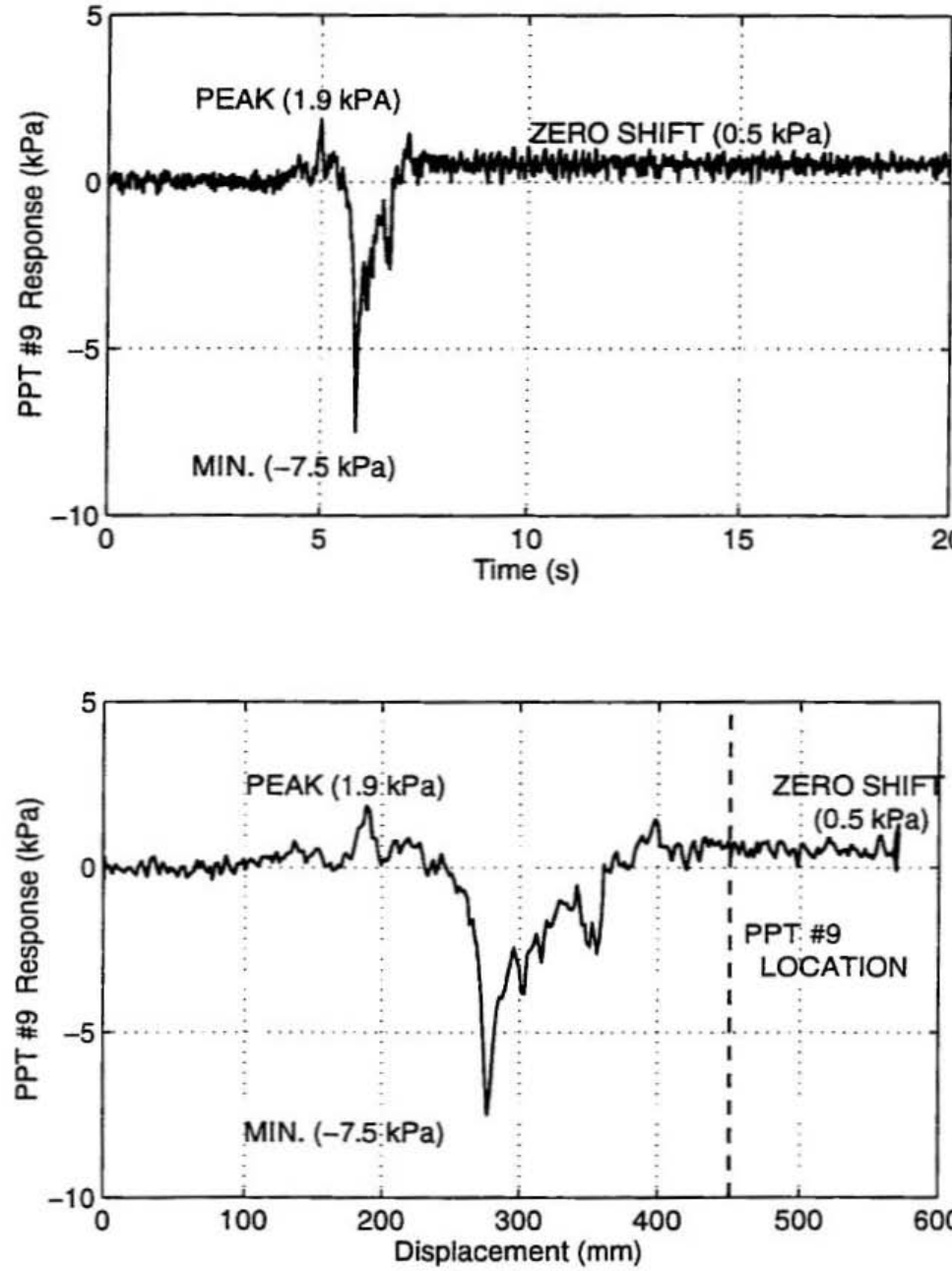

Figure A.34 **Scour C, PPT # 9 Response Versus Time and Displacement**

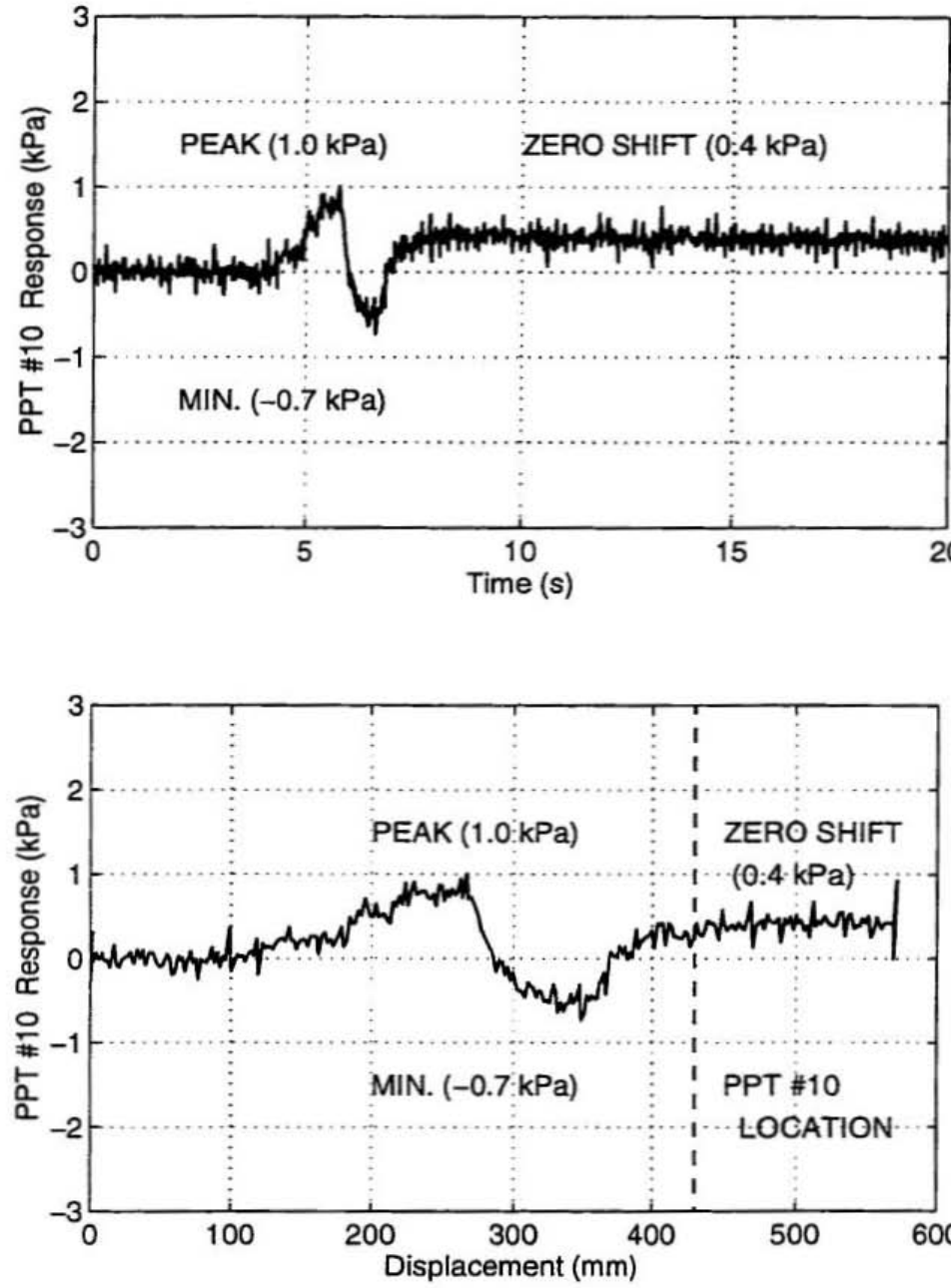

Figure A.35 **Scour C, PPT #10 Response Versus Time and Displacement**

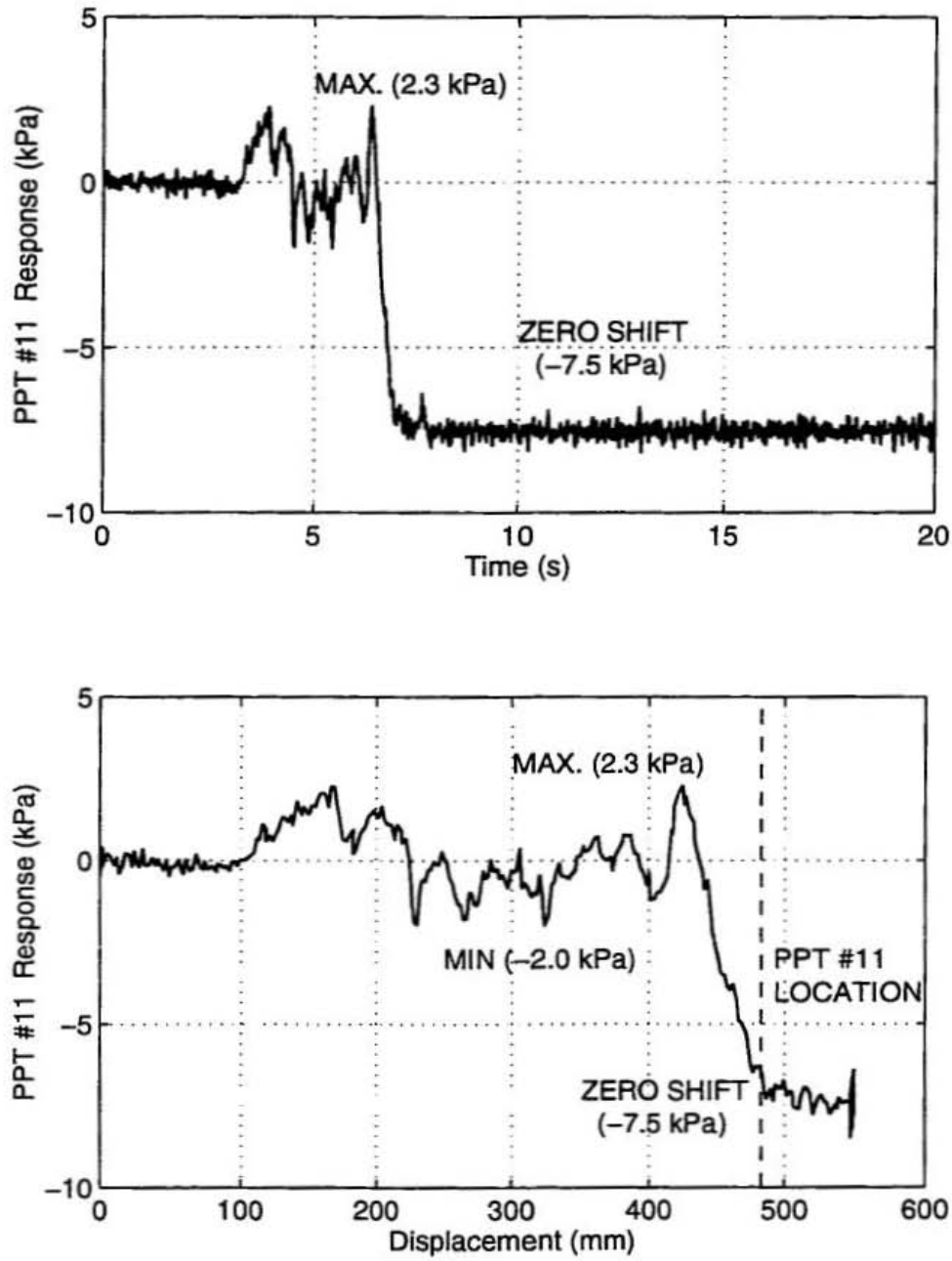

Figure A.36 **Scour D, PPT #11 Response Versus Time and Displacement**

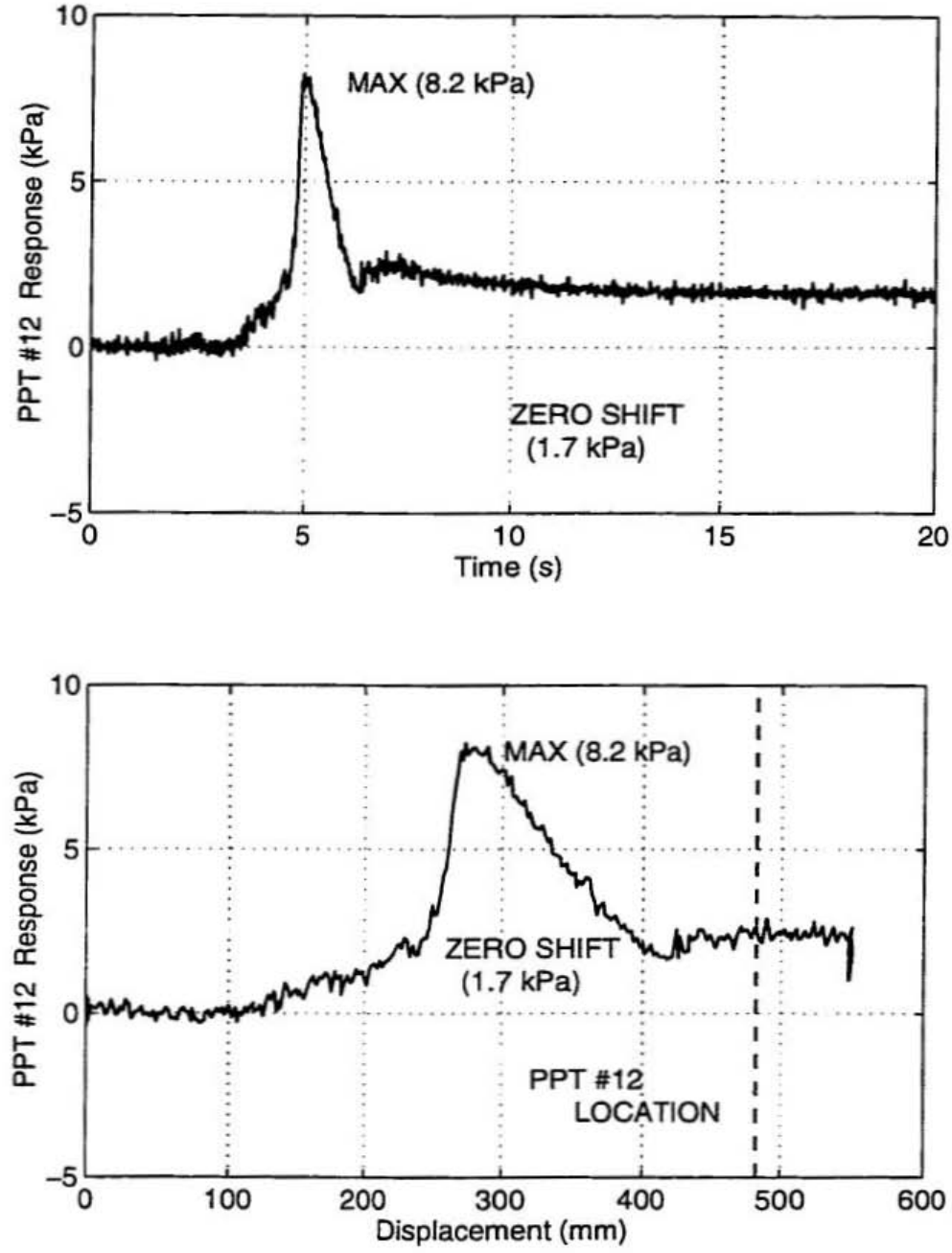

Figure A.37 **Scour D, PPT #12 Response Versus Time and Displacement**

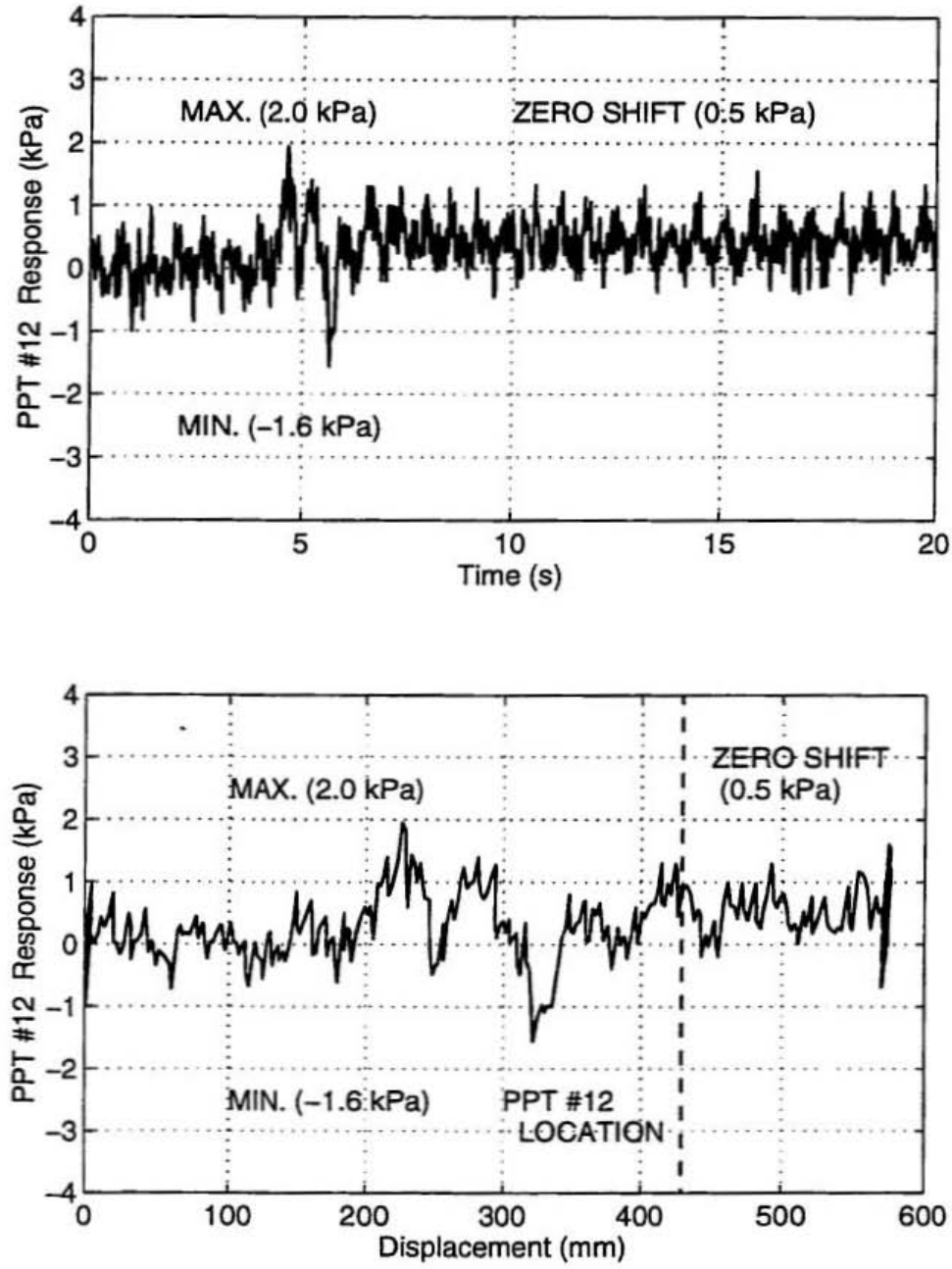

Figure A.38 **Scour E, PPT #12 Response Versus Time and Displacement**

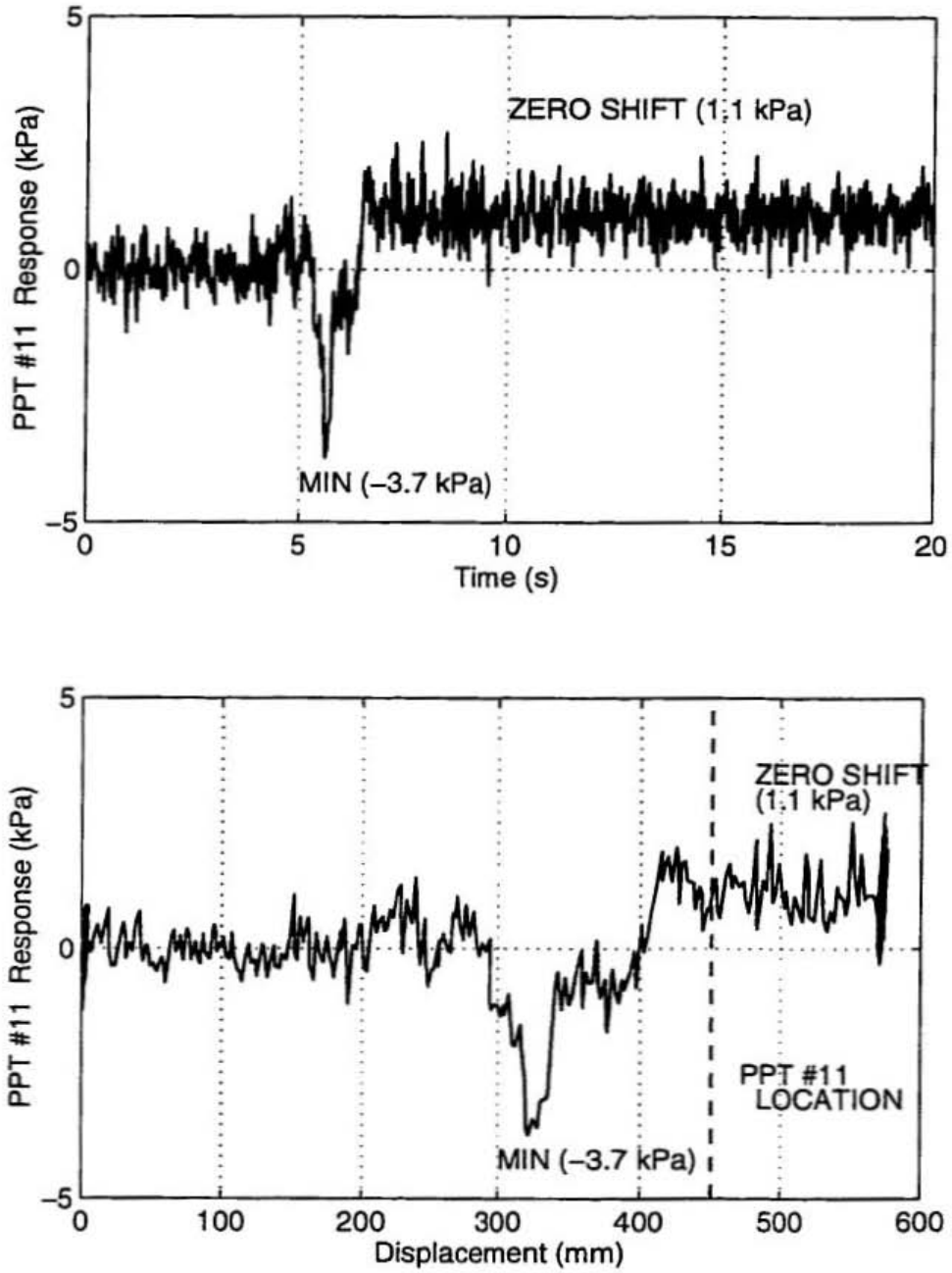

Figure A.39 **Scour E, PPT #11 Response Versus Time and Displacement**

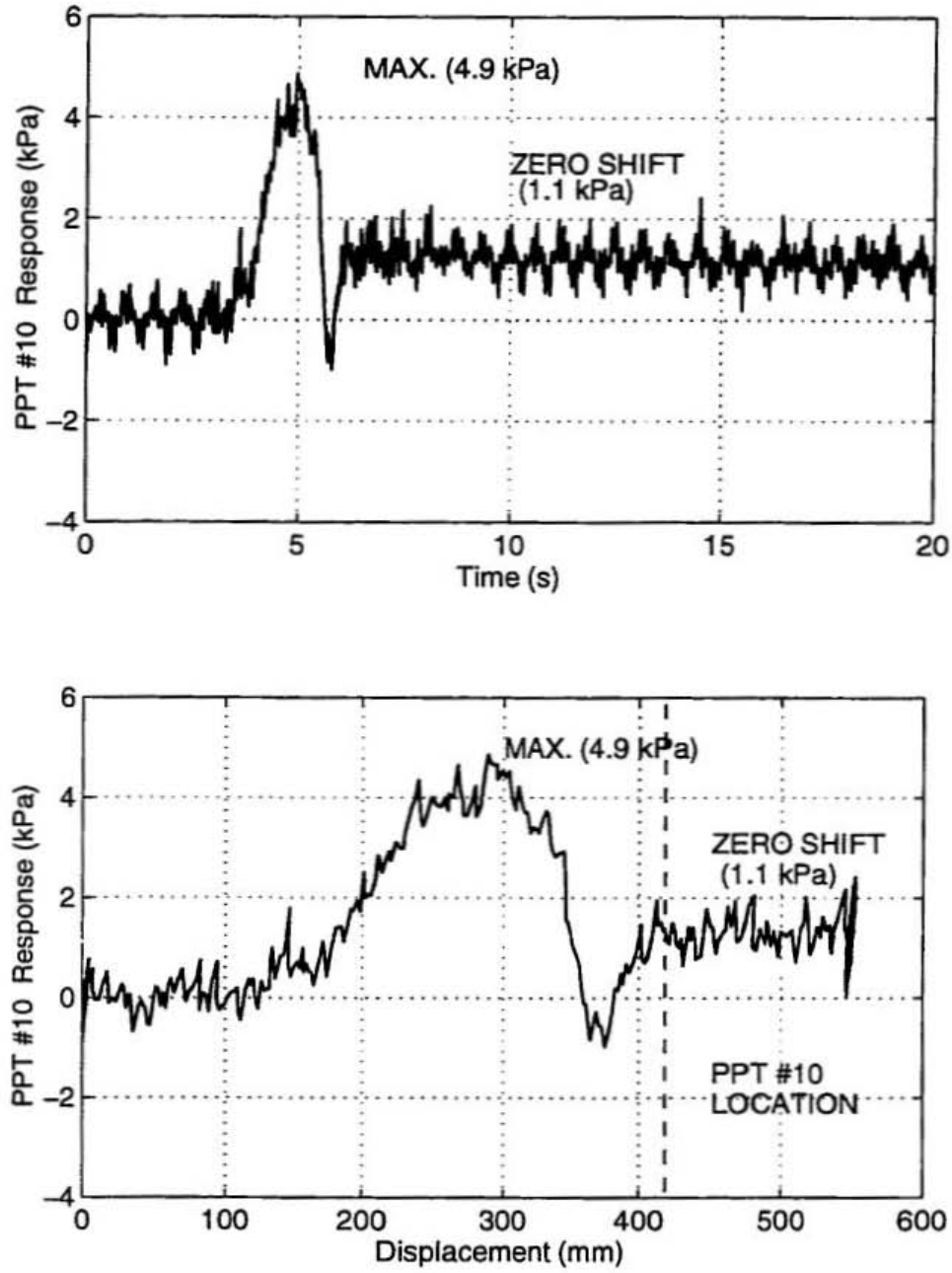

Figure A.40 **Scour F, PPT #10 Response Versus Time and Displacement**

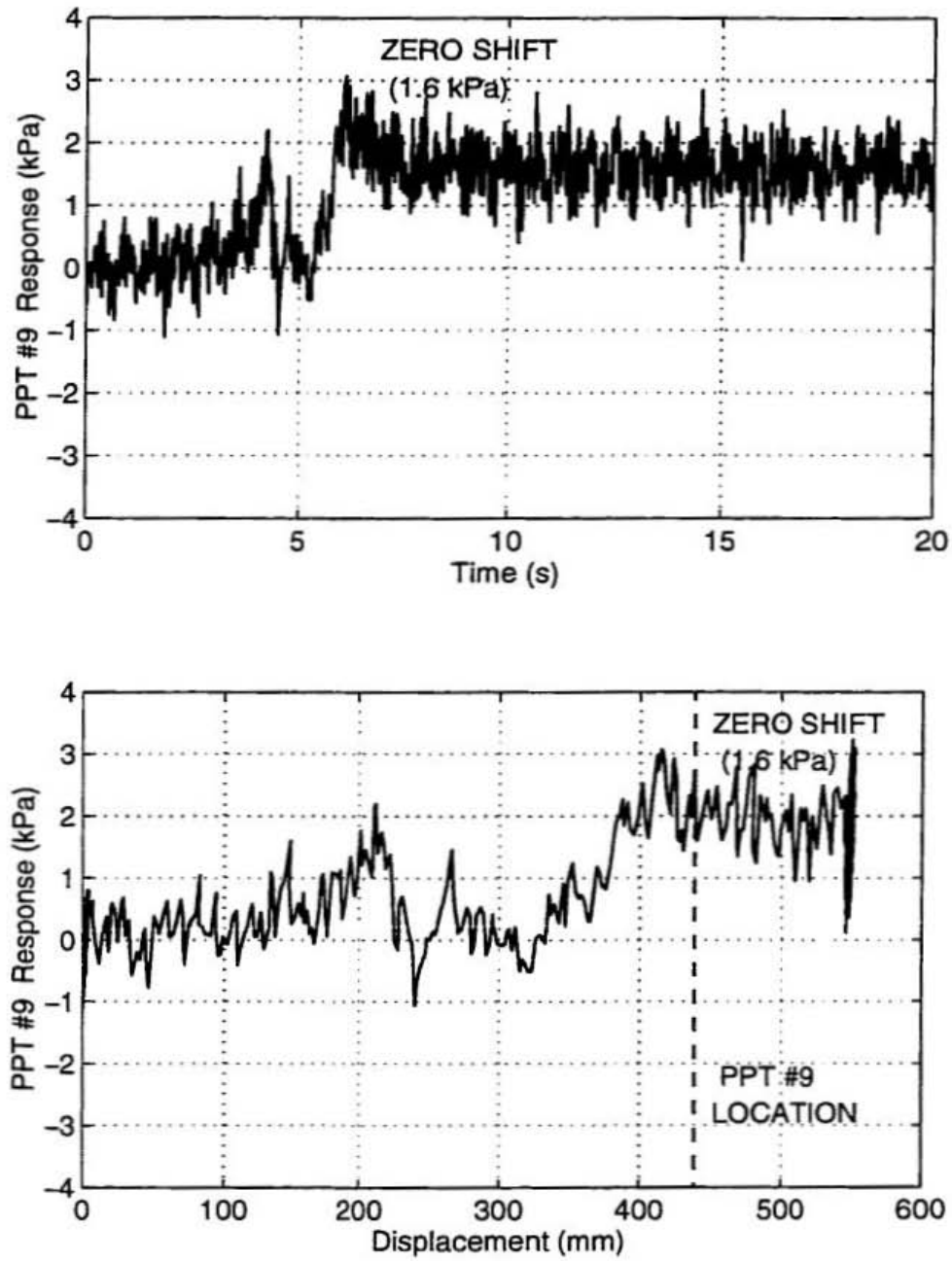

Figure A.41 **Scour F, PPT #9 Response Versus Time and Displacement**

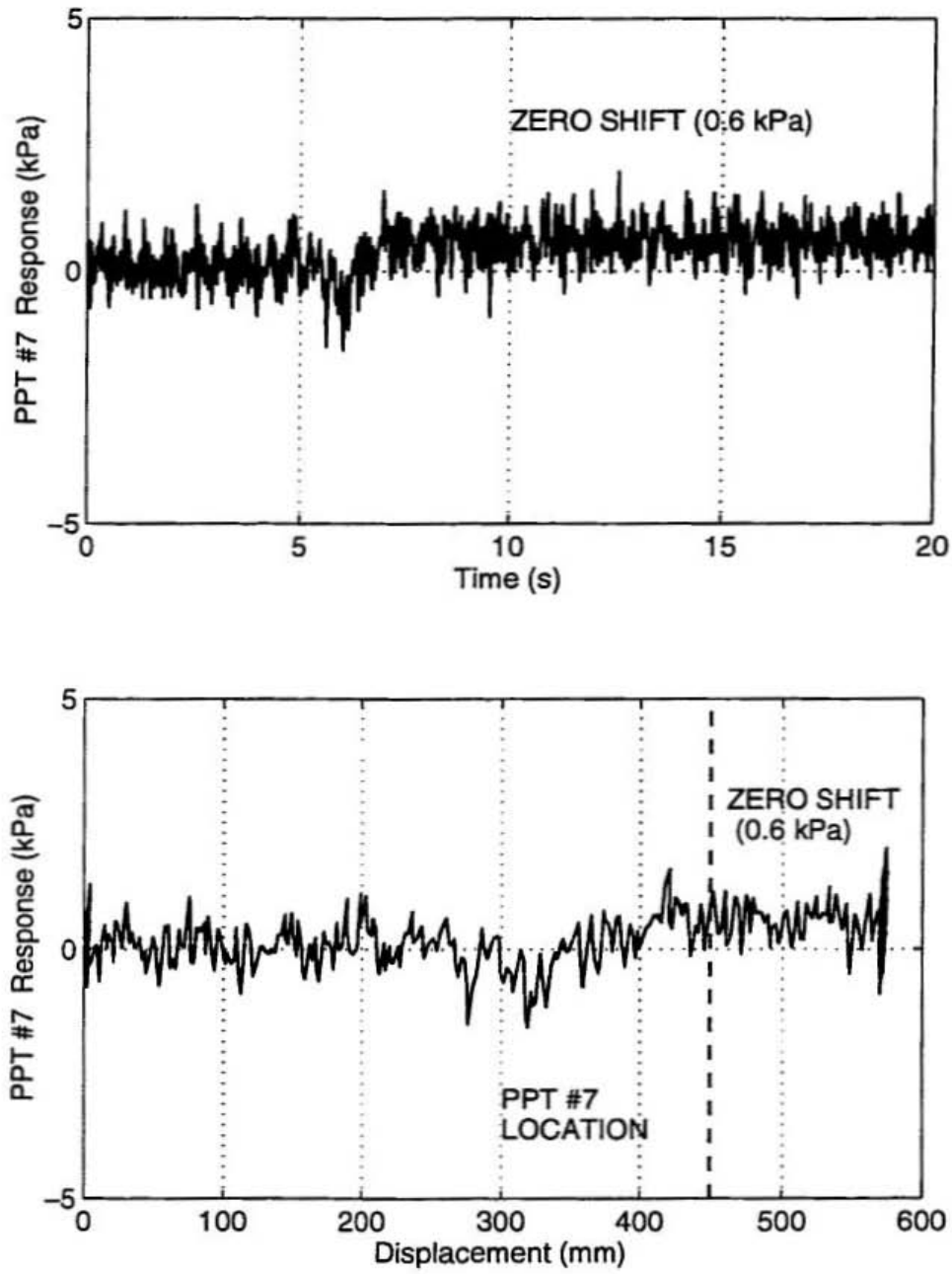

Figure A.42 **Scour G, PPT #7 Response Versus Time and Displacement**

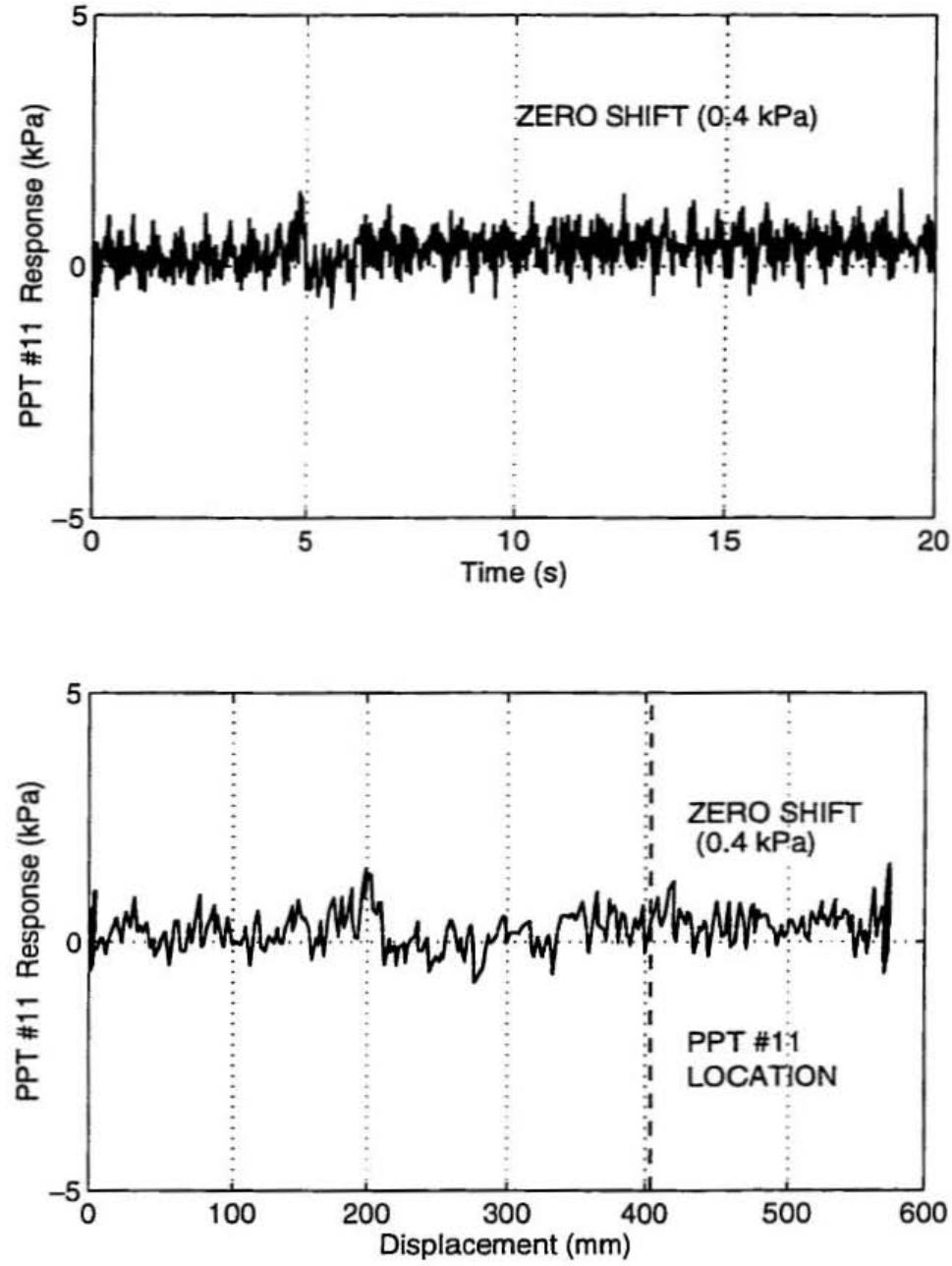

Figure A.43 **Scour G, PPT #11 Response Versus Time and Displacement**

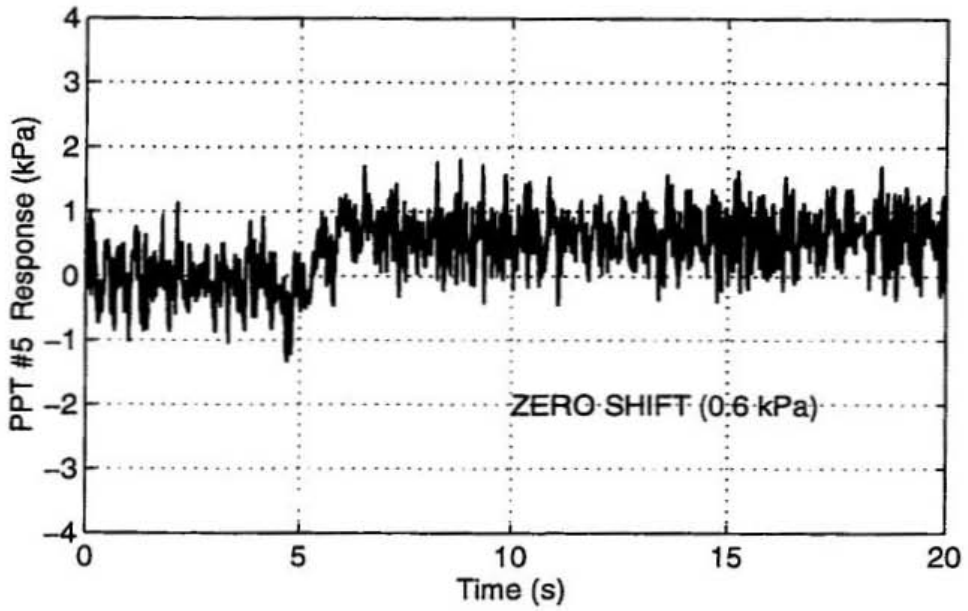

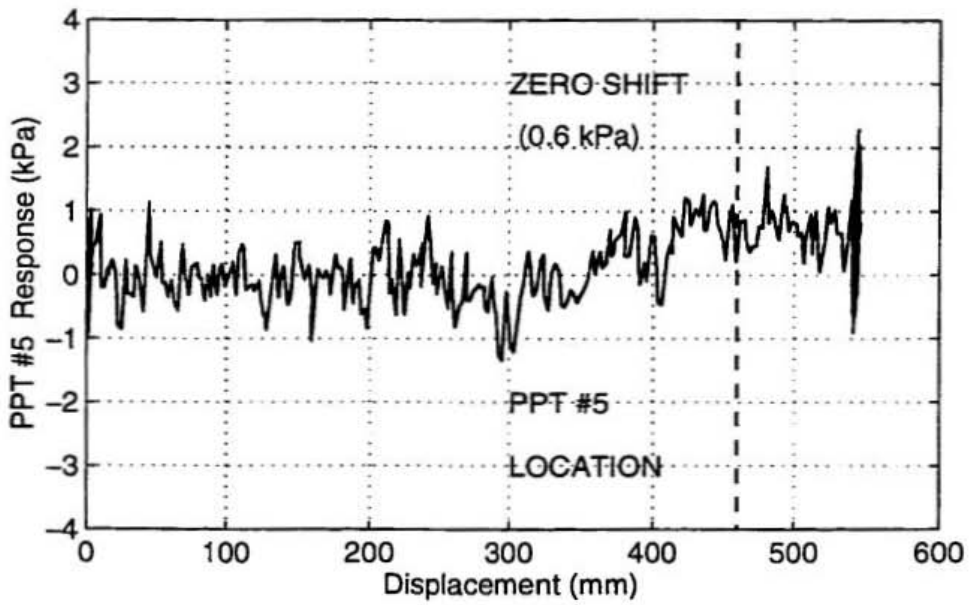

Figure A.44 **Scour H, PPT #5 Response Versus Time and Displacement**

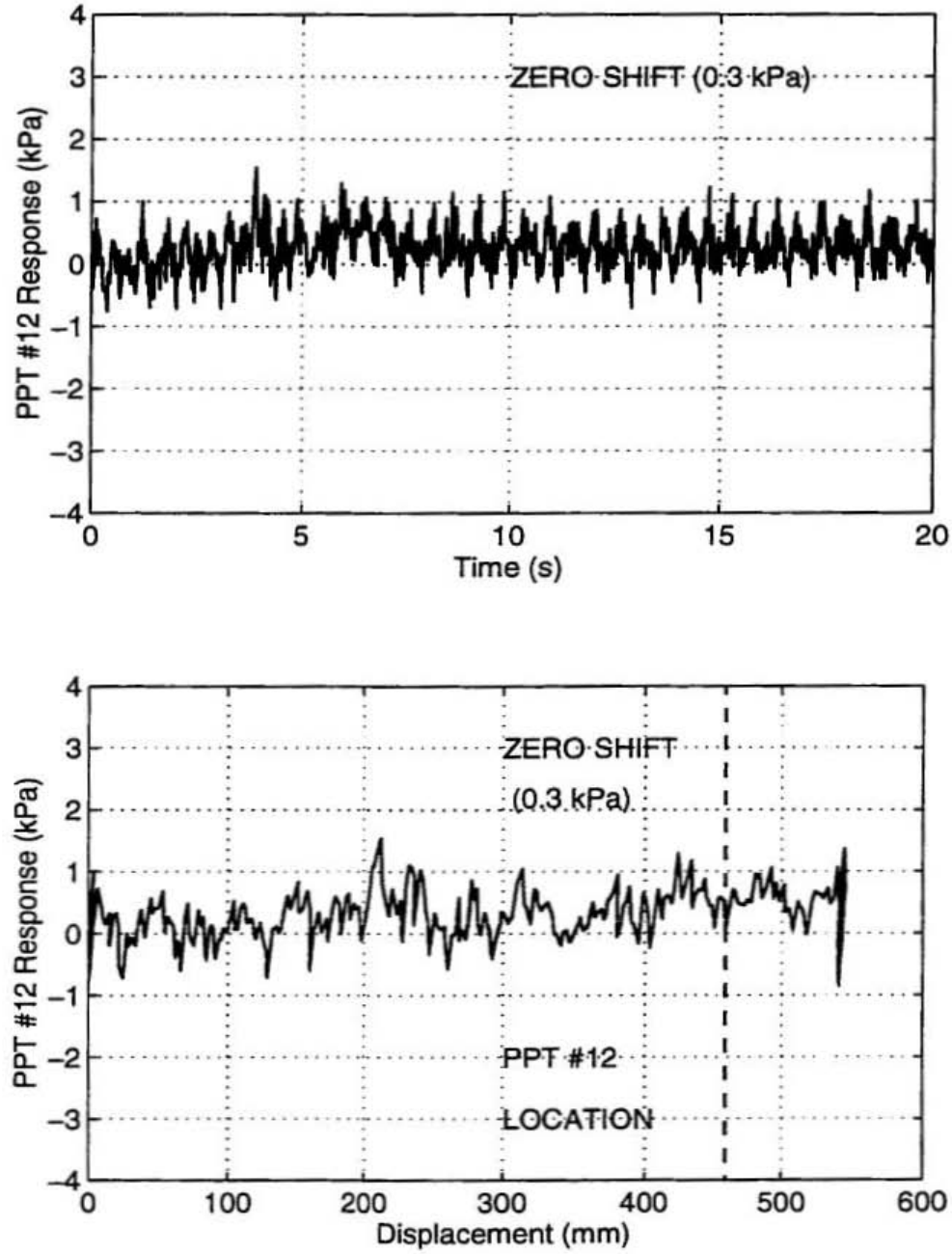

Figure A.45 **Scour H, PPT #12 Response Versus Time and Displacement**

TEST TARGET (QA-3)

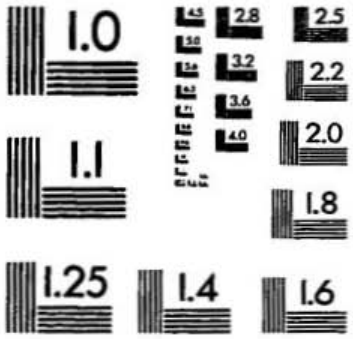

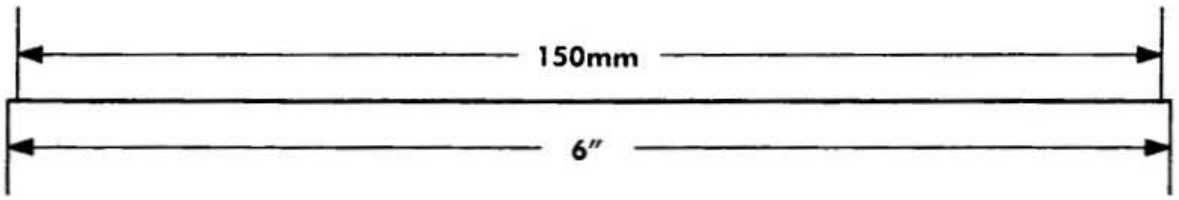

APPLIED IMAGE, Inc
1653 East Main Street
Rochester, NY 14609 USA
Phone: 716/482-0300
Fax: 716/288-5989